



This is to certify that the
dissertation entitled

EQUILIBRIUM AND NON-EQUILIBRIUM CONFORMATION
AND MECHANICAL PROPERTIES OF
NANOPARTICLE/LINEAR POLYMER BLENDS

presented by

DAVID ANDREW BOHNSACK

has been accepted towards fulfillment
of the requirements for the

PhD degree in Chemical Engineering

Major Professor's Signature

30 AUG 2007

Date

PLACE IN RETURN BOX to remove this checkout from your record.
TO AVOID FINES return on or before date due.
MAY BE RECALLED with earlier due date if requested.

DATE DUE	DATE DUE	DATE DUE

**EQUILIBRIUM AND NON-EQUILIBRIUM CONFORMATION AND
MECHANICAL PROPERTIES OF NANOPARTICLE/LINEAR POLYMER BLENDS**

By

David Andrew Bohnsack

A DISSERTATION

**Submitted to
Michigan State University
in partial fulfillment of the requirements
for the degree of**

DOCTOR OF PHILOSOPHY

Department of Chemical Engineering and Materials Science

2007

ABSTRACT

EQUILIBRIUM AND NON-EQUILIBRIUM CONFORMATION AND MECHANICAL PROPERTIES OF NANOPARTICLE/LINEAR POLYMER BLENDS

By

David Andrew Bohnsack

Fillers with characteristic sizes on the nanometer scale and aspect ratios near unity are investigated for their potential to enhance the mechanical properties of a linear amorphous polymer, polystyrene. Four types of nanoparticles with different sizes, structures, and interactions with the matrix have been investigated to better understand the particle-polymer interaction and its significance for mechanical property enhancement. Generally, the particle inclusion increases polymer mobility and free volume. This is observed through decreases in the glass transition temperature, bulk modulus, and internal pressure, as well as increases in the free energy anharmonicity, and strain-to-failure for a sample in tension. The particles behave in a manner similar to a good solvent, swelling the polymer and increasing chain mobility and sample ductility, an observation confirmed by neutron scattering. The details of the particle size, loading, and chemistry introduce other nuances to the polymer-particle behavior. Bulk modulus increases have been observed for many systems, and a general increase in the energy dissipation for a sample in tension is observed with nanoparticle addition. The role of the particles in the orientation of the matrix during uniaxial hot-drawing is studied. In many cases, it is found that equivalent tensile property enhancement can be achieved under more moderate processing conditions by the addition of nanoparticles.

I dedicate this work to my Lord and Savior, Jesus Christ. All that I have is from Him, and all that I do is for Him.

ACKNOWLEDGEMENTS

The work described in this document would not have been possible without the help and collaboration of a number of people.

I am indebted to those people who provided the nanoparticles that were the basis for this work. Specifically, I thank Brooke van Horne and Craig Hawker for the synthesis of the cross-linked polystyrene nanoparticles, Suba Asokan and Michael Wong for the CdSe nanocrystals, and Guangui Chen and Zhibin Guan for the hyperbranched polyethylene. I have been especially reliant on the kind and capable staff of the two neutron sources where I performed experiments. I deeply valued the help of Boualem Hammouda at NIST and Denis Wozniak, Venky Pingali, and Pappanan Thiyagarajan at IPNS. Their help in conducting the experiments and suggestions for interpreting the results have been invaluable.

I consider myself fortunate to have worked under the direction of Prof. Michael Mackay. I am grateful for the tremendous amount that I learned from him. His enthusiasm and commitment to his students is apparent and appreciated in both our professional and personal development. In that vein, he has built a strong research group of which I am proud to have been a member. I am grateful to the group alumni, R.S Krishnan, Leslie Passeno, and Anish Tuteja, for helping me to find my way in the lab. I am also grateful to the newer group members, Jonathan Kiel, Erin McGarrity, Megan Romanowich, Jonathan Seppala, and Erica Tseng, for their contribution of new ideas and enthusiasm at a time when both were flagging. I have especially valued my contemporaries, Tiffany Bohnsack and Melissa Yaklin. Their support as we navigated the waters of graduate school has made the journey more than bearable, even pleasurable.

I have also benefited greatly from a wonderful group of friends and family who have supported me throughout my tenure at MSU. In addition to my friends in the Mackay Group, I am grateful to my other colleagues in the department, Brian Hassler, Troy Hendricks, Aaron Greiner, and Steven Nartker. I am especially grateful to my family for their love and support, not only at this time of my life, but for all the years leading up to this, and those yet to come. I thank my parents, Rich and Kathy, for encouraging me to set high goals and always assuring me that they were within my reach. It is the foundation they laid for me that has allowed me to achieve what I have. I thank my elder siblings, Rob and Carin. Their interest and support in all that I have attempted has been a source of great encouragement. Finally, I thank my wife Tiffany. Her support both in and out of the lab has been instrumental in the completion of this work. I am grateful for her patience, motivation, inspiration, encouragement, perspective, and love.



C
Ch
imp
V
V
V

TABLE OF CONTENTS

List of Tables.....	viii
List of Figures	ix
Chapter I: Introduction	1
I.A. Nanocomposites	1
I.B. Motivation	4
I.C. Equilibrium interactions between particles and polymers	5
I.D. Alignment of neat polymers	9
I.E. Objectives.....	13
Chapter II: The effect of intramolecularly cross-linked polystyrene nanoparticles on the thermal and mechanical properties of linear polystyrene.....	14
II.A. Introduction	14
II.B. Experimental	16
II.C. Results and Discussion.....	21
II.C.1. Equilibrium Thermal Analysis	21
II.C.2. Non-Equilibrium Tensile Behavior	31
II.D. Conclusion.....	36
Chapter III: A small-angle neutron scattering (SANS) study of the anisotropic conformation of linear polystyrene in the presence of intramolecularly cross-linked polystyrene nanoparticles	37
III.A. Introduction	37
III.B. Experimental	44
III.C. Results & Discussion	45
III.D. Conclusion.....	53
Chapter IV: The effect of C₆₀ addition on the thermal and mechanical behavior of PS55	
IV.A. Introduction	55
IV.B. Experimental	58
IV.C. Results & Discussion	58
IV.C.1. Equilibrium Thermal Analysis	58
IV.C.2. Non-Equilibrium Tensile Behavior	67
IV.D. Conclusion.....	71
Chapter V: Dispersion of hyperbranched polyethylene in polystyrene leading to improvements in stiffness and ductility	72
V.A. Introduction	72
V.B. Experimental	73
V.C. Results & Discussion	73
V.C.1. Equilibrium Thermal Analysis	73

V.C.2. Non-Equilibrium Tensile Behavior	79
V.D. Conclusion.....	83
Chapter VI: Rigid nanoparticle inclusion with polystyrene	85
VI.A. Introduction	85
VI.B. Experimental	85
VI.C. Results & Discussion	86
VI.D. Conclusion.....	91
Chapter VII: Conclusions	93
Appendix A. Notes on PVT Analysis	95
Appendix B. Additional Tensile Data	103
References	104

LIST OF TABLES

Table II-1: Molecular weights and distributions of linear polystyrene and intramolecularly cross-linked polystyrene nanoparticles	17
Table III-1: Summary of previous work on alignment by hot drawing and their test parameters.	39
Table III-2: Molecular weights and distributions of linear polystyrene and intramolecularly cross-linked polystyrene nanoparticles	44
Table A-1: Values of free volume layer sizes based on the bulk moduli of composites at 200 °C.....	97
Table A-2: Tait EOS parameters in the melt state of polymer/nanoparticle blends	98
Table A-3: Simha-Somcynsky EOS parameters in the melt state of polymer/nanoparticle blends	100

LIST OF FIGURES

- Figure I-1. Typical process for fiber stretching. Extruded fibers pass over rollers that turn at controlled, increasing speeds. This difference in roller speed induces strain, and therefore alignment, in the fiber spinning direction. 10
- Figure I-2. The room temperature stress-strain curves of unfilled PS 393 kD drawn in tension at five hot draw ratios. PS processed to a hot draw ratio of 2 or greater exhibits ductile failure where a less oriented specimen fails by a brittle process..... 11
- Figure I-3. Schematic depiction of a typical necking process. Regions i and vi are regions of primarily elastic deformation, while regions ii, iii, iv, and v are regions of primarily plastic deformation. The initiation of a necked region (ii and iv) and the propagation of those regions (iii and v) are demonstrated by a series of plateaus in the engineering stress. 12
- Figure II-1. Cross-linked polystyrene nanoparticles are synthesized from a random copolymer of styrene and benzocyclobutene (BCB). When thermally activated, the BCB groups bond with one another to form an intramolecularly cross-linked particle. 16
- Figure II-2. Change in glass transition with addition of PSNP. At low loadings the T_g is reduced, contrary to the prediction based on relative weight fraction (indicated by open symbols and dashed lines), suggesting additional molecular mobility at the particle interface. Error bars indicate the initiation and completion temperatures of the glass transition process..... 22
- Figure II-3. DSC traces for PS, PSNP 78 kD, and a 5% blend of PSNP 78 kD in PS..... 24
- Figure II-4. Bulk modulus and thermal expansivity of a PS with PSNP 78 kD. The cross-linked particles tend to decrease the bulk modulus and increase the thermal expansivity slightly (a). These two effects are suggestive of the introduction of a small region of unoccupied volume around the surface of the fillers. Similar trends are seen in the bulk modulus both above (200 °C) and below (50 °C) the glass transition temperature. Prediction of the bulk modulus with a free volume layer of 1.2 nm provides a satisfactory fit to the measured bulk modulus at 200 °C (b). The prediction for no free volume is for an increase in K_0 , which is not observed..... 25
- Figure II-5. Schematic representation of a particle (p) surrounded by a layer of free volume (f) within a continuous matrix phase (c). The particle has a radius, a , and the free volume region has a thickness, l_f 27
- Figure II-6. The free volume asymmetry number, and internal pressure as function of PSNP 78kD volume fraction in PS 393kD. The free volume asymmetry number is increased with nanoparticle addition, suggesting an increased energetic penalty to compression as compared to dilation. The internal pressure is decreased by particle addition, consistent with a decrease in the strength of intermolecular interactions..... 28

Figure II-7. The dimensionless free energy as a function of relative density. The anharmonic potential shows an equivalent free energy change for compression or dilation. The addition of PSNP 78kD is seen to exacerbate the asymmetry of the free energy profile, with dilation being energetically favored over compression. 29

Figure II-8. Stress-strain curves for unfilled polystyrene and polystyrene filled with three different PSNP types, each processed to a hot draw ratio of 1.75. The two larger PSNP species induce ductile failure under conditions for which the unfilled polymer and the polymer filled with PSNP 41 kD fail by a brittle mechanism at low strains. 32

Figure II-9. The Young's Modulus (a), strain to failure (b), ultimate tensile strength (c), and tensile energy to break (d) of hot-drawn PS 393 kD with PSNP as a function of hot draw ratio. Larger PSNP species have very little effect on Young's Modulus or ultimate tensile strength, while smaller (41 kD) particles increase these properties for the unprocessed and slightly processed case. The ductility (b) is increased for all cases at low draw ratios and at all draw ratios for PSNP 78 kD, which gives rise to an increase in the material toughness (d). 33

Figure III-1. The background signal is assumed to be constant at all wave vectors, at reasonable approximation for the predominantly incoherent scattering observed for protonated PS. 43

Figure III-2. The anisotropic SANS pattern of a non-equilibrium, hot stretched PS film (left). The scattering profiles parallel and perpendicular to the stretch direction are shown on the right. 46

Figure III-3. The Lorentzian exponent of PS with and without PSNP addition as a function of hot draw ratio. The Lorentzian exponent for a Gaussian chain is 2. Swollen coils exhibit a reduced dependence of I on q at higher wave vectors. 48

Figure III-4. The characteristic size development of anisotropic PS with and without PSNP 78 kD as a function of hot draw ratio. The macromolecular size is calculated according to either the Debye form factor (a) at all wave vectors, or the Lorentzian scattering function at high wave vectors. In both cases a discontinuity is observed for the nanoparticle-laden sample at $\lambda=1.75$, the hot draw ratio at which ductile fracture behavior is observed in tension. A small increase is observed in the long axis size of the polymer at the highest draw ratio by both methods of calculation..... 50

Figure III-5. The aspect ratio development of anisotropic PS with and without PSNP 78 kD as a function of hot draw ratio. The aspect ratio is calculated according to either the Debye form factor (a) at all wave vectors, or the Lorentzian scattering function at high wave vectors. In both cases a discontinuity is observed for the nanoparticle-laden sample at $\lambda=1.75$, the hot draw ratio at which ductile fracture behavior is observed in tension. The dashed line represents the aspect ratio for a chain that deforms affine to the bulk sample, the maximum attainable orientation in the absence of an additional driving force. 52



Figure IV-1. Change in glass transition with addition of C₆₀. Extremely low concentrations - corresponding with an interparticle half-gap of similar size to the statistical Kuhn segment length of polystyrene - of C₆₀ show an increase in T_g that corresponds to a reduction in polymer mobility. Higher, but still homogeneously dispersed, loadings show a T_g reduction. 59

Figure IV-2. Bulk modulus and thermal expansivity of a polystyrene/buckminsterfullerene blend. At very low volume fractions for which the interparticle gap is greater than the statistical segment length of the matrix polymer, the bulk modulus is reduced and the thermal expansivity is increased. At higher loadings, the C₆₀ is spaced closer than the Kuhn segment length of polystyrene and the bulk modulus is increased and the thermal expansivity is decreased. Similar trends are seen in the bulk modulus both above (200 °C) and below (50 °C) the glass transition temperature. Prediction of the bulk modulus with a free volume layer of 0.26 nm provides a satisfactory fit to the measured bulk modulus at 200 °C (b). The prediction for no free volume is for a much greater increase in K₀ than is observed experimentally. 62

Figure IV-3. The free volume asymmetry number, and internal pressure as function of C₆₀ volume fraction in PS 393 kD. The free volume asymmetry number goes through a maximum before decreasing with increasing particle loading. The internal pressure is decreased by particle addition, consistent with a decrease in the strength of intermolecular interactions. 64

Figure IV-4. The Young's Modulus (a), strain to failure (b), ultimate tensile strength (c), and energy to failure (d) of hot drawn PS 393 kD with buckminsterfullerenes as a function of hot draw ratio. The modulus (a) and ultimate tensile strength (c) are unchanged for the undrawn case and increased by C₆₀ inclusion at low draw ratios for both loadings. At higher loading (2.5v%) the modulus and ultimate tensile strength are reduced at draw ratios greater than 2.5. The ductility (a) is increased for both loadings at moderate (1.75 to 2.5) draw ratios. At higher draw ratios the samples with low loading (1v%) are similar to unfilled PS while the higher loading (2.5v%) is much less ductile than the neat polymer. 68

Figure V-1. DSC traces of pure PELP and blends of PELP with linear PS. Phase separation becomes apparent in the DSC trace for the 5% blend. 75

Figure V-2. Bulk modulus and thermal expansivity of a polystyrene/hyperbranched polyethylene nanoparticle blend. The PELP decreases the modulus and increases the thermal expansivity as expected for a system with little chemical interaction. Similar trends are seen in the bulk modulus both above and below the glass transition temperature. 76

Figure V-3. The free volume asymmetry number, and internal pressure as function of PELP volume fraction in PS 393 kD. The free volume asymmetry number is increased with nanoparticle addition, suggesting an increased energetic penalty to compression as compared to dilation. The internal pressure is decreased by particle addition, consistent with a decrease in the strength of intermolecular interactions. 78

Figure V-4. The Young's Modulus (a), strain to failure (b), ultimate tensile strength (c), and tensile energy to break (d) of hot-drawn PS 393 kD with 3v% PELP as a function of hot draw ratio. All four key tensile properties are increased at draw ratios less than five. At higher draw ratios, the behavior of the matrix dominates and the composite follows the tensile properties of unfilled polystyrene. 80

Figure V-5. Stress-strain curves for polystyrene with (green diamonds) and without (black circles) PELP, each processed to a hot-draw ratio of 1.5. The PELP induces ductile failure under conditions for which the unfilled polymer fails by a brittle mechanism at low strains. 82

Figure VI-1. The Young's Modulus (a), strain to failure (b), ultimate tensile strength (c), and tensile energy to break (d) of hot-drawn PS 393 kD with 1v% CdSe-pyr as a function of hot draw ratio. The modulus and tensile strength are both increased at all draw ratios less than five. The strain to failure and tensile energy are increased at moderate (2 to 2.5) draw ratios but unchanged from the unfilled polymer under other processing conditions. 88

Figure VI-2. TEM micrograph of CdSe-pyr in PS. The wrinkles in the film are a familiar artifact of ultramicrotomy, reflecting imperfections in the knife edge. The particles are oriented perpendicular to these striations, suggesting that the particles are disturbed during the microtomy process and deposited intermittently as the knife moves across the sample..... 91

Figure VII-1. The calculated free volume layer size (a) and free volume fraction relative to particle volume fraction (b) for nanoparticles for four different sizes. The free volume thickness associated with the particle addition increases with particle size. With the exception of the extreme case of C60 ($a = 0.38$ nm), the ratio of free volume to particle volume is independent of particle size. 94

Figure A-1. The measured specific volume (a) of polystyrene-nanoparticle blends. Blends of polystyrene with nanoparticles follow close to a rule-of-mixtures type trend for specific volume. The deviation from that trend is apparent in the Excess Free Volume (b) for which a positive value represents the presence of free volume in the blend. It must be noted that the measurement technique is very subject to environmental variations and small changes in free volume may not be apparent in specific volume measurements....95

Figure A-2. The Simha-Somcynsky statistical hole fraction for blends of PS 393 kD with four different nanoparticle types..... 102

Figure B-1. The Young's Modulus (a), strain to failure (b), ultimate tensile strength (c), and tensile energy to break (d) of hot-drawn PS 393 kD with PSNP as a function of hot draw ratio. Blends of 1% PSNP are represented by open symbols while blends of 5% PSNP are represented by closed symbols. Larger PSNP species have very little effect on Young's Modulus or ultimate tensile strength, while smaller (41 kD) particles increase these properties for the unprocessed and slightly processed case. The ductility (b) is

increased for all cases at low draw ratios and at all draw ratios for PSNP 78 kD, which gives rise to an increase in the material toughness (d).....103

Chapter I: Introduction

I.A. Nanocomposites

The development of techniques to create well-defined structures with characteristic dimensions less than 100 nm has led to new possibilities for structural enhancement of polymers. The general strategy for the formulations of these nanocomposites is similar to traditional composites; a material of higher modulus and aspect ratio is incorporated into the weaker matrix material with the objective of concentrating stress on the higher modulus material, thereby strengthening the composite. A number of types of nanoparticles which have a multitude of properties have received particular attention. In contrast to this traditional mode of enhancement, we hypothesize that the small characteristic length scale of these additives and their close proximity to one another presents the opportunity to alter the structure of the matrix material itself, thereby strengthening it directly.

The development of characterization techniques suitable for probing length scales in the nanometer range has given momentum to the design and characterization of nanocomposites. Microscopy techniques which are different, but complementary to one another, allow visualization of particles and structures with feature sizes on the order of 1 nm. While microscopy can be used to visualize local features, scattering methods provide an avenue for evaluating the overall, average, morphology of a given system.

Scanning electron microscopy (SEM) facilitates visualization of surface topographies and limited compositional information based on Z-contrast. A key obstacle in the use of this technique is the need for the sample to be electrically conductive. This requirement can be circumvented by coating the sample with a thin layer of conductive

material, often gold. Unfortunately, this coating layer may obscure the smallest topographical features. Environmental SEM (ESEM) can also be used to characterize insulating samples without the need for a conductive layer. This is achieved by immersing the sample in a conductive environment, generally water vapor, rather than the high vacuum used in traditional SEM.

Transmission electron microscopy (TEM) and atomic force microscopy (AFM) allow the visualization of particles and structures with length scales close to 1 nm. TEM samples must be sufficiently thin so that the number of scattering events per electron is close to one. Contrast is achieved in TEM imaging through Z contrast and, to a lesser degree, mass density. Where sufficient natural contrast is not present, it can be enhanced through the use of TEM-specific stains. Heavy metal compounds such as OsO_4 or RuO_4 will preferentially bind to certain chemical environments, especially unsaturated carbon-carbon bonds. This allows Z-contrast to be induced where previously only chemical differences were present. AFM relies on the physical interaction between a probe having a radius of curvature less than 20 nm and the sample surface. Primarily used for profilometry, AFM can also be used as a relative measure of sample stiffness, as regions of different modulus cause the cantilever tip to oscillate at different frequencies. While the vertical resolution attainable by AFM is close to 1 nm, the lateral resolution is limited by the probe tip radius and is often an order of magnitude greater than the vertical resolution.

In addition to microscopic techniques, scattering methods provide a means to understand the average size and structure of a particular species. The variety of scattering methods available – light, x-ray, neutron – ensures that a suitable technique will likely be

available based on the type of contrast that is available for a given sample. A key advantage of scattering methods is that an average measurement is made over billions of scatterers, in contrast to microscopy methods with which at most order of one hundred objects are characterized. While scattering and microscopy are the key methods for visualizing or deciphering nanostructures, the range of bulk characterization methods also reveal nanoscale features such as the strength of interaction at nanoscale interfaces or the presence of free volume.

A number of length scales that are significant in a filled system are affected greatly by the reduction in the filler size. One such length scale is the interparticle half-gap, h , which is determined by the particle radius, a , the particle volume fraction, φ , and the maximum random packing fraction, φ_m , for the particle geometry in question.

$$\text{Eq. 1} \quad h/a = (\varphi_m/\varphi)^{1/3} - 1$$

For the case of a colloidal (1 μm radius) particle versus a nanoscale (5 nm radius) particle the reduction in radius at constant volume fraction results in a reduction of the interparticle half-gap from ~ 1300 nm to ~ 7 nm at a modest loading of 5v%. When included in a matrix of moderately high molecular weight (500 kD) polystyrene, the interparticle half-gap of the colloidal system is nearly 70 times the radius of gyration (R_g) of the host polymer, while the half-gap in the nanosize system is only one third of the polymer's R_g . This geometric evaluation makes it clear that a polymer chain of this molecular weight could not reside between neighboring nanoparticles without becoming distorted from its equilibrium conformation. Systems for which the interparticle half-gap is less than the matrix polymer's R_g are referred to by us as confined, and have been

a
c
8
t
P
f
le
co
th
na

de
ran
as
sof
ma
the
the
cred

shown to display behavior that is substantially different than that of the neat polymer or of a traditionally modeled system.

A decrease of the individual particle size at constant volume fraction naturally also increases the number concentration of particles. For the present example of a colloidal versus nanoscale particle, the number concentration is increased by a factor of 8×10^6 , which obviously increases the surface area for interaction. If one assumes that the polymer within a certain layer thickness, l , is directly affected by the presence of the particle, then the increase in surface area will also increase this volume of interaction. In fact, if one assumes that the thickness of the interaction is similar to the Kuhn segment length of the polymer – 1.8 nm for polystyrene – then for the present example of the colloidal versus nanoscale filler the interaction volume increases by a factor of 240 for the nanoscale filler over the colloidal filler and can represent ~3 % of the volume for the nanoscale system.

I.B. Motivation

Much effort has been devoted to mimicking the hierarchical structures demonstrated by natural systems which often exhibit key features in the nanometer size range. The controlled liquid crystallinity of silkworm¹ and spider²⁻⁴ silk has been studied as a potential route to high modulus synthetic fibers⁵ and the layered structure of hard and soft components in nacre has been studied⁶ in hopes of achieving a similarly strong material through structural control of synthetic composite materials. The recognition that these naturally occurring systems that exhibit desirable end-use properties rely heavily on the structures and interactions that occur over nanometer length-scales lends further credence to the importance of controlling these behaviors in synthetic systems.

One product area that is especially appealing for the application of nanocomposites is protective materials, especially body armor. The ability to produce synthetic fibers with very high modulus supports the development of woven fabrics that can be used as body armor. Kevlar, for example, has been used to achieve extremely high modulus predominantly through strong interchain hydrogen bonding between the polyaramid chains which is enhanced by the polymer chain alignment.⁷ Ultra-high molecular weight polyethylene (UHMWPE), sold commercially as Dyneema or Spectra, owes its very high impact strength to the extreme length of its chains and their high parallel orientation (up to 95%).

In addition to high modulus materials, flexible fibers that effectively dissipate energy prior to failure are needed as restraints. These restraint and cushion materials must deform to gently bring their cargo to a stop in the event of a sudden impact or change in velocity.

It has been found that, in some cases, the addition of nanoparticles to a polymer can reduce the polymer's viscosity,^{8, 9} resulting in a reduction of energy needed for processes like extrusion and injection molding. While this is beneficial from a processing standpoint, in order to be industrially viable the additives must, at the least, not diminish the end use properties of the product. Particles that also provide an improvement to the end use properties in addition to facilitating processing would be particularly desirable.

I.C. Equilibrium interactions between particles and polymers

The ability to uniformly disperse nanoparticles within a linear polymer matrix is significant for the development of functional polymer composites, as well as a new route to enhanced processing or end-use properties through nanoparticulate additives. While

the phase stability of these blends has been studied,¹⁰ the filler-particle interaction of the binary system is insufficiently understood. Some effort has been devoted to the interactions of nanocomposites of inorganic fillers with high aspect ratios.¹¹⁻¹⁴ These studies often involve melt-compounded clays with high surface energy and a strong attractive interaction with the polymer melt. Due to the strong van der Waals forces present between individual clay sheets, adequate exfoliation of the sheets and subsequent intercalation of the polymer between the sheets is often problematic. Once these obstacles are overcome, the frequent result is a tendency towards adsorption of the polymer on the clay surface, resulting in the “hairy clay platelet” structure which has an abnormally high polymer density at the clay surface.

The situation of a filler particle with an aspect ratio approaching unity and a characteristic length on the nanometer scale is much different, as it lacks the large smooth surface that leads to a concentration of van der Waals forces. A considerable amount of theoretical and simulation work has been devoted to understand the conformation and behavior of a polymer chain confined near a spherical surface.¹⁵⁻¹⁹ In molecular dynamics simulations of a rigid spherical particle in a polymer matrix, Brown *et al.*²⁰ showed that the polymer can orient parallel to the particle surface, leading to radial density fluctuations very close to the particle surface. This interphase region has a reduced bulk modulus due to the distortion of the melt structure and regions of low density. Very high loadings of the nanoparticle result in a high volume fraction of this interphase which reduces the total bulk modulus to a value less than that of the neat polymer. Papakonstantopoulos *et al.*¹⁸ studied the effect of the polymer-particle interaction force, finding that attractive polymer-particle interactions lead to the formation of a glassy

interphase layer around the particle, increasing the shear and Young's moduli. Repulsive particle-polymer interactions, on the other hand, produced an interphase region with a modulus less than the bulk, surrounded by a region with modulus greater than the bulk. The net effect of this is reduction of the overall modulus and glass transition temperature of the composite system. These simulations are computationally difficult, however, especially because the time scale of large polymer relaxation is much greater than the time scales that can generally be probed by molecular dynamics simulations.^{21, 22} The alternatives to rigorous simulations of long chain polymers include limiting simulations to oligomeric systems which may overlook entanglement or entropic effects,¹⁸ or simulating only a few phantom chains by attempting to mimic the behavior of a single chain in a continuum melt.¹⁷

While simulation efforts have shed light on the problem, there is less experimental work devoted to this situation of spherical fillers with radii less than or equal to the R_g of the matrix polymer.²³ In one case described by Merkel *et al.*,²³ spherical fumed silica particles were incorporated into a membrane material of glassy, amorphous poly(4-methyl-2-pentyne). The result was an increase in the gas permeability and an increase in the size of one type of free-volume void as observed by positron annihilation lifetime spectroscopy (PALS). By performing similar tests with particles of varying size but constant volume fraction, it was concluded that smaller particles cause greater disruption to the polymer matrix, likely due to their increased surface area. The maximum particle size that affected a change in the free volume or permeability for this system was found to be 50 nm.

The glass transition temperature (T_g) is an indicator of polymer chain mobility in amorphous polymers. More mobile chains require less thermal energy to initiate the Brownian motion of 20 to 50 carbon atoms that is characteristic of a material above its T_g .²⁴ This transition is sensitive to the polymer's chemical structure and molecular weight, as well as the environment in which it is located. Studies have shown that placing a polymer in a thin film, pore, or other confined geometry alters its conformation sufficiently to change the T_g .²⁵⁻²⁷ Studies of the effect of nanofillers on the glass transition temperature have shown that they can increase or decrease T_g by as much as 30 °C.²⁸

In a study of PDMS networks filled with 10 nm silica particles, Fragiadakis *et al.*²⁹ found that the T_g was not significantly changed, but the shape of the calorimetric step change was altered with the particle addition. Dielectric measurements confirmed the presence of a second slower α -relaxation indicative of the restricted motion of polymer chains near the particle surface.

Bansal *et al.*³⁰ studied the effect of wetting behavior on T_g of nanocomposites by grafting oligomeric polystyrene chains onto silica spheres in a polystyrene matrix. By increasing the molecular weight of the matrix polymer, the system transitions from wetting to dewetting behavior. In the case of the low molecular weight, wetting system, the strong interface reduced chain mobility and increased the T_g by as much as 4 °C. The high molecular weight, dewetting system showed a T_g reduction of as much as 4 °C, caused by the introduction of a free interface that increased chain mobility at each particle surface. This behavior is similar to the behavior observed for T_g changes in thin polymer films.³¹ In similar work, Rittigstein and Torkelson³² prepared nanoparticle filled

1

i
c
th
a
m
st

films and observed the change in both T_g and physical aging rate. For poly(2-vinyl pyridine) filled with 47 nm alumina particles which had an attractive wetting interaction the T_g increased by 16 °C and the rate of physical aging, another measure of molecular mobility, decreased by a factor of 17. A non-wetting system of alumina particles in poly(methyl methacrylate) showed a T_g reduction of 5 °C and the same particles in polystyrene had a wetting, but not attractive interaction, causing the T_g to be unchanged by the particle addition.

Another method of nanoparticle inclusion is grafting particles directly onto polymer chains as random copolymers, a method often employed with polyhedral oligomeric silsesquioxane (POSS). Xu *et al.*³³ studied the thermal effect of POSS inclusion with poly(acetoxystyrene) (PAS). Their study revealed competing and adverse effects on T_g ; at low POSS concentration, the POSS disrupted the dipole-dipole interaction of the PAS chain, decreasing the T_g . At higher POSS concentration the T_g increased as dipole-dipole interactions between POSS and polar PAS moieties became more significant.

I.D. Alignment of neat polymers

Introducing global alignment to otherwise amorphous materials is known to increase their tensile strength in the direction of alignment.^{34, 35} This has been demonstrated for linear polymers by introducing axial strain to a sample above its T_g , then quenching it well below T_g , locking the polymeric chains in their nonequilibrium anisotropic conformation. This process is representative of typical polymer processing methods that consist of fiber formation by either melt or gel spinning, followed by hot-stretching which is controlled by passage over rollers that move at progressively

increasing speed. The process is completed by cooling the sample through immersion in a low temperature bath and optional cold-stretching below T_g (Figure I-1).³⁵

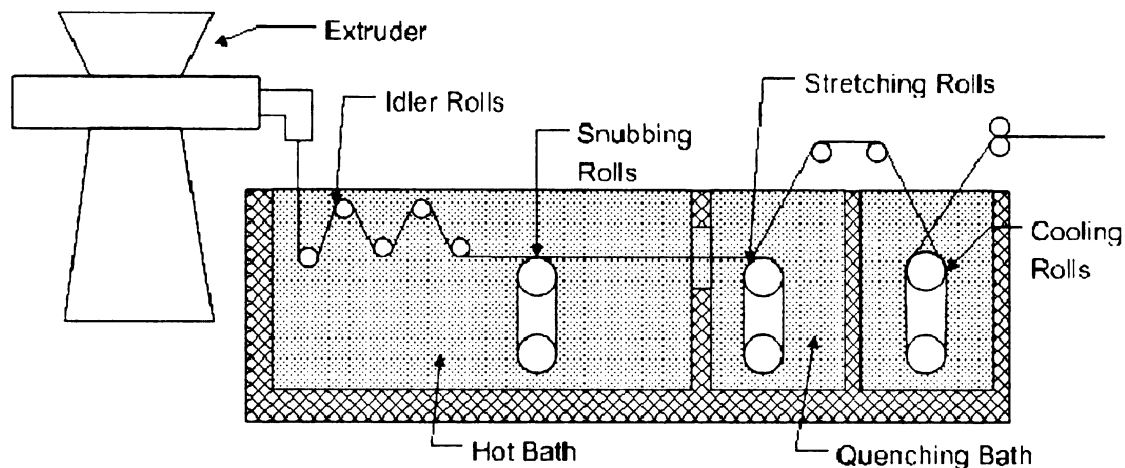


Figure I-1. Typical process for fiber stretching. Extruded fibers pass over rollers that turn at controlled, increasing speeds. This difference in roller speed induces strain, and therefore alignment, in the fiber spinning direction.

In addition to a simple increase in tensile modulus or ultimate tensile strength, chain alignment by hot-stretching has been shown to increase the material's strain-to-failure. At low draw ratios, this is manifested as an incremental increase in the strain-to-failure, while still fracturing by the brittle mechanism that is expected for amorphous polymers below their T_g . At higher draw ratios, a change is typically seen in the failure mechanism as the sample begins to exhibit ductile fracture behavior. The stress-strain curves for PS 393 kD are shown in Figure I-2 for samples processed to a number of hot draw ratios. Ductile failure initiates after a maximum in the stress-strain curve after which the sample cross-section decreases locally, creating a "neck" in the sample which propagates along the sample in the stretch direction as plastic deformation proceeds.

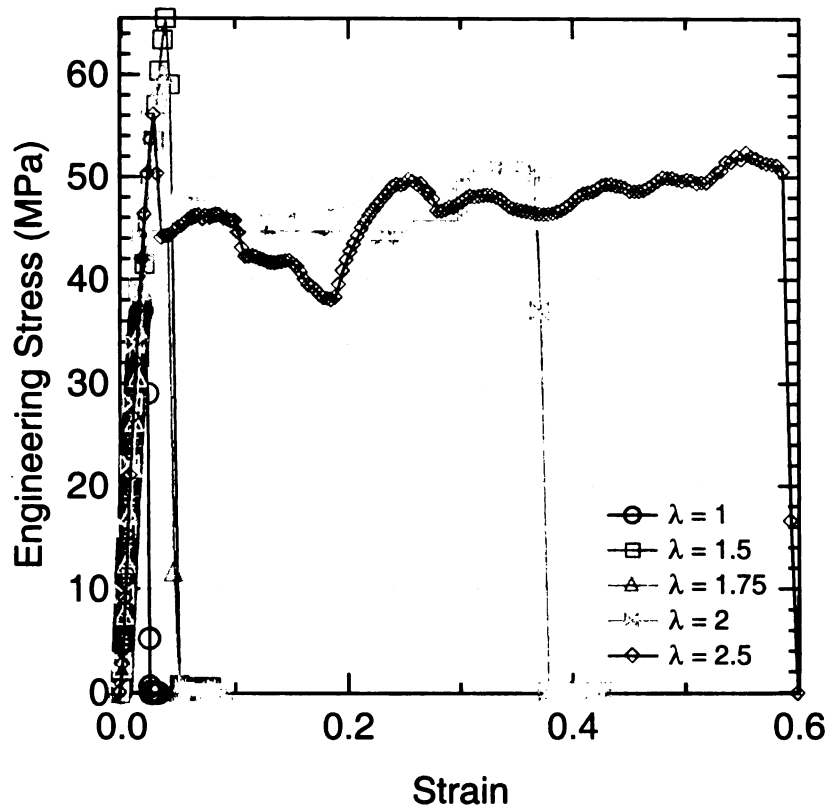


Figure I-2. The room temperature stress-strain curves of unfilled PS 393 kD drawn in tension at five hot draw ratios. PS processed to a hot draw ratio of 2 or greater exhibits ductile failure where a less oriented specimen fails by a brittle process.

The origin of ductility and necking – a schematic illustration of the morphological changes and corresponding stress-strain response is depicted in Figure I-3 – in aligned samples is attributed to an increase in the ability of the sample to distribute stress along the length of the sample.^{36, 37} Whereas an isotropic sample concentrates stress at sample flaws or cross-sectional area minima, a sample with axial orientation can distribute stress along the polymer chain backbone which is aligned in the stress direction. This more even distribution of stress means that regions of the sample with sufficient local freedom to deform can do so, relieving stress from those regions without sufficient mobility to deform without fracturing.

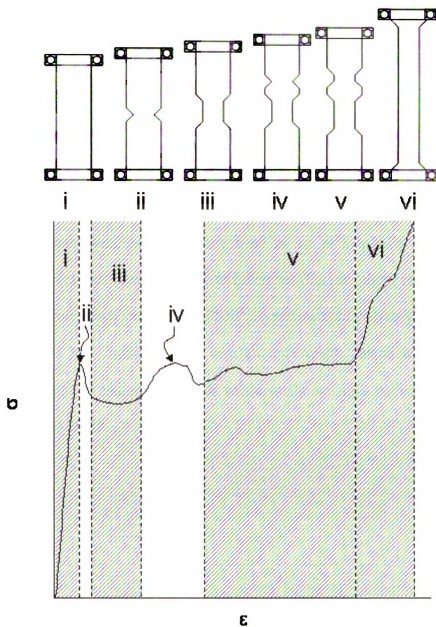


Figure I-3. Schematic depiction of a typical necking process. Regions i and vi are regions of primarily elastic deformation, while regions ii, iii, iv, and v are regions of primarily plastic deformation. The initiation of a necked region (ii and iv) and the propagation of those regions (iii and v) are demonstrated by a series of plateaus in the engineering stress.

I.E. Objectives

In the present work, blends of linear polystyrene with four primary types of nanoparticles are investigated. The blends are investigated in their equilibrium state by DSC and PVT. The tensile properties of the blends are also measured in both their equilibrium state and in their non-equilibrium state following chain alignment by uniaxial hot drawing. In some cases, the conformation of the polymer chain following this alignment process is evaluated by small angle neutron scattering. Cross-linked polystyrene nanoparticles (PSNP) are used as an enthalpically simple system with moderate particle stiffness. Buckminsterfullerenes (C_{60}) are rigid, high modulus particles with a size scale much smaller than PSNP. Hyperbranched polyethylene macromolecules (PELP) are a low modulus filler with an unfavorable interaction with PS. Finally, pyridine stabilized cadmium selenide nanocrystals are rigid particles with a size scale comparable to PSNP.

1
s
c
th
sy

Chapter II: The effect of intramolecularly cross-linked polystyrene nanoparticles on the thermal and mechanical properties of linear polystyrene.

II.A. Introduction

A key factor in any study of composites is the enthalpic interaction between the host matrix and the filler particle. In the case of traditional composites with macroscopic fillers this interaction is largely responsible for the filler-matrix bonding that dictates how well stress will be transferred across the interface. Poor interaction leads to poor stress transfer, weakening the material. The issue of chemical compatibility becomes even more important as the filler size is reduced, increasing the interfacial area and decreasing the interparticle gap at equivalent volume fraction as well as increasing the particle mobility. An unfavorable interaction will cause the filler and matrix to phase separate, leading to an inhomogeneous dispersion and the reduction of mechanical properties. In addition to the thermodynamics, the average interparticle gap is important to any analysis of a system filled with nanometer-scale particulates since small gaps can lead to depletion flocculation. The gap, $2h$, is given by the equation

$$\text{Eq. 2} \quad h/a = (\varphi_m/\varphi)^{1/3} - 1$$

and depends on the particle radius, a , the particle volume fraction, φ , and the maximum packing fraction for the particle geometry, φ_m .

The unfavorable interaction state is often ameliorated by chemically attaching a species that interacts favorably with the matrix to the exterior of the filler particle. In the case of polymer nanocomposites, the stabilizing species is often an oligomeric chain of the matrix polymer. This strategy is often successful for enhancing the stability of the system but, in addition to adding a synthetic obstacle, this strategy complicates analysis

by introducing a third, often ill-defined phase. Furthermore, the stabilizing ligand generally does not possess the desired reinforcing character of the filler particle, thereby acting against the desired effect of composite formulation.

One way to circumvent the practical difficulties of ligand stabilization is to synthesize a nanoparticle that is itself chemically similar to the matrix polymer. Harth *et al.*³⁸ demonstrated a method for preparing cross-linked nanoparticles with well defined sizes that are chemically similar to polystyrene (PS). This is accomplished by producing a random copolymer of styrene with benzocyclobutene (BCB). The butyl group on the BCB moiety can be thermally activated for potential cross-linking, leading it to bond with a similarly activated group located elsewhere on the same chain. By activating the reaction under ultra-dilute conditions it can be assured that each copolymer chain will cross-link only with itself, producing an intramolecularly cross-linked nanoparticle that has a well-defined size and is chemically similar to polystyrene. The degree of cross-linking, and therefore the extent to which the macromolecule behaves in a manner more consistent with a particle than a Gaussian chain, is controlled by the relative proportion of BCB to styrene. While the ideal reaction cross-linking reaction is one in which two identical cross-linking groups bond with one another, this is not the only possible outcome. The activated cross-linking moiety may also capture a styrene backbone hydrogen and bind at this newly activated site along the backbone. While this does not functionally change the resulting product – an intramolecularly cross-linked structure is created in either case – it should be noted that the structure may vary from the idealized scheme, a representation of which is shown in Figure II-1.

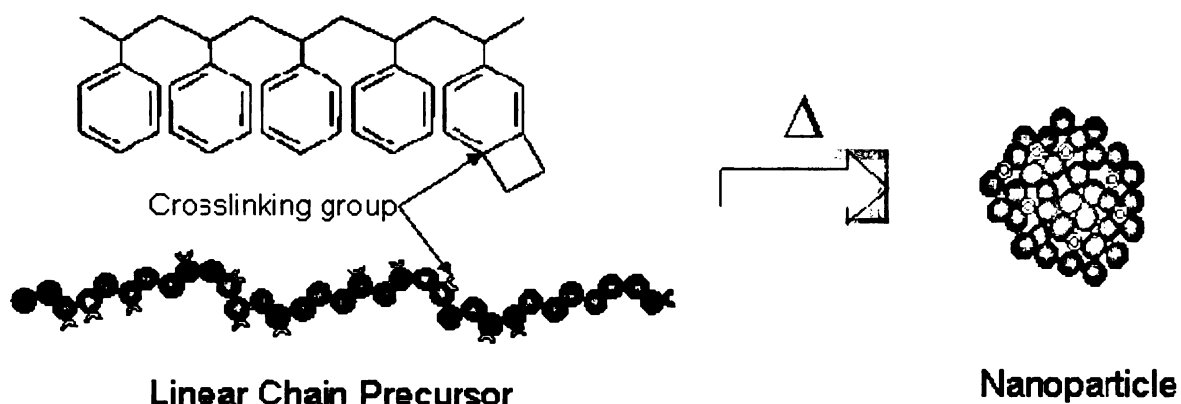


Figure II-1. Cross-linked polystyrene nanoparticles are synthesized from a random copolymer of styrene and benzocyclobutene (BCB). When thermally activated, the BCB groups bond with one another to form an intramolecularly cross-linked particle.

In the present study, the nature of the polymer-particle interaction is studied by equilibrium DSC and PVT measurements. These complimentary techniques are used to elucidate the system mobility and the introduction of free volume to the system by PSNP addition.

The addition of the polystyrene nanoparticles (PSNP) to linear PS has been shown previously³⁹⁻⁴² to decrease the viscosity of the melt, aiding processing. Evidence that these particles don't diminish the mechanical performance of the polymer, or that they even improve it, would lend additional credence to the application of these particles as processing aids. To this end, the solid-state mechanical properties of the PS/PSNP blends in tension are also examined. Specifically, a hot drawing scheme that approximates an industrial fiber spinning process is used to understand how the PSNP influences the non-equilibrium alignment of PS chains.

II.B. Experimental

Polystyrene standards were purchased from Scientific Polymer Products (Ontario, NY). Intramolecularly cross-linked polystyrene nanoparticles were synthesized according

to the process described by Harth *et al.*⁹ The particles contained potentially cross-linking benzocyclobutane (BCB) groups randomly distributed along the chain in a ratio of 4 styrene monomers: 1 BCB. Particle molecular weight values and distributions were measured by an HPLC system with a Wyatt Technologies (Santa Barbara, CA) DAWN EOS static light scattering detector, and an Optilab Rex refractive index detector. Samples for HPLC were prepared in tetrahydrofuran and filtered through 0.02 μm filters prior to characterization.

Table II-1: Molecular weights and distributions of linear polystyrene and intramolecularly cross-linked polystyrene nanoparticles

Sample Name	M_w (g/mol)	M_n (g/mol)	PDI	R_g (nm)*
PS	393,400	339,140	1.16	17.3
PSNP 41kD	42,520	41,090	1.04	2.5
PSNP 78 kD	89,020	77,830	1.14	3.1
PSNP 211 kD	278,400	211,200	1.32	4.3

* R_g for the linear polymer is based on molecular weight of PS. Radii for particles are based on the bulk density of PS

Linear polymer/nanoparticle blends were made by dissolving both the linear polymer and nanoparticle in a mutual solvent, toluene. The solution was then dripped into a mutual non-solvent, methanol, where the polymer and nanoparticles rapidly precipitated, forming an intimately mixed, homogeneous dispersion of nanoparticles in the linear polymer.⁴³ After removing the majority of the liquid from the sample by decanting and vacuum filtration with copious methanol rinsing, the blend was dried for a week in an oven at 50 °C and under rough vacuum.

Differential scanning calorimetry measurements were conducted using a TA Instruments (New Castle, DE) Q-1000. The instrument was fully calibrated using indium and sapphire standards. All tests were conducted using the modulated DSC (MDSC)

o
A
(
C
s
s
c
o
b
v
sp
M
vo
det

heat-only test type with a modulation period of 40 s and an overall heating rate of 5 °C min⁻¹ under a nitrogen atmosphere. Each sample was heated three times to erase the thermal effects of processing and measurements were taken from the third heating. The glass transition temperature is reported as the inflection of the step change in reversible heat flow as a function of temperature. The onset and offset points of the transition are indicated in the figure as bars above and below the point.

Pressure-Volume-Temperature measurements were conducted using a Gnomix (Boulder, CO) bellows type PVT apparatus.⁴⁴ This automated, programmable instrument was used to measure the change in specific volume to within 0.0001 cm³ g⁻¹ as a function of pressure and temperature in an operating range of 10-200 MPa and ambient to 400 °C. A hydrostatic pressure is achieved by immersing the sample in an inert confining fluid (mercury), which is contained in a steel sample cell at one end of which is a steel bellows of known cross-sectional area. The sample is prevented from adhering to the side of the sample cell – which would result in only a quasi-hydrostatic pressure – by placing the sample in a flexible Nickel foil cup. Expansion of the sample, confining fluid, and sample cup are translated to the bellows, which deforms linearly, allowing quantitative observation of the change in sample volume as a function of pressure and temperature in both the solid and melt states. The measured quantity is the change in sample specific volume, ΔV . The actual specific volume, V , is the sum of the measured ΔV and the specific volume at the initial test condition, V_0 . Because the minimum test pressure is 10 MPa, an extrapolation of ΔV to zero pressure was used to ascertain the true specific volume under ambient conditions. The sample specific volume at zero pressure was determined based on the buoyancy of the sample in water, according to a procedure

C

S

P

n

P

fr

er

Th

un

be

Re

car

trn

sub

adapted from ASTM D792. Prior to data collection, the sample was allowed to anneal within the PVT cell for one hour at 150 °C to ensure that all measured properties were equilibrium properties, and not influenced by processing conditions. Data were collected using isothermal run cycles from 10 to 200 MPa and distributed at 10 °C increments from 30 °C to 200 °C; isothermal run cycles were used to prevent sample degradation at high test temperatures from influencing subsequent runs.

Samples for PVT analysis were made by compression molding 200 – 400 mg cylinders under vacuum to ensure that air was not incorporated into the sample. All samples were annealed at 180 °C under no pressure for an hour or more to ensure that polymer chains had sufficient time to relax and equilibrate prior to testing. A sufficient number of cylinders were pressed to make the total sample size 1 g, the standard size for PVT measurement.

Samples for mechanical testing were prepared by compression molding a void-free pellet under vacuum. All samples were annealed at 180 °C for one hour or more to ensure that polymer chains had sufficient time to relax prior to the next processing step. Thin (*ca.* 0.3 mm) sheets were made by pressing the pellet in a sheet press at 160 °C under a load of *ca.* 1 ton. Sheet thickness was dictated by placing steel shim stock between the press plates. Sheets were annealed after pressing at 160 °C for two hours. Rectangular strips were cut from the subsequent sheet using a razor blade with the sample carefully positioned on a hard cutting surface to prevent any torsional stresses during trimming. Dog bone shaped specimens were avoided, as they would unduly complicate subsequent processing.

to
c
t
l
t
n
s
th
f
R
w
co
str
pro
fro
to

Uniaxial processing was conducted using TA Instruments (New Castle, DE) RSA 3. Rectangular samples were affixed to the rectangular film sample geometry and heated to the processing temperature (115 °C, *ca.* $T_g + 10$ °C) and allowed to equilibrate for 8 min. After heating, the gap was increased to take up slack in the sample caused by thermal expansion of the tool and sample. The sample was then subjected to a constant Hencky strain rate of 0.1 s^{-1} ($\epsilon_H = L^{-1} (dL/dt)$). The draw ratio ($\lambda = L/L_0$) was predetermined by setting the sample deformation time. Once the deformation was complete the sample was cooled using the instrument's forced air environmental control unit followed by exposure to ambient lab air. Cooling to below T_g generally occurred in less than 15 s, with cooling to ambient temperature happening within 3 min. During this time, the grips were held in place to prevent gross chain retraction. Samples were removed from the instrument and measured to determine the minimum deformed cross-sectional area. While the deformation surfaces were not uniformly parallel, a region in the midsection of the sample usually had parallel surfaces, and this was the region used for subsequent tensile testing.

Mechanical testing was carried out using a TA Instruments (New Castle, DE) RSA 3 at ambient conditions and a constant Hencky strain rate of 0.01 s^{-1} . Strain values were corrected for the measured compliance of the instrument and Young's modulus was computed from the slope of the low strain linear region of the stress-strain curve. Many stress-strain curves exhibit a toe region at low strains that is not indicative of any material property, rather it is due to the take-up of sample slack at the test start. This deviation from zero strain is corrected by extrapolating the linear portion of the stress-strain curve to zero stress and setting this point as the strain origin. Tensile Energy to Break was

computed as the numerical integral of the stress-strain curve from the corrected strain origin to the breaking strain. All mechanical properties are computed as the average of three to five samples with error bars indicating the standard error between measurements.

II.C. Results and Discussion

II.C.1. Equilibrium Thermal Analysis

The glass transition temperature (T_g) is an indicator of polymer chain mobility in amorphous polymers. More mobile chains require less thermal energy to initiate the Brownian motion of 20 to 50 carbon atoms that is characteristic of a material above its T_g .²⁴ This transition is sensitive to the polymer's chemical structure and molecular weight, as well as the environment in which it is located. Studies have shown that placing a polymer in a thin film, pore, or other confined geometry alters its conformation sufficiently to change the T_g .²⁵⁻²⁷ One possible route to increase chain mobility is an increase of free volume. As obstacles to motion are reduced, especially by the introduction of unoccupied area (free volume), the thermal energy needed to initiate free motion of the amorphous chains is decreased, leading to a reduction in the glass transition temperature.

The effect of three PSNP sizes on the glass transition temperature (T_g) of polystyrene is shown as a function of particle volume fraction in (Figure II-2). In all three cases the T_g is decreased by nanoparticle addition at low (1%) loadings. At higher loadings the glass transition temperature increases, eventually surpassing that of the neat polymer. The glass transition temperatures of the PSNP particles themselves are 15 to 20 °C greater than polystyrene. A general, rule of mixtures, approach to the T_g of the polymer-particle blend would suggest that the glass transition temperature of the blends

F
re
sy
in
tr

Th

2 =

cor

file

should increase in a linear fashion between the T_g of polystyrene and the T_g of the pure particles as a function of the volume fraction, ϕ , of the particle.

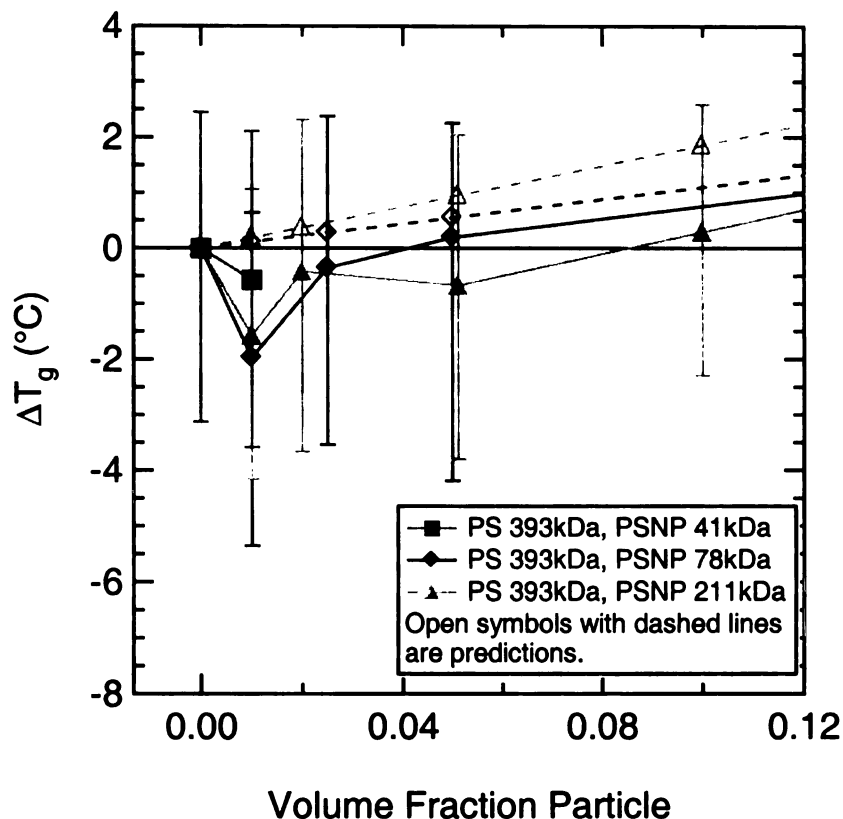


Figure II-2. Change in glass transition with addition of PSNP. At low loadings the T_g is reduced, contrary to the prediction based on relative weight fraction (indicated by open symbols and dashed lines), suggesting additional molecular mobility at the particle interface. Error bars indicate the initiation and completion temperatures of the glass transition process.

$$\text{Eq. 3} \quad T_g(\phi) = (1 - \phi) \times T_g(\phi=0) + \phi \times T_g(\phi=1)$$

This expected behavior is shown in the figure for comparison.

In this enthalpically simple case of PSNP in PS the T_g decreases slightly (*ca.* 2 °C) at 1v% loading, then increases as the loading increases. While the samples are confined ($h < R_g$) even at 1v%, the interparticle half-gap is greater than the radius of the filler particle ($h > a$). At loadings for which the T_g increases to PS's unfilled value, the

interparticle half-gap has been reduced to be less than the nanoparticle radius ($h < a$), suggesting that a rogue nanoparticle would be hindered in its attempt to diffuse freely through the polymer/nanoparticle medium. Previous measurements⁴⁵ of the diffusivity of nanometer-sized CdSe nanocrystals have shown the nanoparticles to diffuse anomalously fast. If particle diffusion plays a significant role in the overall mobility of the system, then this critical “jamming,” which occurs at $\phi \geq 8\%$, would understandably contribute to a reduction of system mobility and an increase in T_g when $h < a$. While this condition serves as a helpful benchmark, interparticle interference to diffusion may become operable at loadings even less than that.

The DSC traces of the individual species and blends of the two also shed light on the quality of dispersion. Figure II-3 shows the DSC traces of PS 393 kD, PSNP 78 kD, and a blend of 5% PSNP 78 kD in PS 393 kD. The step change in the reversible heat flow that is indicative of the glass transition is clearly visible for all three samples between 100 and 135 °C. The step change of the PSNP trace is more broad, and an endothermic melting peak is seen near 20 °C. The trace for the PS-PSNP blend shows a single T_g and no apparent melting peaks, suggesting phase stability. Phase separated samples, on the other hand, often show the distinct features of the constituent species. While the DSC trace is not a guarantee of phase behavior,⁴⁶ it is a good indicator.

F

in

sp

m

In

th

str

an

obs

beh

How

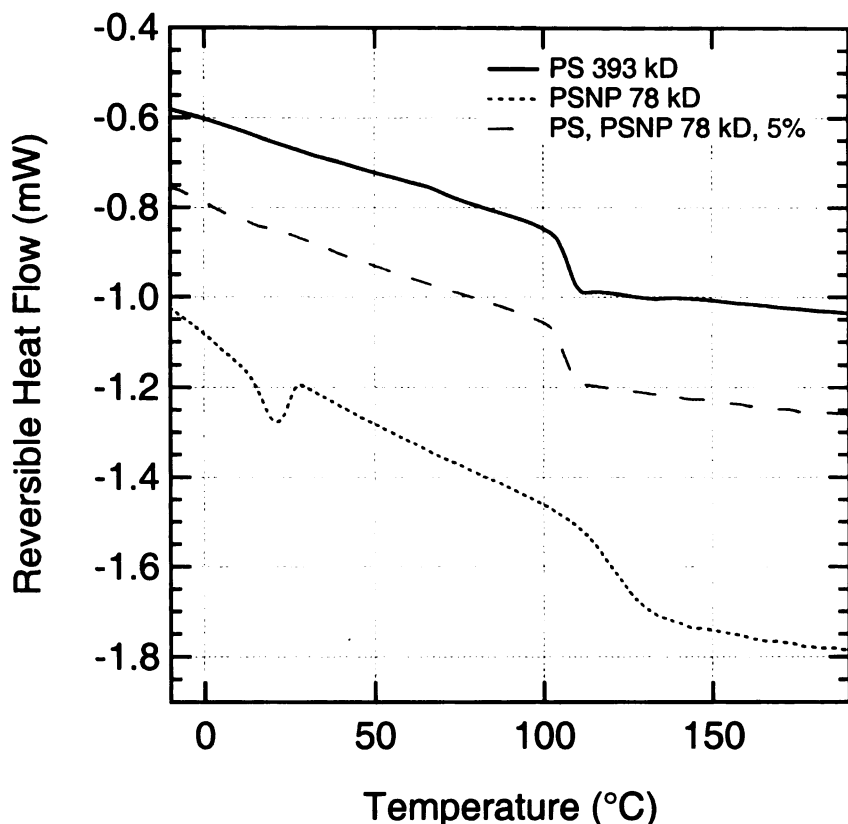


Figure II-3. DSC traces for PS, PSNP 78 kD, and a 5% blend of PSNP 78 kD in PS.

The overall compressibility of the system and its volumetric response to changes in temperature and pressure are sensitive to internal structure and the presence of void space. Engineering properties of interest that can be derived from PVT data are the bulk modulus, $K = -V(\partial P/\partial V)_T$, and the coefficient of thermal expansion,⁴⁷ $\alpha = V^{-1}(\partial V/\partial T)_P$. In the case of the bulk modulus, changes brought about by particle addition result from the interplay of two competing factors. Due to their intramolecularly cross-linked structure, the PSNP are expected to have a bulk modulus greater than that of the analogous linear polymer. This tendency toward more rigid, solid-like behavior has been observed through the elevated T_g of the particle compared to PS and through their flow behavior,⁴⁸ exhibiting a yield stress rather than acting as a simple viscoelastic fluid. However, the presence of free volume at the particle surface in the blend, as suggested by

v
s
E
i
n

K
(c)

Fig
lin
slig
un
mo
of t
me
in E

am

the reduction of T_g , simultaneously reduces the bulk modulus of the nanocomposite. In the case of PSNP 78kD in PS it appears that these two factors are well-balanced, resulting in a modest reduction in K_0 , the bulk modulus extrapolated to zero pressure, at 200 °C (Figure II-4). In fact, while PVT measurements are only strictly valid in the melt state, where pressure is uniformly hydrostatic, similar trends are also observed for the solid state bulk modulus, measured at 50 °C (Figure II-4a). The reduction of the bulk modulus provides strong evidence in support of an increase in free volume caused by PSNP incorporation; if there were no additional free volume introduced, K_0 would certainly be increased by the addition of these semi-rigid macromolecules (Figure II-4b).

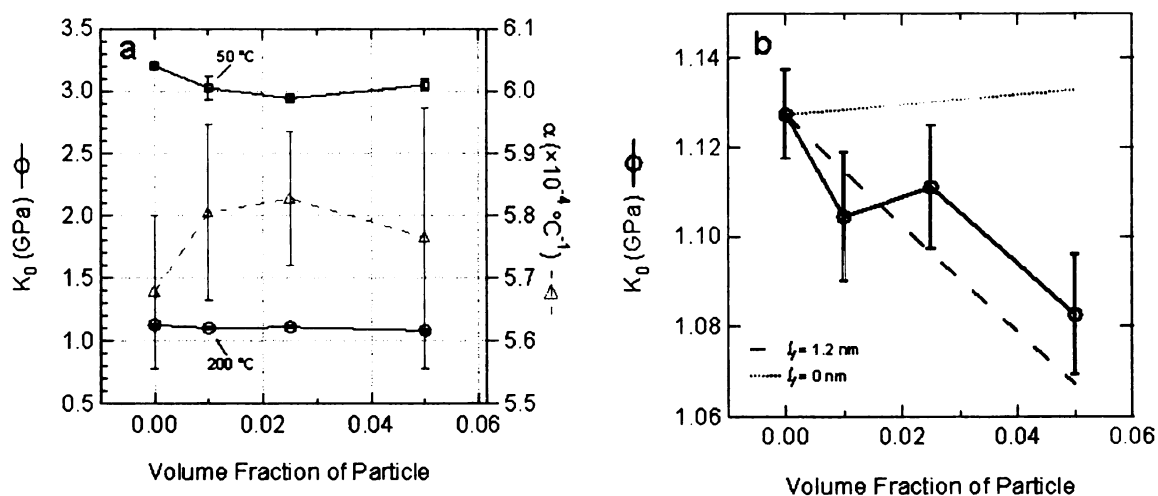


Figure II-4. Bulk modulus and thermal expansivity of a PS with PSNP 78 kD. The cross-linked particles tend to decrease the bulk modulus and increase the thermal expansivity slightly (a). These two effects are suggestive of the introduction of a small region of unoccupied volume around the surface of the fillers. Similar trends are seen in the bulk modulus both above (200 °C) and below (50 °C) the glass transition temperature. Prediction of the bulk modulus with a free volume layer of 1.2 nm provides a satisfactory fit to the measured bulk modulus at 200 °C (b). The prediction for no free volume is for an increase in K_0 , which is not observed.

If an estimate of the bulk modulus for the nanoparticles is assumed, a relative amount of free volume present in the sample can be computed based on a volumetric

average of the moduli of the three components: the continuous PS (c), particulate PSNP (p), and free volume (f).

$$\text{Eq. 4} \quad 1 = \varphi_c + \varphi_p + \varphi_f$$

$$\text{Eq. 5} \quad K_0 = \varphi_p K_{0,p} + \varphi_c K_{0,c}$$

The known bulk modulus of the composite, K_0 , and the nominal volume fraction of filler, $\varphi_{n,p}$, can be used to calculate the free volume fraction.

$$\text{Eq. 6} \quad \varphi_{n,p} = V_p / (V_p + V_c)$$

$$\text{Eq. 7} \quad \varphi_f = 1 - K_0 [(1 - \varphi_{n,p}) K_{0,c} + \varphi_{n,p} K_{0,p}]^{-1}$$

If one assumes that the free volume is concentrated in an even layer around the particle, with a radius a , the free volume layer thickness, l_f , can also be calculated.

$$\text{Eq. 8} \quad l_f = a [(((\varphi_p + \varphi_f) \varphi_p^2)^{1/3} / \varphi_p) - 1]$$

It is likely that the presence of cross-linking increases the bulk modulus of the particle beyond that of simple PS, so the pure polymer's bulk modulus of 1.13 GPa is used as a lower bound on the bulk modulus of PSNP. One might estimate that the modulus scales as the coordination number. Monomers of the unfilled polymer have an average coordination number of 2, while the monomers of the cross-linked particle have an average coordination number of 2.2, based on 20% of the monomers having a nominal coordination number of 3. This leads to a scaled estimate of the particles bulk modulus of 1.24 GPa which serves as a conservative upper-bound. Based on these values, the average thickness of the excluded volume shell (Figure II-5) around each particle is between 0.65 and 1.8 nm. Volumetric estimates of the bulk modulus based on a PSNP bulk modulus of 1.24 GPa and free volume layer thickness of 1.2 nm lie within the experimental error of the bulk modulus measurements of the PS-PSNP blends (Figure

II-4b). A similar free volume size can be calculated from the solid state bulk modulus and values of this calculation are tabulated in Appendix A.

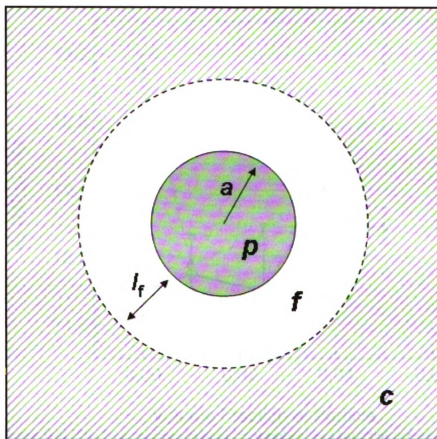


Figure II-5. Schematic representation of a particle (p) surrounded by a layer of free volume (f) within a continuous matrix phase (c). The particle has a radius, a , and the free volume region has a thickness, l_f .

The calculation of increased free volume according to the bulk modulus is supported by the observed increase in the thermal expansivity (Figure II-4a), which has been attributed to an increase in the overall free volume of a sample.⁴⁹⁻⁵²

In addition to the value of bulk modulus at zero pressure, it is instructive to measure the slope of the bulk modulus as a function of pressure close to zero pressure, K_1 (Figure II-6). For PSNP 78kD in PS 393kD at low loading (1% to 2.5%) the value of K_1

appears to change little compared to the unfilled polymer. However, at a volume fraction of 5% the value of K_1 increases by *ca.* 10%.

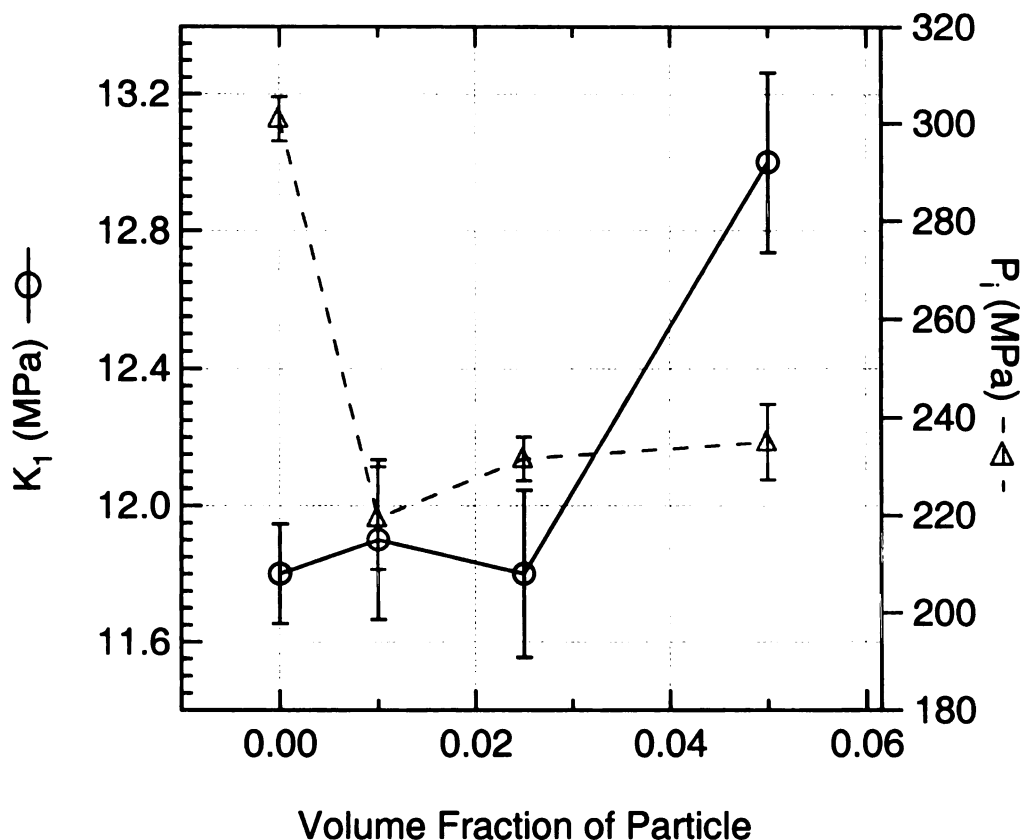


Figure II-6. The free volume asymmetry number, and internal pressure as function of PSNP 78kD volume fraction in PS 393kD. The free volume asymmetry number is increased with nanoparticle addition, suggesting an increased energetic penalty to compression as compared to dilation. The internal pressure is decreased by particle addition, consistent with a decrease in the strength of intermolecular interactions.

The quantity, K_1 , is related to the shape of the free energy minimum and is referred to as the free energy anharmonicity.⁵³ A K_1 value of five is equivalent to a harmonic potential, for which compression and dilation are equally favorable processes. However, intuition and experience suggest that K_1 is generally greater than five, consistent with a material for which dilation is favored relative to compression. Typical K_1 values for polymeric materials are 11.0 ± 1.5 .⁵³ It has been shown through the

reduction of T_g and K_0 that the addition of PSNP introduces a driving force towards free-volume expansion within the nanocomposite. This driving force is also manifested in an increase in the free-volume anharmonicity, K_1 , as the system becomes increasingly biased towards dilation over compression. The shape for of the dimensionless free-energy as a function of relative density is shown in Figure II-7 for three value of K_1 , the harmonic potential, and the values for unfilled PS and PS filled with 5% PSNP 78 kD. The free energy contour illustrates the increasing bias towards dilation compared to compression.

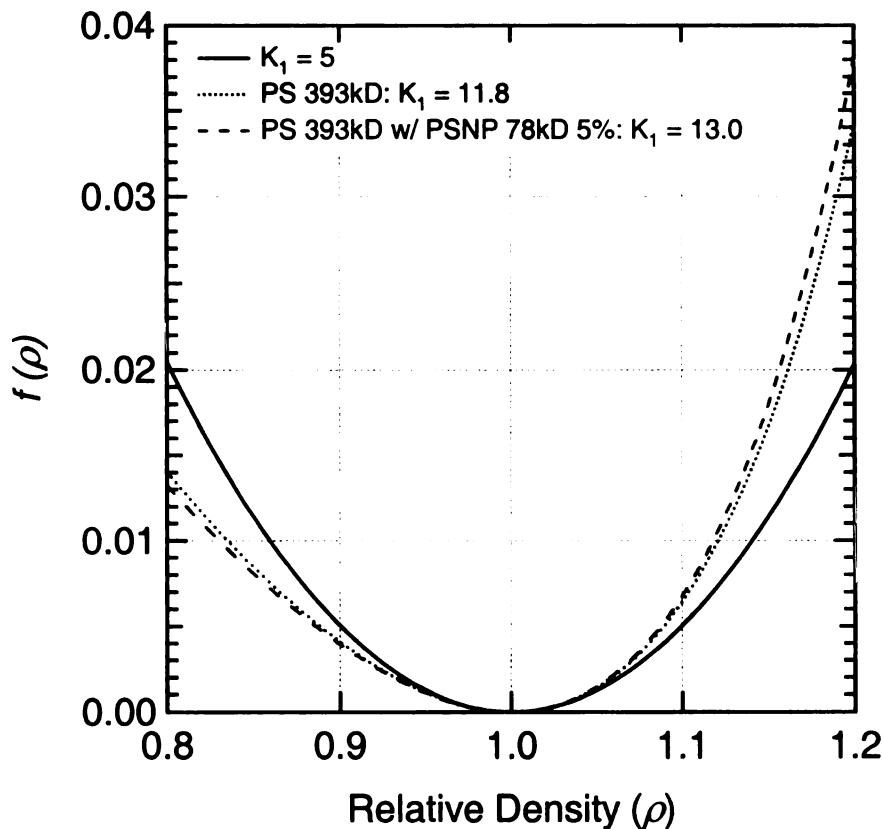


Figure II-7. The dimensionless free energy as a function of relative density. The anharmonic potential shows an equivalent free energy change for compression or dilation. The addition of PSNP 78kD is seen to exacerbate the asymmetry of the free energy profile, with dilation being energetically favored over compression.

In addition to the shape of the free energy well, the sensitivity of internal energy to volumetric changes can be calculated from PVT data. This sensitivity is defined as the

internal pressure, P_i .⁵⁴ The internal pressure is not a direct measure of the magnitude of intermolecular interaction energy, but rather a measure of the response of this energy to a change in volume.⁵² The direct measure of the interaction energy between molecules is the Cohesive Energy Density (CED) which is defined⁵⁵ as

$$\text{Eq. 9} \quad \text{CED} = U/V$$

In the past, the difference between CED and P_i has sometimes been wrongly neglected and values of P_i have been used for CED. While not strictly correct, it was shown by Hildebrand *et al.*⁵⁶ that the ratio, n , of P_i to CED is approximately one for low molecular weight liquids. In further analysis Sauer and Dee⁵⁵ showed for a number of polymeric materials that n is between 0.88 and 1.35.

The internal pressure is strictly defined as the response of the internal energy to a change in volume:

$$\text{Eq. 10} \quad P_i \equiv (\partial U / \partial V)_T$$

$$\text{Eq. 11} \quad P_i = T (\partial S / \partial V)_T - P$$

The internal pressure can also be written as the difference between the thermal pressure ($T\alpha K$) and the system pressure (P).

$$\text{Eq. 12} \quad P_i = T\alpha K - P$$

As free volume is increased in a system, additional regions are introduced for stress relief in the event of a change in volume. This diminishes the system's energetic response to changes in volume, and therefore reduces P_i . This effect is observed for the PS-PSNP 78kD system. Similar to the change in T_g , at extremely low loadings (1%) the mobility of the system is maximized, reflected by a nearly 30% decrease in P_i . Much like the trend seen in T_g , this reduction becomes less drastic at higher particle loadings, increasing

slightly compared to the 1% blend. This confirms the notion that optimum mobility enhancement occurs at very low particle loadings for which free volume introduction dominates, prior to particle crowding effects becoming more significant.

II.C.2.Non-Equilibrium Tensile Behavior

The observed increase of free volume with PSNP addition has consequences for the tensile behavior of the nanocomposite material. The presence of nanometer sized voids that increase polymer mobility in a material encourages plasticization of the matrix.^{51, 57, 58} The even distribution of stress across the sample may prevent the stress concentration at a specific larger flaw that otherwise leads to stress concentration and failure.^{59, 60} This increase in ductility may manifest itself as an incremental change in the strain-to-failure, ϵ_f , or it may result in a shift in the failure mechanism. In concert with the stress distribution brought about by the small, homogeneous regions of low density (free volume), alignment of the matrix polymer has been shown to promote stress propagation in the direction of orientation. In its unprocessed state, unfilled PS 393kD fails by the low-strain brittle mechanism that is typical for amorphous polymer below their T_g . When sufficiently oriented ($\lambda=2$ for the processing conditions of the current study) by a hot drawing process, PS undergoes ductile failure characterized by neck formation and failure at higher strain values.

Studying the solid state stress-strain curves of the nanocomposites reveals that blends of PS with the two larger PSNP types fail by the ductile mechanism at a lower draw ratio ($\lambda=1.75$) than the unfilled system (Figure II-8). While stress-strain curves are only shown for 1% loading, PSNP 78kD and PSNP 211kD also exhibit ductile failure at $\lambda=1.75$ for 5% loading. The transition to ductility occurs when the stress to flow initiation

is less than the stress to failure. This shift may be due to an increase in alignment, the added stress distribution facilitated by the particle-induced free volume increase, or a combination of the two.

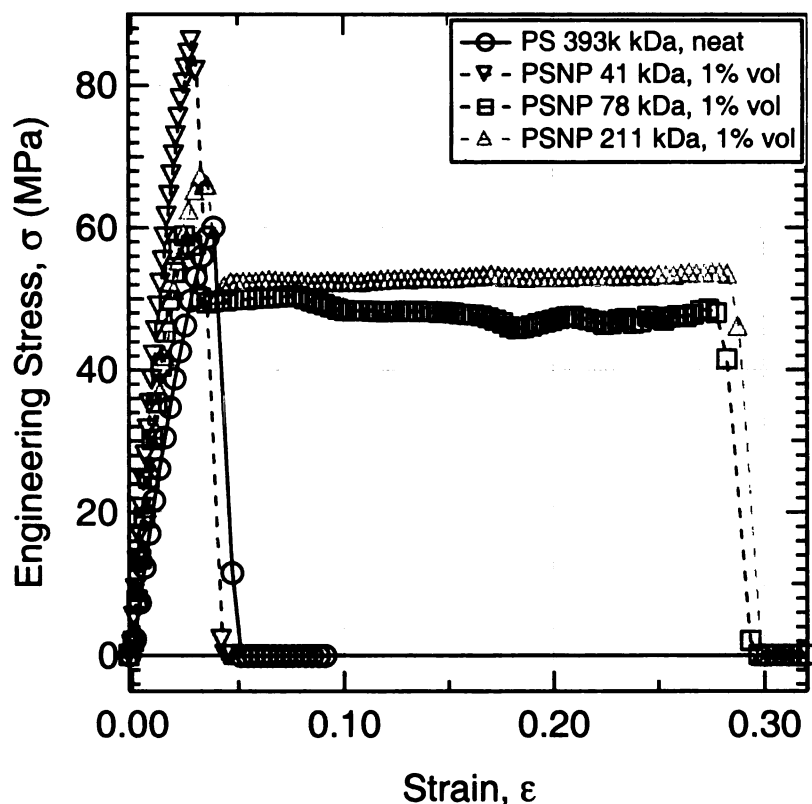


Figure II-8. Stress-strain curves for unfilled polystyrene and polystyrene filled with three different PSNP types, each processed to a hot draw ratio of 1.75. The two larger PSNP species induce ductile failure under conditions for which the unfilled polymer and the polymer filled with PSNP 41 kD fail by a brittle mechanism at low strains.

In addition to the shift in fracture mechanism to increase ductility, ϵ_f is increased for the particle blends at low to moderate draw ratios (Figure II-9b). From the stand-point of material design, this increase in ductility also increases the Tensile Energy to Break (TEB) (Figure II-9d). This is an attractive benefit for the design of safety devices that need to effectively dissipate energy before failure. The increases in toughness and

ductility are primarily applicable for low to moderate ($\lambda < 5$) draw ratios. At higher draw ratios, the polymer chain is oriented to such a degree that stress is being applied more directly along the chain back-bone.^{34, 35} In this case, stress relief by increased mobility can do little to ameliorate the strain being applied directly to the rigid covalent bonds.

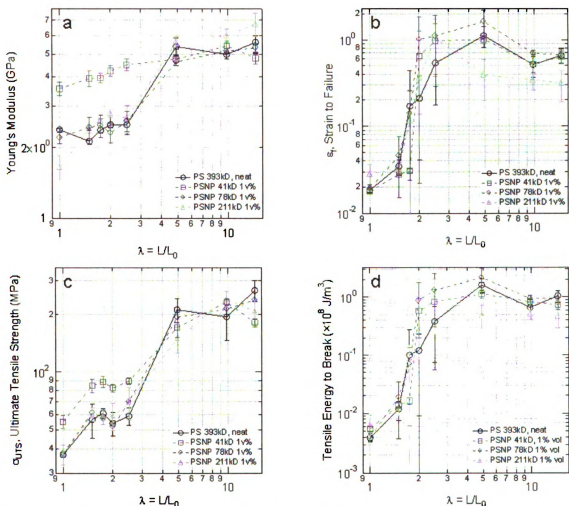


Figure II-9. The Young's Modulus (a), strain to failure (b), ultimate tensile strength (c), and tensile energy to break (d) of hot-drawn PS 393 kD with PSNP as a function of hot draw ratio. Larger PSNP species have very little effect on Young's Modulus or ultimate tensile strength, while smaller (41 kD) particles increase these properties for the unprocessed and slightly processed case. The ductility (b) is increased for all cases at low draw ratios and at all draw ratios for PSNP 78 kD, which gives rise to an increase in the material toughness (d).

Also, it should be noted that the most substantial increases in ductility occur for the 1% blend of PSNP 78kD in PS. The low loading, 1% blend was also shown by changes in T_g and P_i to be most effective at improving system mobility, a key factor in enhancing ductility. Higher loadings, which were previously associated with the development of interparticle interference effects, show a reduction in TEB relative to PSNP 78kD 1% (Appendix B).

It was suggested earlier that the increase in ductility may be due to either an increase in free volume or chain alignment. Choi, Spruiell, and White⁶¹⁻⁶³ studied the orientation development developed in PS by a hot drawing process and correlated the optical birefringence – a measure of monomer orientation – with tensile property changes. The authors found that of the tensile properties studied, ϵ_f is the most sensitive to chain orientation, but Young's modulus, E , and the ultimate tensile strength, σ_{UTS} are also dependent on orientation. In the case of PSNP 78kD and PSNP 211kD in PS, however, there is no discernible trend of either of these other properties (Figure II-9a, c) with PSNP inclusion. The absence of an observed increase in Young's modulus or ultimate tensile strength may indicate that no significant change is occurring to the chain orientation. However, the weaker dependence of E and σ_{UTS} on orientation demonstrated by Choi, Spruiell, and White, also suggests that the increase is more subtle than the resolution of measurement. From the present data, it is unclear whether changes in tensile behavior brought about by PSNP inclusion are due to increases in free volume or chain orientation.

It should also be noted that, while no specific increase is observed for E or σ_{UTS} , no significant decrease is observed either. Traditional plasticizers increase ductility at the

expense of reduced stiffness. This ability to increase ductility without reduction in E or σ_{UTS} shows that the nanoparticle inclusion may provide a more attractive route to ductility and toughness enhancement than traditional additives.

The exception to the trend of strict ductility enhancement is the blend of 1% PSNP 41kD in PS. This system shows moderate ductility increase relative to unfilled PS at low draw ratios and notable increases in strength and modulus at low draw ratios. Contrary to the previously described PSNP behavior, this is consistent with a view of enhanced orientation. However, the stiffness increase is not due solely to orientation development. The fact that E and σ_{UTS} are increased for even the undrawn ($\lambda=1$) sample shows that the PSNP 41kD imparts some inherent stiffness to the system. The deviation from the behavior observed for the larger particles may reflect a size dependence of the PS-PSNP interaction. The measured radius of the PSNP 47kD is 2.8 nm, which is less than twice the statistical segment length of polystyrene, 1.8 nm. This presents a challenge to polymer to efficiently pack in the vicinity of the particle. This is consistent with a view of free volume introduction around the periphery of the particle as suggested by the reduction of T_g (Figure II-2), but reflects the strained nature of the polymer near the particle.

The processing space for which most property enhancement has been demonstrated is for low to moderate draw ratios ($\lambda < 5$). These draw ratios are well below the extremely high elongations utilized in fiber spinning applications but these effects are, nonetheless, significant. Other polymer materials production processes lead to the moderate orientation of polymer chains. Injection molding is one such application for which there may be room to exploit the illustrated particulate enhancement effect.

Inje

cha

geon

cont

proc

if na

prod

nano

mobi

parti

inter

beha

modu

from

impor

size t

vicin

Injection molding, however, is often limited by a poor ability to carefully control the chain alignment, and the stresses often vary widely across a given part, based on the mold geometry. In biaxially oriented polystyrene, on the other hand, the stresses are well-controlled and uniform, but much lower than for fiber spinning. This manufacturing process could benefit from the reduced neat for processing to achieve similar results if nanoparticles similar to those utilized in the present work are incorporated into the production feedstock.

II.D. Conclusion

When added to linear polystyrene, intramolecularly cross-linked polystyrene nanoparticles are shown to increase free volume and mobility. The increase in polymer mobility is the greatest at low loadings, for which free volume has been introduced at the particle surface, but at sufficiently low loadings that particle-particle crowding does not interfere with overall system mobility. For larger particles, this leads to plasticizing behavior and tendency toward ductility, but it doesn't necessarily diminish Young's modulus. It is difficult to disambiguate the additional mobility caused by free volume from the plasticizing effect of orientation enhancement. The smaller particles reveal the importance of filler size in determining mechanical properties. The similarity of the filler size to the persistence length of the matrix polymer creates an obstacle to packing in the vicinity of the particle and a stiffening behavior.

Chapter III: A small-angle neutron scattering (SANS) study of the anisotropic conformation of linear polystyrene in the presence of intramolecularly cross-linked polystyrene nanoparticles

III.A. Introduction

Introducing global alignment to otherwise amorphous materials is known to increase their tensile strength in the direction of alignment. This has been demonstrated for linear polymers by introducing axial strain to a sample above its T_g , then quenching it well below T_g , locking the polymeric chains in their nonequilibrium anisotropic conformation. This process is representative of typical polymer processing methods that consist of fiber formation by either melt or gel spinning, followed by hot-stretching which is controlled by passage over rollers that move at progressively increasing speed. The process is completed by cooling the sample through immersion in a low temperature bath and optional cold-stretching below T_g (Figure I-1).

The effect of uniaxial processing strain on fiber properties has been studied for neat polystyrene under a number of processing conditions and the induced alignment has been observed by optical birefringence measurements^{64, 65} and small angle neutron scattering (SANS).⁶⁶ Optical birefringence was the first experimentally feasible method for evaluating the orientation of amorphous polymers. However, birefringence measurements often present a misleading understanding of the chain's orientation. In the case of polystyrene, it is the large, flat phenyl rings that dominate the optical character of the polymer. Consequently, an aligned chain has phenyl rings oriented perpendicular to the chain backbone, resulting in a negative birefringence. The alignment being probed, therefore, is that of the individual chain segments, rather than the entire chain.

Dominated, as these short segments are, by extremely short relaxation times they are not a good indicator of the overall orientation of the chain backbone, which has a total relaxation time orders of magnitude larger than the segmental relaxation time. Indeed, it is the long scale orientation that has been shown to be most important for determining the solid state mechanical properties of a polymer system.¹⁰

While a great deal of work has been conducted towards understanding the strain-induced alignment process, very little agreement exists regarding appropriate processing methods or parameters. So while general trends can be observed and confirmed or disputed, quantitative comparison is often impractical. A summary of some existing work and the disparate processing and evaluation methods employed is presented in Table III-1. Especially noteworthy is the inconsistency between definitions of the time dependence of the sample strain. While some groups have processed their material by imparting a constant strain rate, many researchers process their samples based on a constant cross-head speed, resulting in a strain rate that diminishes exponentially during the process. The latter method makes lesser demands on instrumentation, but convolutes the experimental conditions, as most material properties are rate, rather than speed, dependent. A constant-rate process is also more consistent with industrial application of the process than a constant-speed process.

Table III-1: Summary of previous work on alignment by hot drawing and their test parameters.

<i>First Author</i>	<i>Draw Temperature (°C)</i>	Drawing	Tensile Testing	
		<i>Draw Ratio</i>	<i>Initial Draw Rate (s⁻¹)</i>	<i>Initial Testing Rate (s⁻¹)</i>
Cleereman ³⁵	99 – 132	50% - 1200% ≤ 12000%	NS	NS
Cheatham ³⁴	145	†	NS	1.6×10 ⁻⁵ - 0.167
Ender ⁶⁷	115	NS	NS	NS
Picot ⁶⁴	110 – 130	≤ 4.5	0.18	NA
Tanabe ⁶⁸	197	NS	NS	0.0167*
Boue ⁶⁹	113 – 134	3	0.06 – 0.189	NA
Choi ^{61, 63}	110	1.6 - 2.5	0.0833	NA
Choi ^{61, 63}	120	3 - 7.2	0.0767	0.00328*
Ramzi ⁶⁵	134	1.2 - 3	NS	NA
Pellerin ⁷⁰	120	2	0.791*	NA
Bent ⁷¹	170	NA	.01-3.0	NA
Stendahl ³⁷	108	250%, 1000%	0.00654*	NS*
De Francesco ⁷²	105 - 130	2, 4, 6	0.0119*	10 ⁻⁴
Theodorou ⁷³	105	NS	0.00333*	NA
Yokouchi ⁷⁴	105	≤7, 5	NS	.0029 - 230
Dvoranek ⁷⁵	225 - 265	NS	NS	0.00242*
Han ⁷⁶	100 - 115	2 - 5	.0048-.0033*	NA
Embery ⁶⁶	113, 148	1 - 5	NS*	NA

*: Sample was deformed at a constant cross-head speed. The instantaneous strain rate was determined from the cross-head speed and the initial gauge length.

†: Draw ratio was determined by the change in the cross-sectional area

NS: Not clearly specified

NA: Not applicable, the specified process was not conducted

While the orientation of high aspect ratio nanoparticles for use as composite filler has been studied, little work has been conducted to understand the orientation of the surrounding matrix, especially in the case of fillers that have an aspect ratio approaching unity. Work has been conducted to quantify the equilibrium conformation of linear polymers surrounding spherical nanoparticles. It has been shown through previously described (I.C) simulations by Brown *et al.*²⁰ that polymer chains orient in layers perpendicular to the particle surface. Mackay *et al.*⁷⁷ have demonstrated that the presence of certain nanoparticles leads to an increase in the radius of gyration (R_g) of the matrix polymer. It is believed that this swelling behavior may make the linear polymer more susceptible to the strains that lead to orientation under uniaxial processing conditions.

A key factor in any study of composites, and especially a study of the matrix conformation, is the chemical (enthalpic) interaction between the matrix polymer and the filler species. In the case of traditional composites with macroscopic fillers this interaction is largely responsible for the filler-matrix bonding that dictates how well stress will be transferred across the interface. A poor interaction leads to poor stress transfer, which weakens the material. The issue of chemical compatibility becomes even more important as the filler size is reduced and the particles gain mobility within the system. An unfavorable interaction will cause the filler and matrix to phase separate, leading to an inhomogeneous dispersion and the generally negative effects on the mechanical properties.

The unfavorable interaction state is often ameliorated by chemically attaching a species that interacts favorably with the matrix to the exterior of the filler particle. In the case of polymer nanocomposites, the stabilizing species is often an oligomeric chain of

the matrix polymer. This strategy may be successful for enhancing the stability of the system but, in addition to adding a synthetic obstacle, this strategy complicates analysis by introducing a third, often ill-defined phase. Furthermore, the stabilizing ligand generally does not possess the desired reinforcing character of the filler particle, thereby acting against the desired effect of composite formulation.

One way to circumvent the analytical, as well as practical, difficulties of ligand stabilization is to synthesize a nanoparticle that is itself chemically similar to the matrix polymer. Harth *et al.*³⁸ demonstrated a method for preparing cross-linked nanoparticles with well defined sizes that are chemically similar to polystyrene. This is accomplished by producing a random copolymer of styrene with benzocyclobutene (BCB). The butyl group on the BCB moiety can be thermally activated for potential cross-linking, leading it to bond with a similarly activated group located elsewhere on the same chain. By activating the reaction under ultra-dilute conditions it can be assured that each copolymer chain will cross-link only with itself, producing an intramolecularly cross-linked nanoparticle that has a well-defined size and is chemically similar to polystyrene. The degree of cross-linking, and therefore the extent to which the macromolecule behaves in a manner more consistent with a particle than a Gaussian chain, is controlled by the relative proportion of BCB to styrene.

Small angle neutron scattering (SANS), allows characterization of a broader range of molecular length scales⁷⁸ than optical birefringence measurements. It is especially well-suited to evaluating macromolecular feature sizes, including the R_g of a polymer chain. The general equation for the scattered intensity, $(\partial\Sigma/\partial\Omega)$, as a function of wave

vector, q ($q = 4\pi/\lambda_n \sin(\Theta/2)$ where Θ is the scattering angle and λ_n is the neutron wavelength), is given by Eq. 13

$$\text{Eq. 13} \quad (\partial\Sigma/\partial\Omega)(q) = NV^2 (\Delta\rho)^2 P(q) S(q) + B$$

The incoherent background scattering is defined as B . The number fraction of scatterers, N , their individual volume, V , and the scattering length density contrast, $\Delta\rho$, are independent of wave vector and are often grouped together and referred to as the scale factor, or the intensity at zero wave vector, I_0 .

$$\text{Eq. 14} \quad I_0 = NV^2 (\Delta\rho)^2$$

Information about the size and shape of an individual scattering center is given by the form factor, $P(q)$, while the long range order of scatterers is defined by the structure factor, $S(q)$, both of which tend towards unity at low values of q . For very dilute, amorphous systems, the structure factor can be set to one at all wave vectors, leaving only the parameters of the form factor to be determined. Form factors have been determined for a number of scatterer geometries and one of particular interest to polymer science is that of the Debye distribution of a Gaussian.

$$\text{Eq. 15} \quad P(q) = 2 (\exp(-q^2 R_g^2) + q^2 R_g^2 - 1) (q^2 R_g^2)^{-2}$$

In addition to simplifying the filler-matrix interaction, using a filler with a similar chemical structure to the matrix simplifies the neutron beam contrast. The scattering length density, ρ , depends only on the chemical composition and the bulk density of the scatterer. As these two quantities are similar for the PS and PSNP, scattering from a composite of the two can be reasonably approximated as a constant intensity regardless of wave vector.

The conformation of individual matrix chains can be studied by substituting a small fraction (2v%) of the protonated matrix polymer with a deuterated chain of the same size and type. It is then a simple matter to subtract a measured background scattering signal for the purely protonated sample. Alternatively, the largely incoherent scattering of the background can be treated as a constant background value and estimated from the plateau at high values of the scattering vector. This is found to be a satisfactory assumption (Figure III-1) for the scattering of the background and it avoids the error propagation that accompanies background sample scattering subtraction.

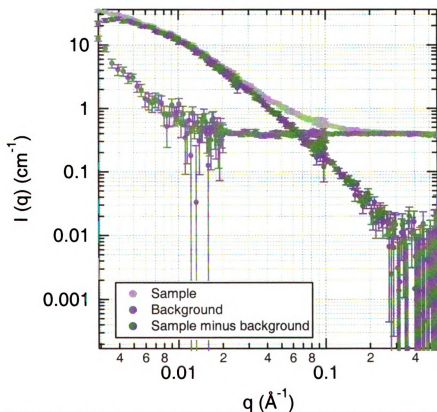


Figure III-1. The background signal is assumed to be constant at all wave vectors, at reasonable approximation for the predominantly incoherent scattering observed for protonated PS.

III.B. Experimental

Protonated polystyrene (PS) was purchased from Scientific Polymer Products (Ontario, NY) and deuterated polystyrene (dPS) was purchased from Polymer Source (Montreal, QC). Linear polymer/nanoparticle blends were made by dissolving the linear polymer(s) and nanoparticle in a mutual solvent, toluene. The solution was then dripped into a mutual non-solvent, methanol, where the polymer(s) and nanoparticles rapidly precipitated, forming an intimately mixed, homogeneous dispersion of nanoparticles in the linear polymer.⁴³ After solvent removal by decanting and filtration the blend was dried for a week in an oven at 50 °C and under rough vacuum.

Table III-2: Molecular weights and distributions of linear polystyrene and intramolecularly cross-linked polystyrene nanoparticles

Sample Name	M_w (g/mol)	M_n (g/mol)	PDI
PS	393,400	339,140	1.16
dPS	420,200	373,200	1.26
PSNP 41 kD	42,520	41,090	1.04
PSNP 78 kD	89,020	77,830	1.14
PSNP 211 kD	278,400	211,200	1.32

Samples for neutron scattering were prepared by the method described in section II.B. Measurements of orientation were made *ex situ*, after the drawing process was completed and the sample was cooled to ambient conditions.

Small angle neutron scattering tests were conducted using the NG7 30-m Small Angle Scattering Instrument at the NIST Center for Neutron Research (Gaithersburg, MD). The instrument is a variable geometry instrument with a sample to detector distance of 1.0 to 15.3 m and an associated wave vector range of 0.0008 to $.7 \text{ \AA}^{-1}$. The source to sample distance is also variable, but was held constant in the present work at 15m. The detector is 640×640 mm with 5×5 mm resolution.

III.C. Results & Discussion

Primary SANS studies were conducted for two sample compositions: 98% PS, 2% dPS and 97% PS, 1% PSNP 78kD, 2% dPS, each measured in the solid state, below their glass transition temperature. For each sample, background samples were measured for which the dPS was replaced by PS and processed by the same conditions. In light of this it was found to be preferable to assume a constant value for the background based on the high- q plateau. Each sample was evaluated at a number of hot draw ratios in order to quantify the development of orientation in the matrix polymer.

The data analysis method for isotropically scattering samples includes averaging of points with the same scattering vector, regardless of their azimuthal angle. In the case of non-equilibrium, oriented films, the scattering is asymmetric and this circular averaging would be invalid. Instead, the 2-dimensional scattering profile can be divided into angular regions parallel and perpendicular to the direction of stretch (Figure III-2) and these regions can be treated separately, averaging the individual data segments at each q -value and generating two intensity profiles for each sample. The process of separating the data azimuthally involves a trade-off between attaining sufficient counting statistics to provide an adequately high quality signal, and capturing the direction specific size scale that is brought about by the hot drawing process. For the present study azimuthal sections were analyzed with a width of 40°.

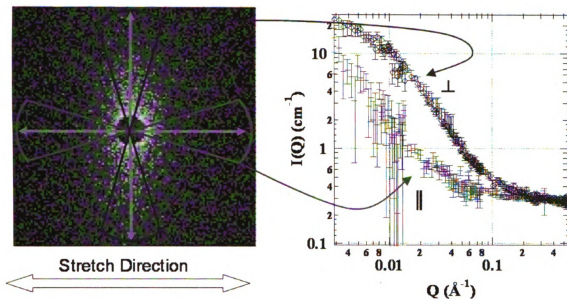


Figure III-2. The anisotropic SANS pattern of a non-equilibrium, hot stretched PS film (left). The scattering profiles parallel and perpendicular to the stretch direction are shown on the right.

Even with care taken to select a sufficiently large wedge size to provide high quality data, difficulties arise for this type of analysis. The applicable q -range for a given feature size is based approximately on the inverse of the characteristic length scale to be measured. A high molecular weight was selected for this study of orientation because higher molecular weight chains are more sensitive to orientational flow than lower molecular weight chains, due to their longer relaxation times. This presents a challenge to the low- q resolution of the instrument, a challenge which increases as the size of the chains' long axis is increased by the extensional flow. Consequently, the short axis – perpendicular to the draw direction – data are easier to interpret and less error prone for low to moderate q -range analyses.

To simplify the fitting procedure and reduce the number of degrees of freedom for analysis, the intensity at zero wave-vector, I_0 and often referred to as the scale factor, was held constant for all samples and draw ratios. I_0 is dependent on the volume of the

scatterer, its number fraction, and the scattering length density contrast between the scatterer and background. As none of these quantities are expected to change with draw ratio or PSNP inclusion, this is viewed as a reasonable assumption. The value of I_0 was determined from the fit of the undrawn PS-dPS scattering profile to the form factor for a Gaussian chain.

A useful and accurate method for interpreting the collected scattering profiles is by fitting to a previously derived form factor that is appropriate for the shape of the scatterer under investigation. For the system in question, the expectation is that the chains will conform to the form factor of a Gaussian chain in each direction. This would allow determination of the R_g in the directions parallel and perpendicular to the stretch direction. In order to confirm the suitability of the proposed Debye form factor for the system in question, the low and high q intensity profiles can be analyzed to ensure consistency with the limits of the form factor. The low- q trend can be checked by the Guinier approximation, for which a plot of $\ln(I(q))$ versus q^2 should tend towards a straight line in the range of $q R_g < 1$. Due to the aforementioned limitation on the low- q data, the Guinier analysis is not feasible for the present system. In the high- q range ($q > 5 R_g^{-1}$), the scattering profile of a Gaussian chain can be treated with the Kratky approximation, reaching a plateau at $I_0 R_g^{-2}$ when plotted as Iq^2 versus q . Rather than simply looking for a plateau in the Kratky plot, the high- q data can also be fit to the Lorentzian function

$$\text{Eq. 16} \quad I(q) = I_0 / (1 + q^n L^n)$$

and values of the Lorentzian exponent and screening length determined. For a Gaussian chain the exponent is equal to 2 and the screening length is equal to the radius of

gyration. For a swollen coil in a good solvent, the value of the exponent is less than 2,^{65, 79} decreasing with increasing solvent quality. The screening length is a characteristic size of the polymer, but not strictly equivalent to the radius of gyration. The values of the Lorentzian exponent determined from fits of the high- q scattering profiles to Eq. 16 are shown in Figure III-3 as a function of the hot draw ratio.

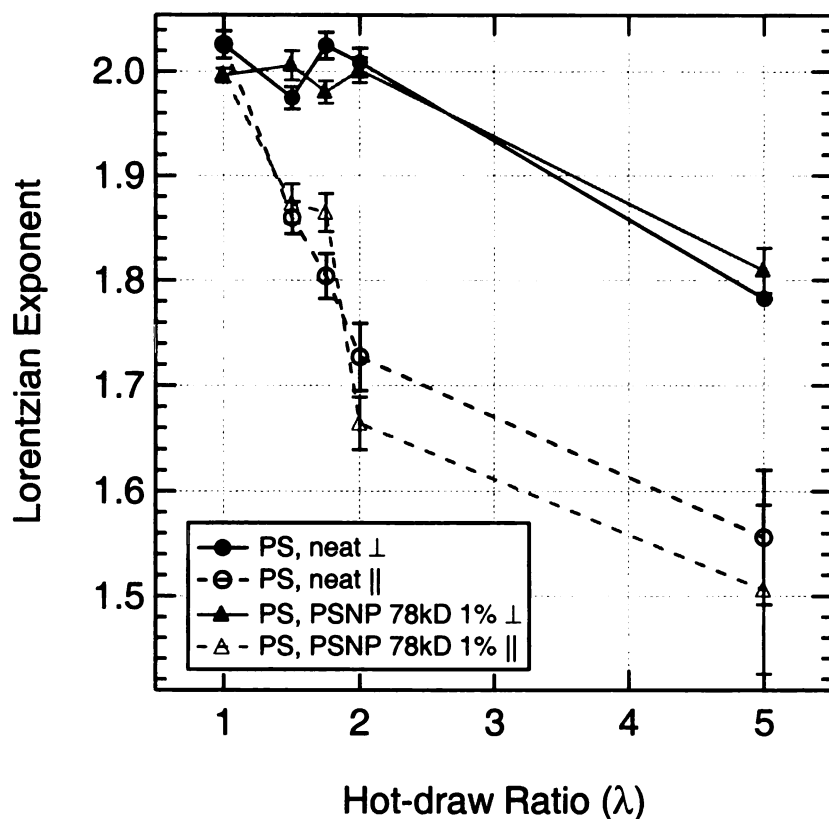


Figure III-3. The Lorentzian exponent of PS with and without PSNP addition as a function of hot draw ratio. The Lorentzian exponent for a Gaussian chain is 2. Swollen coils exhibit a reduced dependence of I on q at higher wave vectors.

The results of the hot drawing process are largely dependent on the initial state of the material before drawing. To this end, the high- q dependence of the scattering intensity provides a measure of the conformation of the unperturbed system. The nanoparticle laden system is seen to have a slightly lower value of the Lorentzian

exponent than the unfilled polymer. This is consistent with the view of the nanoparticle swelling the linear polymer, as has been demonstrated in previous studies of the dependence of R_g on nanoparticle addition.¹⁰ This also sheds light on the particle-polymer interaction, suggesting that the polymer may partially wrap around the particle, rather than simply confining the particle to a space between isolated polymer chains. The observed decrease of the Lorentzian exponent suggests that the chain adopts a swollen coil conformation, which is expected to increase the radius of the polymer chain. This increase in radius is observed as a small increase in the Lorentzian screening length for the undrawn sample (Figure III-4b). If the scattering from the nanoparticle-laden chains is treated as a Gaussian chain and fit to the Debye form factor (Eq. 15), disregarding the high- q deviation, the R_g is also seen to increase by *ca.* 1% (Figure III-4a), consistent in magnitude with the results of Mackay *et al.*¹⁰ for a high molecular weight chain blended with a similar size and type of nanoparticle at a low loading.

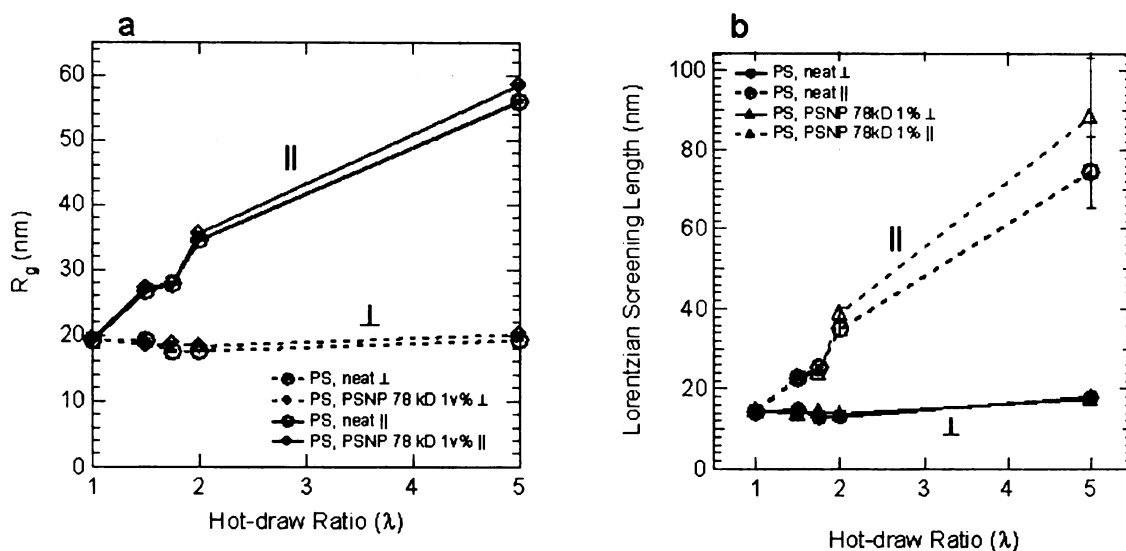


Figure III-4. The characteristic size development of anisotropic PS with and without PSNP 78 kD as a function of hot draw ratio. The macromolecular size is calculated according to either the Debye form factor (a) at all wave vectors, or the Lorentzian scattering function at high wave vectors. In both cases a discontinuity is observed for the nanoparticle-laden sample at $\lambda=1.75$, the hot draw ratio at which ductile fracture behavior is observed in tension. A small increase is observed in the long axis size of the polymer at the highest draw ratio by both methods of calculation.

In studying the drawn samples by this high- q approximation it is important to consider the quality of data. The assumptions for the high- q trends in the scattering profile are generally considered valid for values of $q > 5 R_g^{-1}$. Based on instrumental limitations, however, scattering data is rarely reliable beyond a value of the scattering vector of 0.5 \AA^{-1} . This means that for a larger scatterer, or data for a chain parallel to the draw direction, there is a wider range of high- q data available for analysis than for a smaller scatterer, or data for a chain perpendicular to the draw direction. Also, separating the scattering profiles into separate sections parallel and perpendicular to the draw direction reduces the quality of the data. While the Lorentzian scattering function may provide a more accurate representation of the non-Gaussian chain behavior, the additional

degree of freedom introduced by the unknown Lorentzian exponent increases the possibility of an errant fit to noisy data. With this in mind, it is worthwhile to consider the results based on both the Lorentzian function (Eq. 16) and the Debye form factor (Eq. 15).

Analysis of the Lorentzian exponent with increasing draw ratio shows that the exponent for both filled and unfilled PS decreases for the data parallel to the draw direction as the hot draw ratio increases. This is reasonable behavior and has been shown previously,^{64, 65} showing that the chain is drawn to a size greater than its equilibrium, Gaussian, distribution. The Lorentzian exponent for the data perpendicular to the stretch direction also decreases with λ , reflecting the perturbed shape of the coil in both directions. Very low draw ratio behavior is similar for the samples with and without particles, as their exponents are nearly the same at a draw ratio of 1.5. At a draw ratio of 1.75, however, the exponent of the particle filled system is greater than the unfilled system. At higher draw ratios, this trend reverses, as the exponent of the filled system exceeds the unfilled system. The screening length in the parallel direction also increases with λ and shows trends similar to the dependence of the exponent with λ .

Perhaps more illustrative than the individual length scales, is the ratio of these length scales (Figure III-5). This provides a molecular aspect ratio, $\xi = L_{\parallel} / L_{\perp}$, of the overall chain and measure of orientation. As a reference for the extent of orientation, the affine limit of the aspect ratio can be calculated, which scales as $\xi = \lambda^{3/2}$. This is the maximum aspect ratio that is to be expected for the given draw ratio. ξ increases with hot draw ratio, adhering closely to the affine limit at low draw ratios, but deviating substantially at $\lambda = 5$. For the draw ratios of 1.5, 2, and 5, the aspect ratios calculated

from the Lorentzian Screening Lengths of the dPS chain in the particle filled system are greater than the unfilled system, but not beyond the range of error for the measurement (Figure III-5b). According to the Debye fit, the aspect ratios at these draw ratios are essentially unchanged by nanoparticle addition.

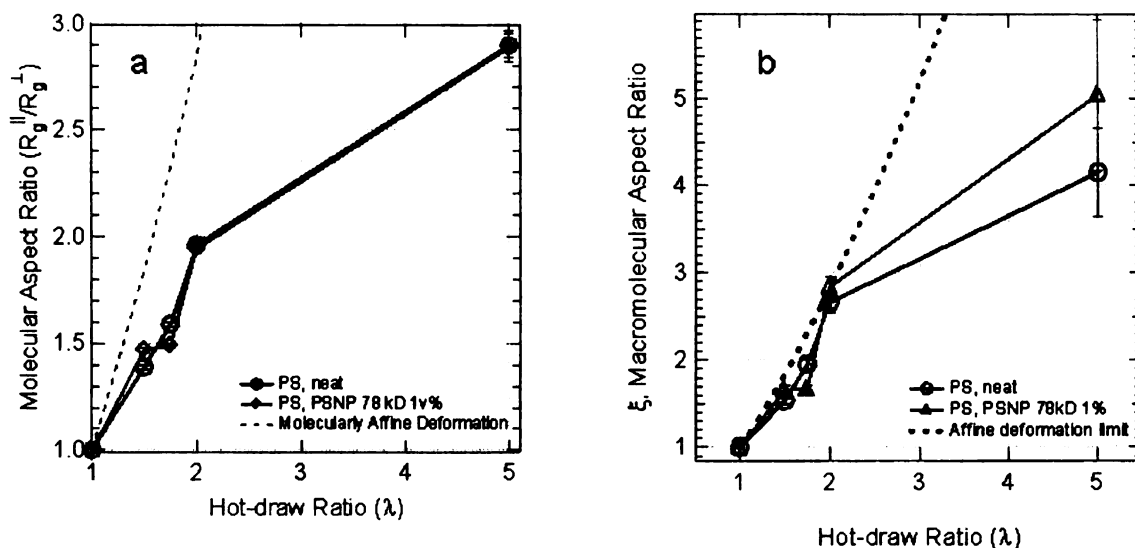


Figure III-5. The aspect ratio development of anisotropic PS with and without PSNP 78 kD as a function of hot draw ratio. The aspect ratio is calculated according to either the Debye form factor (a) at all wave vectors, or the Lorentzian scattering function at high wave vectors. In both cases a discontinuity is observed for the nanoparticle-laden sample at $\lambda=1.75$, the hot draw ratio at which ductile fracture behavior is observed in tension. The dashed line represents the aspect ratio for a chain that deforms affine to the bulk sample, the maximum attainable orientation in the absence of an additional driving force.

At the intermediate draw ratio of 1.75, however, there is a significant difference between the two systems, the PSNP-filled system showing a lower aspect ratio than the unfilled system. It has been shown previously (Chapter II:) that PSNP-filled PS undergoes tensile failure by a ductile mechanism accompanied by neck formation when processed to a hot draw ratio of 1.75, while unfilled PS fails by a brittle mechanism under the same conditions. The primary obstacle to polymer chain orientation in a flow field is the relaxation of the polymer from its strained state; for example, low drawing

temperatures have been shown to enhance orientation by increasing the relaxation time of the polymer chain. This decrease in the aspect ratio for the PSNP-filled system suggests that the relaxation time of a polymer chain is decreased by the presence of nanoparticles. This is consistent with previously described observations of increased chain mobility by PSNP addition as measured by a decrease in the equilibrium T_g and an increase of the strain-to-failure for nanoparticle filled samples tested in tension. The decrease of the relaxation time decreases the orientation, and therefore ξ , at $\lambda=1.75$. However, the lower relaxation time also improves chain mobility which leads to ductile failure when stressed in tension

III.D. Conclusion

Small angle neutron scattering has revealed a number of key features about the influence of PSNP addition on the polymer conformation of both isotropic, equilibrium chains, and anisotropic, non-equilibrium chains. The polymer chain is shown to swell to a form that is larger than a simple Gaussian distribution, as reflected by the reduction of the Lorentzian exponent. This chain swelling relative to the unfilled polymer is also seen at higher draw ratios, accompanied by an increase in the chain aspect ratio at high draw ratios. In mechanical studies of tensile behavior, a transition to a ductile fracture mechanism after processing to a hot draw ratio of 1.75 was observed for the PSNP filled system. This has been corroborated by a reduction in the matrix chain aspect ratio at this processing condition, reflecting a decrease in the relaxation time of the matrix, decreasing orientation but also increasing the mobility of the chain. The increased chain mobility, coupled with the swelling of the polymer conformation shows that the cross-linked

nanoparticles act as a solvent for the PS matrix. This solvent-like behavior is unusual for a material with a cross-linked structure, high modulus, and T_g greater than PS.

Chapter IV: The effect of C₆₀ addition on the thermal and mechanical behavior of PS

IV.A. Introduction

Fillers with high aspect ratios such as carbon nanotubes⁸⁰⁻⁸⁴ and clay particles^{15, 39-41, 83, 85, 86} are popular fillers for creating aligned nanocomposites. Work has even been conducted to evaluate the ability to induce orientation of the filler particle³⁹⁻⁴² and the effect this has on mechanical properties.

Miaudet *et al.*,⁴⁰ for example, showed that the hot drawing of wet-spun fibers containing poly(vinyl alcohol) (PVOH) and multi-walled carbon nanotubes (MWNT) or single-walled nanotubes (SWNT) increases a number of desirable end-use fiber properties, including energy absorption at low strain and moisture resistance. These property enhancements were attributed to the alignment of the polymer and nanotube moieties. The hot drawing process was shown to increase the alignment of PVOH from $\pm 27^\circ$ from the fiber axis for the as-spun fiber to $\pm 4.3^\circ$ and $\pm 6.3^\circ$ for the hot drawn fibers containing SWNT and MWNT, respectively. The nanotubes had a similar limited orientation in the as-spun case, but hot drawing improved the orientation of the SWNT to $\pm 9^\circ$ and the MWNT to $\pm 11^\circ$. The hot drawing process was also found to increase the PVOH crystallinity.

Minus *et al.*⁸⁶ also studied PVOH fibers with SWNT formed in the presence of a shear flow. They found that the nanotube increased PVOH crystallinity and templated polymer orientation parallel to the nanotube axis, which was parallel to the fiber axis. In the case of poly(acrylonitrile) (PAN), the same group⁸⁵ found that PAN orientation was also enhanced by the addition of SWNT. However, they found that while the average crystalline size was increased, the total crystallinity is reduced. Contrary to the findings

of Miaudet *et al.*,⁴⁰ this group found that the nanotube is more oriented than the surrounding polymer.

Dror *et al.*⁴¹ measured the alignment that developed during electrospinning nanofibers of poly(ethyleneoxide) (PEO) with MWNT. They found that the converging flow geometry led to alignment of the MWNT with the fiber axis. The PEO chains were also found to align, but the presence of the MWNT diminished the alignment of the PEO.

Weon and Sue⁸³ examined the significance of filler aspect ratio and orientation on a composite of nylon-6 and silicate clay. They found that the composites modulus, tensile strength, and distortion temperature all increased with increasing clay aspect ratio and orientation. The opposite dependence on aspect ratio and orientation was observed for composite toughness and ductility.

The development of buckminsterfullerenes (C_{60}) in 1985⁸⁷ and carbon nanotubes (CNT) in 1991⁸⁸ ushered in a new era in composite research. The well-defined molecular structure, potentially high mechanical stiffness, appealing electronic character, and nanoscopic dimensions of these materials made them extremely attractive for use in myriad applications. Buckminsterfullerene has been found to have a truncated icosohedral structure,⁸⁷ with an average radius of gyration equal to 3.82 Å.⁸⁹ This third crystalline form of carbon has been studied theoretically⁹⁰⁻⁹² as well as experimentally⁹³⁻⁹⁷ in order to determine the bulk modulus at zero pressure, K_0 , of individual particles, as well as crystalline assemblies of C_{60} . The values for K_0 that have been suggested range from 6.8 GPa⁹⁷ for an fcc crystal to 20 GPa⁹² for an individual particle. While these values are high, they are less than the bulk modulus of diamond at zero pressure (442-433 GPa⁹⁸), which is one of the hardest known materials and another allotropic form of

carbon. At pressures greater than 70 GPa, however, buckminsterfullerenes come into hard sphere contact with one another and the bulk modulus reaches 600 to 700 GPa⁹⁰⁻⁹² exceeding that of even diamond, making C₆₀ the hardest currently known substance, under certain conditions.

In addition to its high modulus, C₆₀ deserves special attention as a filler for polymeric materials due to its very small size. The radius of the particle (0.38 nm) is much less than the Kuhn segment length, l_K , of polystyrene (PS), *ca.* 1.8 nm. The Kuhn length has been identified as the size scale on which a polymer chain can bend 180° relative to itself, and is *ca.* 8-9 monomers for PS.⁹⁹ This small size of the particle relative to the chain flexibility limit suggests the potential for the particles to occupy space that is otherwise inaccessible to the polymer due to the chains' limited flexibility. While the fullerene cage is open and has a hollow interior, it is unlikely that a polystyrene chain would be able to access the void space. The openings within the C₆₀ cage structure are the same size or smaller than the pendant phenyl rings along the PS backbone, creating an obvious steric obstacle to penetration and leaving C₆₀ to be reasonably considered as a hard, impenetrable sphere.

In the present study, the effect of C₆₀ addition to polystyrene will be studied with regard to developing an understanding of the polymer-particle interface and how this impacts solid state mechanical properties. Of particular interest is the ability for these spherical fillers to perform with respect to a processing environment that imparts alignment to the polymer matrix by aligning the polymer in the melt state, followed by rapid cooling to lock the chains in an anisotropic, non-equilibrium state.

IV.B. Experimental

Polystyrene standard was purchased from Scientific Polymer Products (Ontario, NY) with $M_w = 393,400$ Da and $M_w/M_n = 1.16$. Buckminsterfullerenes were purchased from Term-USA (Moscow, Russia). Linear polymer/nanoparticle blends were made by dissolving both the linear PS and C_{60} in a mutual solvent, toluene. This ternary solution was then dripped into a mutual non-solvent, methanol, where the PS and C_{60} rapidly precipitated, forming an intimately mixed, homogeneous dispersion of C_{60} in the linear PS.⁴³ After removing the majority of the liquid from the sample by decanting and vacuum filtration with copious methanol rinsing, the blend was dried for a week in an oven at 50 °C and under rough vacuum. Sample processing and characterization techniques were identical to those described in section II.B.

IV.C. Results & Discussion

IV.C.1. Equilibrium Thermal Analysis

The effect of buckminsterfullerene inclusion on the glass transition temperature of polystyrene is shown in Figure IV-1. The glass transition temperature is often used as an indicator of polymer mobility, and therefore free volume. As obstacles to motion are reduced, especially by the introduction of unoccupied areas, the thermal energy input required to initiate rapid motion of the amorphous chains is decreased, leading to a reduction in the glass transition temperature. In the case of C_{60} added to PS, the glass transition temperature is seen to decrease relative to the T_g of unfilled PS at loadings greater than 1v%. Extremely low loading of C_{60} (0.5v%), on the other hand, brings about an increase in T_g of the same magnitude as the decrease at 1-2v%.



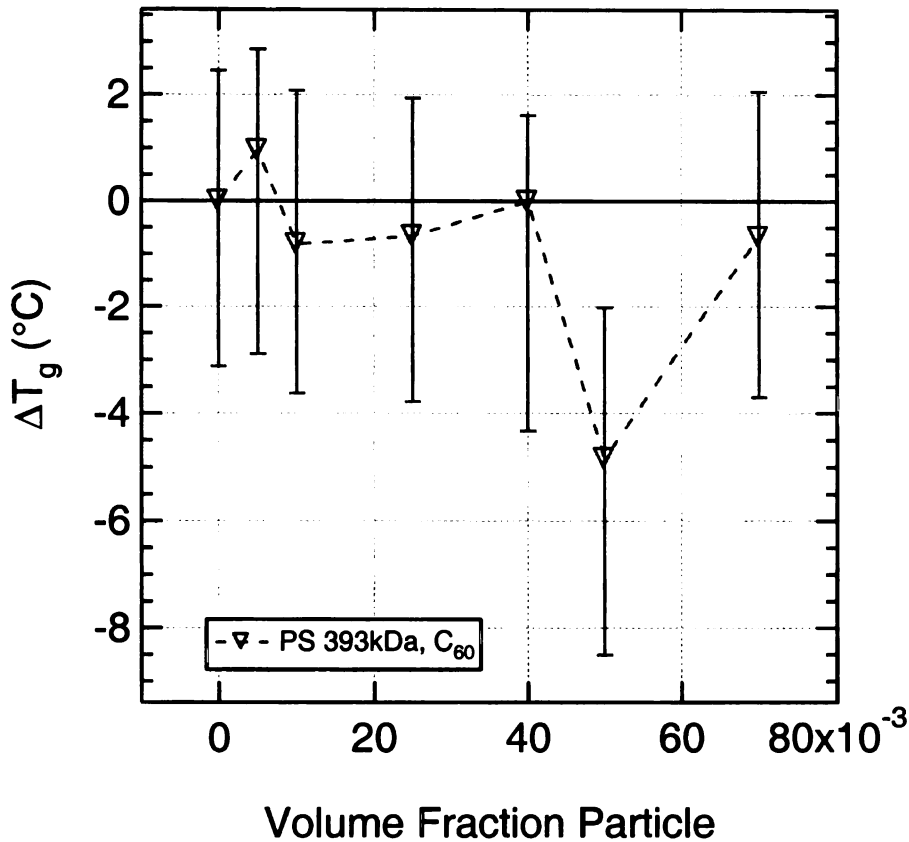


Figure IV-1. Change in glass transition with addition of C₆₀. Extremely low concentrations - corresponding with an interparticle half-gap of similar size to the statistical Kuhn segment length of polystyrene - of C₆₀ show an increase in T_g that corresponds to a reduction in polymer mobility. Higher, but still homogeneously dispersed, loadings show a T_g reduction.

An important parameter to consider in the study of any nanoparticulate filled system is the interparticle gap, $2h$, given by Eq. 17.

$$\text{Eq. 17} \quad h/a = (\phi_m/\phi)^{1/3} - 1$$

At equivalent volume fractions the interparticle gap scales with the particle radius, a . For particles with extremely small radii, such as C₆₀, this gives rise to very small interparticle gaps into which the polymer chain is confined. In fact, for the concentrations at which the glass transition temperature is reduced, the interparticle half-gap is less than the Kuhn segment length, l_K , of polystyrene, 1.8 nm. It is likely that the difference between having an interparticle half-gap that is less than l_K and one that is greater than l_K is sufficient to

delineate two separate regimes of packing and polymer conformation. In the limit of $h \approx l_K$, the polymer is able to pack a full segment or more lengthwise between neighboring particles. It is possible to consider this to be a sort of critically percolated packing state in which the C_{60} limits the polymer mobility.

In the other regime, $h < l_K$, the C_{60} particles are forced into closer proximity with one another. The fact that this space is smaller than that into which PS can freely pack suggests that the C_{60} are relegated to regions that are inaccessible to the polymer, or that the matrix expands to accommodate the particles. The results from DSC suggest that the latter mode of packing is operable. The PS matrix expands to accommodate the ever-encroaching fullerenes, leading to an increase in the overall system mobility and, potentially, free volume.

PVT analysis is a sensitive test of the internal structure and potential presence of free volume within polymeric materials. Engineering properties of interest that can be directly calculated from PVT data include the bulk modulus, $K = -V(\partial P/\partial V)_T$, and the coefficient of thermal expansion,⁴⁷ $\alpha = V^{-1}(\partial V/\partial T)_P$. The bulk modulus is of particular interest in the case of C_{60} because it reflects the cumulative result of two competing effects. As mentioned previously, both simulation and experiment have shown C_{60} to have an extremely high bulk modulus at zero pressure, K_0 , ranging from 6.8 to 20 GPa. While this is a very broad range, it reflects the broad range of forms and interactions that C_{60} can assume and the values are sufficiently high compared to PS (1.13 GPa) as to justify the treatment of C_{60} as a rigid particle. In addition to the rigidity of the particle, the volumetric response of the material will also be influenced by any free volume that may

be introduced to the system. This free volume will act in opposition to the reinforcing effect of the high modulus particle, reducing the modulus of the nanocomposite.

The effect of C_{60} addition to PS on K_0 is shown in Figure IV-2. In fact, while PVT measurements are only strictly valid in the melt state, where pressure is uniformly hydrostatic, similar trends are also observed for the solid state bulk modulus, measured at 50 °C. Similar to the discontinuity seen in the T_g at $\varphi = 0.5\%$, the bulk modulus is reduced by more than 10% for this very low loading. Further addition of C_{60} leads to an increase of K_0 in excess of the value for unfilled PS. The thermal expansivity, α , shows the opposite behavior, increasing by *ca.* 8% for the 0.5v% blend before decreasing to a value that is less than the unfilled polymer and remaining nearly constant with increasing volume fraction.

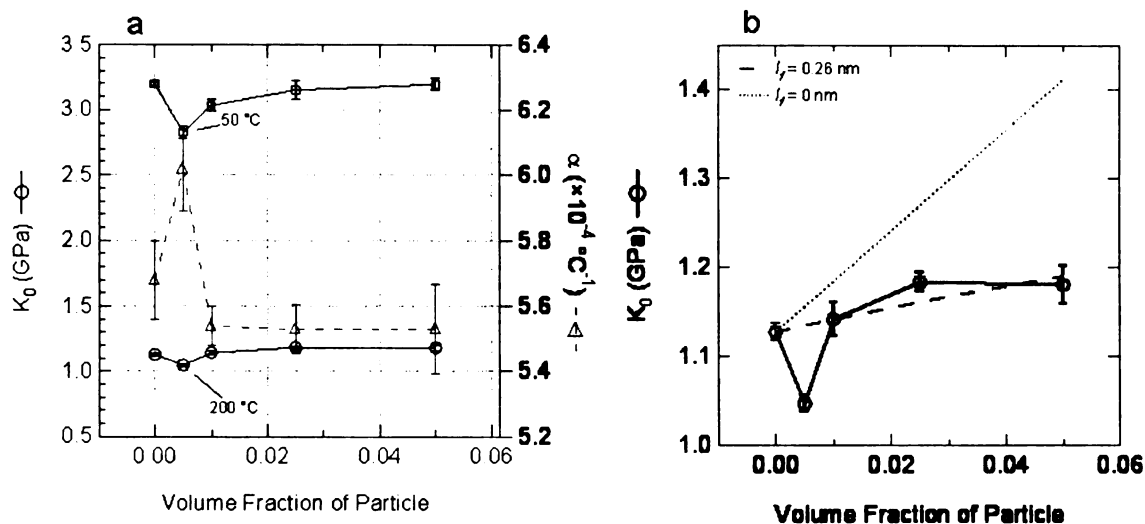


Figure IV-2. Bulk modulus and thermal expansivity of a polystyrene/buckminsterfullerene blend. At very low volume fractions for which the interparticle gap is greater than the statistical segment length of the matrix polymer, the bulk modulus is reduced and the thermal expansivity is increased. At higher loadings, the C_{60} is spaced closer than the Kuhn segment length of polystyrene and the bulk modulus is increased and the thermal expansivity is decreased. Similar trends are seen in the bulk modulus both above (200 °C) and below (50 °C) the glass transition temperature. Prediction of the bulk modulus with a free volume layer of 0.26 nm provides a satisfactory fit to the measured bulk modulus at 200 °C (b). The prediction for no free volume is for a much greater increase in K_0 than is observed experimentally.

Contrary to the T_g observations made by DSC, these PVT quantities suggest an *increase* in free volume for the 0.5v% case and a decrease at higher loadings. However, the types of mobility being probed by the two techniques are not precisely equivalent. DSC results are based on the thermal energy required to initiate motion to transition from the glass to melt state. PVT results, on the other hand, are based on the volumetric response of a material, already in the melt state, to changes in pressure and temperature. This means that PCT is a more direct measure of internal voids, while T_g changes observed by DSC are indicative of mobility, which is a possible result of changes in void space. Furthermore, while the K_0 and α values indicate a reduction in the effect of free

volume at higher C_{60} loadings, they do not preclude the possibility that free volume is still greater than for the unfilled polymer. Recalling that K_0 for pure C_{60} is much higher than for unfilled PS, the addition of 2.5v% C_{60} would be expected to increase the value of K_0 for the blend to 1.27 GPa, based on the lowest estimates of the modulus of C_{60} (Figure IV-2b). This is much higher than the observed value of 1.18 GPa and suggests that highly compressible void space is being introduced with the C_{60} .

If the void space is considered to have an infinite compressibility (K_0^{-1}) and based on the known range of moduli for C_{60} and unfilled PS then the bulk modulus of the composite can be used to estimate the amount of free volume in the sample based on a volumetric average of the bulk moduli of the PS, C_{60} , and free volume (see section II.C.1). For the very low concentration system that showed a stark drop in K_0 , the free volume fraction, ϕ_f is 0.18 to 0.13 and the free volume to C_{60} volume ratio (ϕ_f/ϕ_{C60}) is 43.47 to 30.32. At the higher (1v% to 5v%) loadings of C_{60} , ϕ_f/ϕ_{C60} becomes essentially constant at 3.5 ± 0.5 to 14.8 ± 0.7 . If one assumes that the free volume introduced by C_{60} is located in a layer of constant thickness around the perimeter of the particle, then a value for that layer thickness may be calculated. For the very low concentration system, the free volume layer thickness, l_f is 0.98 to 0.83 nm. At the higher (1v% to 5v%) loadings of C_{60} l_f is 0.25 ± 0.03 to 0.58 ± 0.01 nm. Volumetric estimates of the bulk modulus of PS- C_{60} blend based on a free volume layer thickness of 0.26 nm and a C_{60} bulk modulus of 6.8 GPa are shown in Figure IV-2b and match well with the observed values of K_0 for loadings greater than 0.5v%. These estimates are all less than the previously discussed l_K , even approaching the size of a styrene monomer, lending credence to this as a realistic length scale based on the limited flexibility of the polymer

chain. Moreover, this weak interaction is consistent with a previously suggested¹⁰ slightly repulsive chi-parameter for the PS-C₆₀ interaction.

In addition to the value of bulk modulus at zero pressure, it is instructive to measure the slope of the bulk modulus as a function of pressure close to zero pressure, K_1 (Figure IV-3). For the blends of C₆₀ in PS, K_1 reaches a maximum at a particle volume fraction of 0.5v% to 1v%.

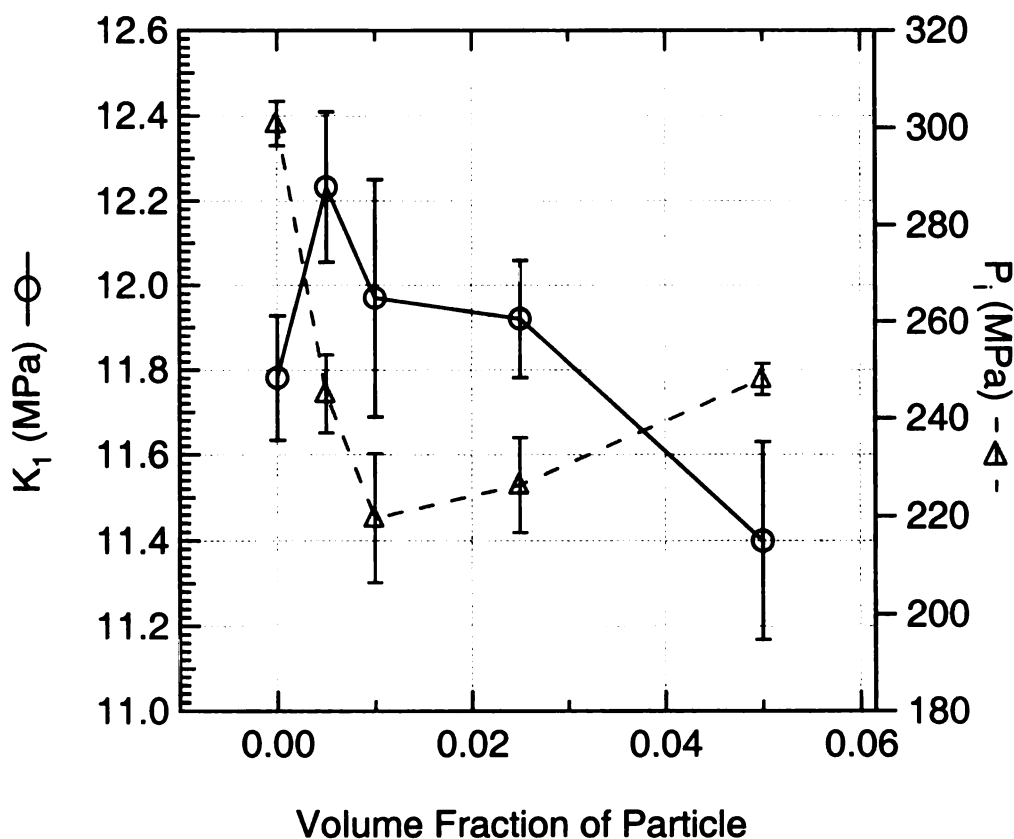


Figure IV-3. The free volume asymmetry number, and internal pressure as function of C₆₀ volume fraction in PS 393 kD. The free volume asymmetry number goes through a maximum before decreasing with increasing particle loading. The internal pressure is decreased by particle addition, consistent with a decrease in the strength of intermolecular interactions.

The quantity, K_1 , is related to the shape of the free energy minimum and is referred to as the free energy anharmonicity.⁵³ A K_1 value of five is equivalent to a

harmonic potential, for which compression and dilation are equally favorable processes. However, intuition and experience suggest that K_1 is generally greater than five, consistent with a material for which dilation is favored relative to compression. Typical K_1 values for polymeric materials are 11.0 ± 1.5 .⁵³

It has been shown through changes to K_0 that the addition of C_{60} introduces a driving force towards free-volume expansion within the nanocomposite. This driving force is also manifested in an increase in the free-volume anharmonicity, K_1 , as the system becomes increasingly biased towards dilation over compression. This is specifically apparent for $\phi=0.5\%$ where a maximum value of K_1 is observed, in concert with the maximum free volume increase calculated according to K_0 values. At a higher volume fraction (5v%) K_1 decreases relative to the unfilled PS. High K_1 values are characteristic of repulsive intermolecular forces, but as material becomes more porous, there is less driving force toward dilation – the system is already in a high volume state – and the free energy well becomes more neutral.

In addition to the shape of the free energy well, the sensitivity of internal energy to volumetric changes can be calculated from PVT data. This sensitivity is defined as the internal pressure, P_i .⁵⁴ The internal pressure is not a direct measure of the magnitude of intermolecular interaction energy, but rather a measure of the response of this energy to a change in volume.⁵² The direct measure of the interaction energy between molecules is the Cohesive Energy Density (CED) which is defined⁵⁵ as

$$\text{Eq. 18} \quad \text{CED} = U/V$$

In the past, the difference between CED and P_i has sometimes been wrongly neglected and values of P_i have been used for CED. While not strictly correct, it was shown by

Hildebrand *et al.*⁵⁶ that the ratio, n , of P_i to CED is approximately one for low molecular weight liquids. In further analysis Sauer and Dee⁵⁵ showed for a number of polymeric materials that n is between 0.88 and 1.35.

The internal pressure is strictly defined as the response of the internal energy to a change in volume:

$$\text{Eq. 19} \quad P_i \equiv (\partial U / \partial V)_T$$

$$\text{Eq. 20} \quad P_i = T (\partial S / \partial V)_T - P$$

The internal pressure can also be written as the difference between the thermal pressure ($T\alpha K$) and the system pressure (P).

$$\text{Eq. 21} \quad P_i = T\alpha K - P$$

As free volume is increased in a system, additional regions are introduced for stress relief in the event of a change in volume. This diminishes the system's energetic response to changes in volume, and therefore reduces P_i . This effect is clearly observed with the addition of C_{60} to PS. The additional free volume introduced to the system leads to a *ca.* 25% reduction of the internal pressure. There is, however, an apparent limit to the P_i reduction that can be caused by particle introduction and the accompanying free volume layer, as P_i increases for C_{60} loadings greater than 1v%. This may highlight the effect of particle crowding; particle addition enhances mobility at low volume fractions, but at higher loadings the particles begin to impinge on another, eventually decreasing mobility by acting as obstacles themselves. This increases the volumetric dependence of free energy as the particles become close enough to interact with one another rather than only interacting with the polymer matrix.

IV.C.2. Non-Equilibrium Tensile Behavior

In addition to equilibrium techniques for understanding the C₆₀-PS interaction, an understanding of the solid state tensile properties is needed to evaluate the potential for application of C₆₀ as a route to structural reinforcement. Of particular interest is the tensile behavior of samples that have been subjected to a uni-axial hot drawing process which introduces alignment to the polymer matrix.

Similar to the previously discussed quantities, a material's strain-to-failure, ϵ_f , may be indicative of free volume introduced near a filler particle surface. The hot draw ratio, λ , dependence of ϵ_f is shown for two C₆₀ loadings in Figure IV-4b. The ductility for both studied C₆₀ loadings is increased compared to unfilled PS at low to moderate (1.75 to 2.5) values of λ . At higher values of λ the blend with a lower concentration of C₆₀ shows a ϵ_f value that is similar to the behavior of the unfilled polymer. The blend with a higher C₆₀ loading, on the other hand, shows a stark drop-off at higher draw ratios, a behavior that will be discussed later.

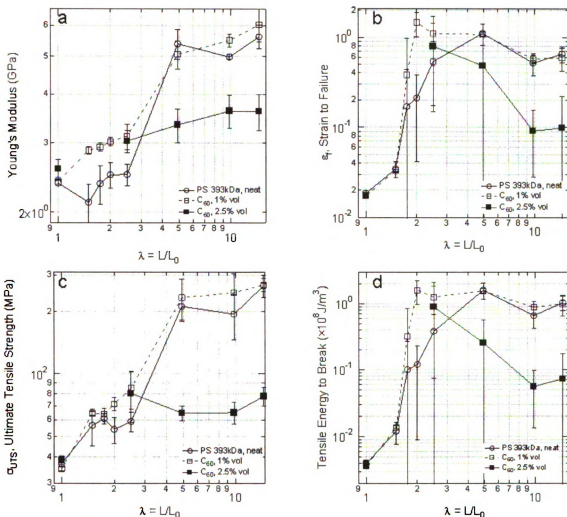


Figure IV-4. The Young's Modulus (a), strain to failure (b), ultimate tensile strength (c), and energy to failure (d) of hot drawn PS 393 kD with buckminsterfullerenes as a function of hot draw ratio. The modulus (a) and ultimate tensile strength (c) are unchanged for the undrawn case and increased by C60 inclusion at low draw ratios for both loadings. At higher loading (2.5v %) the modulus and ultimate tensile strength are reduced at draw ratios greater than 2.5. The ductility (a) is increased for both loadings at moderate (1.75 to 2.5) draw ratios. At higher draw ratios the samples with low loading (1v%) are similar to unfilled PS while the higher loading (2.5v%) is much less ductile than the neat polymer.

Weak interfacial contact between the matrix and filler can enhance ductility by introducing a region of increased polymer mobility which increases the plasticity of the polymer.^{51, 57, 58} In the absence of avenues for uniform stress relief or distribution, stress becomes concentrated at flaws or cross-sectional area minima, which gives rise to catastrophic failure at these points. Added free volume is not, however, the only avenue

for ductility increase for hot drawn films. Previous work with unfilled PS has shown that chain orientation also increases the value of ϵ_f .^{36, 37, 62, 100, 101} This is attributed to an enhanced capacity to distribute stress through the sample along the oriented chain. In addition to stress transfer, the chain orientation may decrease the stress to flow initiation, an important quantity in determining whether or not a sample will break. When the stress to flow initiation is less than the stress to failure, a sample under load will deform, and vice versa. Chains oriented in the direction of flow *and* chains in a higher free volume environment have fewer entanglements in the stress direction, making them more likely to flow than an equivalent unoriented or tightly packed chain.

The increase in the ductility for the blend with a lower C₆₀ loading suggests again that C₆₀ is introducing free volume to the blended sample. The inability of the additive to induce ductility at higher draw ratios is indicative of a maximum in the polymer alignment. Beyond a sufficient alignment, the tensile stress on the material is being applied more directly along the polymer chain backbone. In this case it is the chain bonds themselves that are experiencing stress which cannot be redistributed or relieved.

A study of the Young's Modulus as a function of the hot draw ratio (Figure IV-4a) lends insight to the effects of buckminsterfullerene inclusion on PS alignment. The first thing to note is that despite the remarkably high bulk modulus of buckminsterfullerene, the Young's Moduli of the unstretched samples ($\lambda=1$) are essentially unchanged by the addition of C₆₀. As the draw ratio increases to 2.5, however, Young's Modulus shows immediate improvement for both low (1v%) and moderate (2.5v%) C₆₀ loading. While both these modifications show similar behavior at low draw ratio – E increases from an unstretched value of *ca.* 2.5 GPa to *ca.* 3.0 GPa – the Young's modulus of unfilled PS

increases much less, from *ca.* 2.4 GPa to *ca.* 2.5 GPa. Much higher draw ratios show a volume-fraction dependent behavior. At a draw ratio of 4.5 unfilled PS surpasses PS-C₆₀-2.5v% while PS-C₆₀-1v% continues to show improvement greater than that of the unfilled system. In fact, while PS-C₆₀-2.5 vol.% demonstrates a plateau in Young's Modulus with draw ratio near 4 GPa, unfilled PS continues to increase up to 5.5 GPa at $\lambda=15$ while PS-C₆₀-1 vol.% reaches 6.0 GPa at the same draw ratio.

Trends seen for Young's Modulus become even more obvious for the ultimate tensile strength (Figure IV-4c). At draw ratios of 5 and higher, PS-C₆₀-2.5v% shows marked deterioration of the strain and especially stress to failure. While PS-C₆₀-1v% shows some improvement in ultimate tensile strength, the strain-to-failure is essentially unchanged, leading to little change in the energy required to fracture the specimen.

Larger draw ratios show a deviation from universal enforcement by C₆₀. At draw ratios greater than 2.5, the polystyrene film bearing 2.5v% C₆₀ shows a decrease in Young's modulus, strain-to-failure, and ultimate tensile strength. A reduction in the tensile modulus is often indicative of phase separation, leading to stress concentration at the phase interface. In the case of C₆₀, even strong interfacial contact with the matrix would be insufficient to provide a significant tensile modulus increase, as the extremely small fullerene particles lack the high aspect ratio that is the norm for traditional fillers, making an aggregate of C₆₀ incapable of withstanding even a moderate tensile stress. The notion of strain-induced phase separation is reinforced when one examines the interparticle gap in the blend. The average interparticle gap for a volume fraction of 2.5% is 1.36 nm. If the particles in the composite move relative to one another in an affine fashion during orientation, then two particles oriented perpendicular to the stretch

direction would decrease their interparticle gap during hot drawing. In fact, at a draw ratio of 4, close to the drop-off in tensile properties, the calculated interparticle gap is less than the particle radius. This suggests that forced particle motion during processing may promote phase separation, leading to erosion of mechanical performance.

IV.D. Conclusion

Buckminsterfullerene demonstrates a complex behavior when used as an additive for linear polystyrene. Like some other nanoparticulate fillers, C_{60} introduces a layer of free volume around the particle surface that increases polymer chain mobility, decreasing T_g and increasing ϵ_f in many cases. However, the high modulus of C_{60} leads to an increase in the bulk and tensile moduli of the composite material. Additionally, the very small radius leads to small interparticle gaps that have consequences for particle-particle interaction.

Chapter V: Dispersion of hyperbranched polyethylene in polystyrene leading to improvements in stiffness and ductility

V.A. Introduction

A route to the controlled branching of polyethylene was described by Guan *et al.*¹⁰² in 1999. By controlling the monomer pressure during polymerization, the rate of occurrence of chain-growth steps is controlled.¹⁰³ In the intervening time between chain additions, the active radical is free to isomerize, moving randomly along the chain by a process referred to as chain-walking. According to this mechanism, a chain grown under low monomer pressure (PELP) has been found to have greater branching, and a dendritic-type structure. In the present work, the addition of PELP to linear polystyrene (PS) is studied to understand how the polymer-particle interaction gives rise to changes in the equilibrium thermal, as well as non-equilibrium mechanical properties of the composite. Polyethylene is generally considered to be immiscible in polystyrene, but Mackay *et al.*¹⁰ demonstrated that these hyperbranched PE macromolecules can be stably dispersed, provided a sufficiently high molecular weight of polystyrene is used.

Studies of particle addition to polymers for reinforcement in the literature^{5, 14, 29, 104-106} and in the present work have tended to focus on higher modulus, rigid fillers added to a weaker polymer matrix. In this case, however, the particle additive is quite soft, while still having a defined, branched structure and a radius, a , of 11 nm which is less than the polymer radius of gyration. While this larger size is still within the general limit for particle dispersion defined by Mackay *et al.*¹⁰ ($a < R_g$) it does have consequences for other key characteristics of the nanocomposite. Notably, the interparticle gap, h , of a 3.2v% blend of PELP in PS is greater than the R_g of the polymer. This means that the

polymer is not confined between the particles and is more free to assume its equilibrium, unfilled conformation than a polymer in a confined state would be.

V.B. Experimental

Polystyrene standards were purchased from Scientific Polymer Products (Ontario, NY) with $M_w = 393,400$ Da and $M_w/M_n = 1.16$. Branched polyethylene chains were generously provided by Zhibin Guan and synthesized according to a previously reported method.¹⁰² Linear polymer/nanoparticle blends were made by dissolving both the linear polymer and nanoparticle in a mutual solvent, THF. The solution was then dripped into a mutual non-solvent, methanol, where the polymer and nanoparticles rapidly precipitated, forming an intimately mixed, homogeneous dispersion of nanoparticles in the linear polymer.⁴³ After removing the majority of the liquid from the sample by decanting and vacuum filtration with copious methanol rinsing, the blend was dried for a week in an oven at 50 °C and under rough vacuum. Sample processing and characterization techniques were identical to those described in section II.B.

V.C. Results & Discussion

V.C.1. Equilibrium Thermal Analysis

The glass transition temperature (T_g) is an indicator of polymer chain mobility in amorphous polymers. More mobile chains require less thermal energy to initiate the Brownian motion of 20 to 50 carbon atoms that is characteristic of a material above its T_g .²⁴ This transition is sensitive to the polymer's chemical structure and molecular weight, as well as the environment in which it is located. Studies have shown that placing a polymer in a thin film, pore, or other confined geometry alters its conformation sufficiently to change the T_g .²⁵⁻²⁷ One possible route to increase chain mobility is an

increase of free volume. As obstacles to motion are reduced, especially by the introduction of unoccupied area (free volume), the thermal energy needed to initiate free motion of the amorphous chains is decreased, leading to a reduction in the glass transition temperature.

The glass transition temperature as measured by DSC of PS-PELP blends is found to be lower than that of the unfilled matrix polymer. For measured blends with volume fractions between 1.3v% and 6.4v%, the T_g is reduced relative to PS by 1.72 ± 0.61 °C. The trends in glass transition temperature with PELP addition to PS confirm a number of expectations. First, the glass transition temperature of the PELP is well below 0 °C, although the thermal behavior of the hyperbranched PE macromolecule and its T_g is somewhat difficult to ascertain with certainty. The low T_g of this filler material is expected to, and does, decrease the T_g of the blend. In addition to the low T_g of the filler, PS and PE are known to have a weak, or even repulsive interaction. This negative interaction generates a weak interface, permitting chain mobility.

In addition to the change in T_g , other features of the DSC trace (Figure V-1) reveal information about the particle/polymer blend. Hyperbranched PE shows a large endothermic peak at *ca.* -33 °C. This transition is not clearly apparent for the 1.3v% blend, but a small peak is noticeable for the 6.4v% blend. This suggests, but does not guarantee⁴⁶ that 1.3v% blend is well-dispersed, while the 6.4v% blend seems to indicate the possibility of phase separation in the blend.

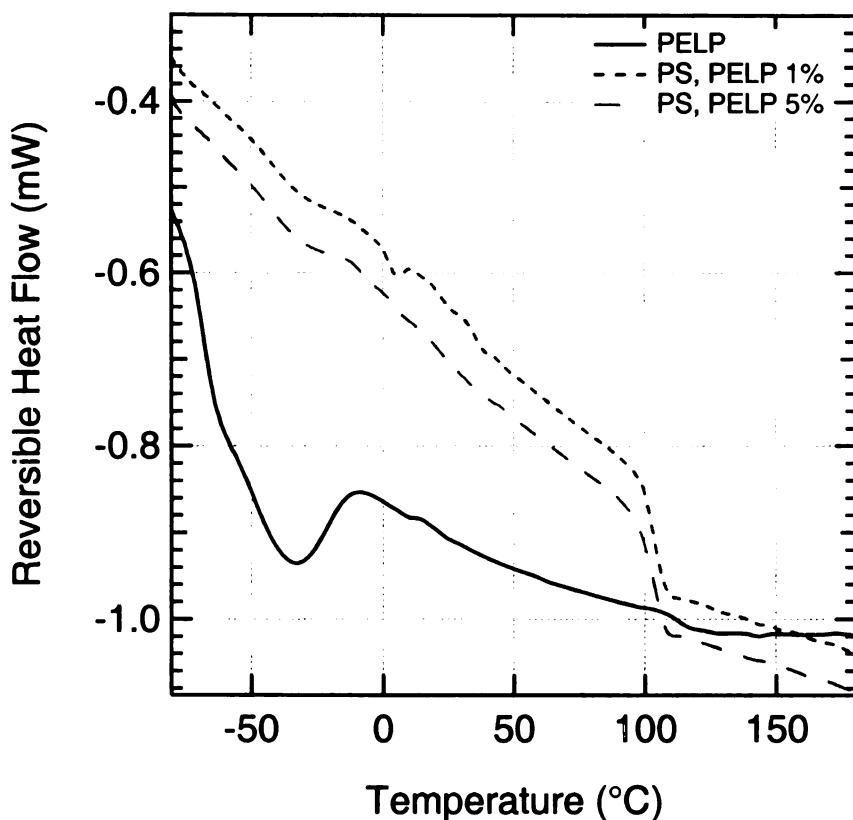


Figure V-1. DSC traces of pure PELP and blends of PELP with linear PS. Phase separation becomes apparent in the DSC trace for the 5% blend.

The overall compressibility of the system and its volumetric response to changes in temperature and pressure are sensitive to internal structure and the presence of void space. Engineering properties of interest that can be derived from PVT data are the bulk modulus, $K = -V(\partial P/\partial V)_T$, and the coefficient of thermal expansion,⁴⁷ $\alpha = V^{-1}(\partial V/\partial T)_P$. Analysis of the volumetric response of PS-PELP blends to temperature and pressure is consistent with expectations based on intuition about the component particles. The hyperbranched polyethylene shares the low T_g of other ethylene based polymers. However, likely due to the steric effects of branching, PELP appears to be hindered in its ability to crystallize at room temperature. Consequently, at ambient conditions and above

the sample is a liquid and is expected to have a very low modulus. This expectation is confirmed by measurements of the bulk modulus of PS-PELP blends as a function of increasing PELP content (Figure V-2). The modulus decreases quickly, falling by 18% at a 3.2v% loading of PELP. At higher loadings, the modulus increases, consistent with the observation made by DSC that phase segregation becomes prevalent at the higher concentration. The decrease in K_0 is quite significant in magnitude. While PELP is expected to have a very low bulk modulus, the reduction observed is greater than that expected for a material with bulk modulus of zero.

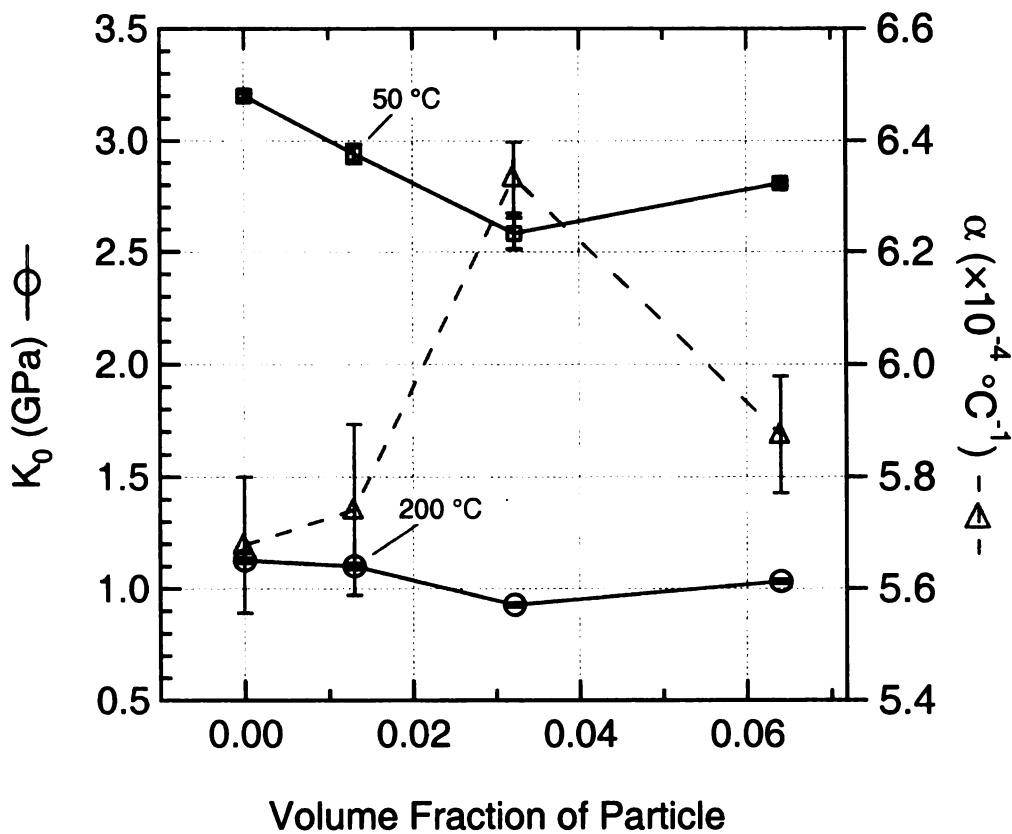


Figure V-2. Bulk modulus and thermal expansivity of a polystyrene/hyperbranched polyethylene nanoparticle blend. The PELP decreases the modulus and increases the thermal expansivity as expected for a system with little chemical interaction. Similar trends are seen in the bulk modulus both above and below the glass transition temperature.

In lieu of the seemingly unphysical conclusion that the bulk modulus of PELP is negative, the system can be viewed as having a layer of free volume surrounding the approximately spherical PELP macromolecules. The void space may be considered to have an infinite compressibility (K_0^{-1}) and for lack of a better estimate of the compressibility of PELP, we also assume infinite compressibility for the dendritic PE. Based on these estimates and the known K_0 of unfilled PS, the bulk modulus of the composite can be used to estimate a lower limit of the free volume in the sample based on a volumetric average of the bulk moduli of the PS, PELP, and free volume, following the method described in section II.C.1. For the stable PELP loadings of 1.3v% and 3.2v%, the calculated size of the excluded volume layer is 3.2 nm and 12.6 nm thick, respectively. It is more likely, however, that the free volume is more evenly distributed throughout the material rather than being located exclusively at the particle surface. In fact, calculations of free volume may be interpreted as diffuse regions of low density, rather than a full region of absolute void space. In either case, the estimate of the free volume is 2v% and 15v% at PELP loadings of 1.3v% and 3.2v%, respectively.

The view of the system as one having a high amount of void space is supported by the trend in thermal expansivity. Systems with high free volume and mobility have been identified as having increased values of α .⁴⁹⁻⁵² For the PELP/PS blend, the thermal expansivity shows a maximum at 3.2v%, concurrent with the minimum in K_0 at the same volume fraction.

The decrease in the bulk modulus suggests a porous, free volume laden structure of the nanocomposite. Additionally, the material also becomes more favored towards dilation with the addition of PELP. This is reflected by the increase in the free energy

anharmonicity, K_1 with PELP content (Figure V-3). This trend emphasizes the unfavorable interaction between the PS matrix and the PE filler, with the blend showing an energetic preference toward dilation – increasing the PS to PELP separation – rather than compression. The internal pressure, P_i , is the sensitivity of the internal energy to changes in volume and is sensitive to porosity, or free volume in the material. An increase in free volume is expected to decrease the volumetric dependence of internal energy as the mean nearest-neighbor spacing increases. This behavior is observed for the PS-PELP blend, with internal pressure decreasing by as much as 30%.

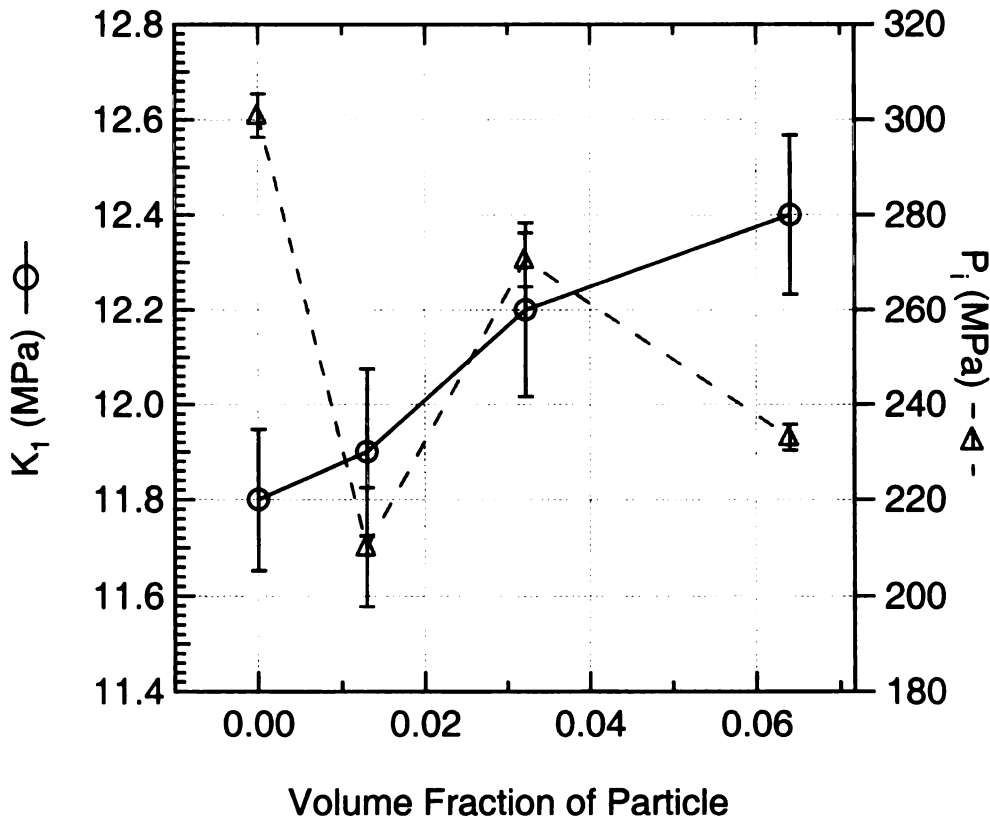


Figure V-3. The free volume asymmetry number, and internal pressure as function of PELP volume fraction in PS 393 kD. The free volume asymmetry number is increased with nanoparticle addition, suggesting an increased energetic penalty to compression as compared to dilation. The internal pressure is decreased by particle addition, consistent with a decrease in the strength of intermolecular interactions.

V.C.2.Non-Equilibrium Tensile Behavior

While dilatometric measures of bulk modulus reflect a volumetric average of the overall sample composition and the interaction between components, the solid state tensile behavior is largely dominated by the state of the continuous matrix. Therefore, a soft filler that weakens the composite when tested in compression may lead to a reduction in bulk modulus but an increase in the tensile modulus. This may occur if the expulsion of the matrix polymer from the vicinity of the filler causes the polymer to be more rigid due to its tendency to shrink away from the unfavorable filler environment. Efforts by the polymer to avoid the unfavorable particle interface may lead to the chains being strained beyond their normal equilibrium state. While this chain stretch would not be in any particular orientation, the strained state could lead to some increase in Young's Modulus, E. Additionally, the already strained polymer should be susceptible to orientation by a hot drawing process, increasing the modulus relative to the undrawn case or an equivalently drawn, but neutral environment chain. A study of the Young's Modulus as a function of the hot draw ratio, λ , for PS samples with and without PELP addition reveals this type of behavior.

The Young's Modulus of the undrawn sample increases from 2.37 to 2.85 GPa (20%) by the addition of 3.2v% PELP (Figure V-4a). The PELP laden sample is highly sensitive to orientation in the low draw ratio regime, increasing in E by 35% at a hot draw ratio of 1.5. By comparison, the unfilled polymer does not increase in E by that much until a draw ratio of more than 2.5. While the strained nature of the chains seems to make them easier to align, it does not appear to improve the maximum alignment, or at least the

maximum Young's Modulus that can be achieved by the hot drawing process. In fact, at the higher draw ratios the modulus of the PELP filled PS is similar to, or slightly less than, the unfilled polymer. The stiffening effect seen for Young's Modulus is also observed for the ultimate tensile strength (Figure V-4b), albeit to a lesser degree.

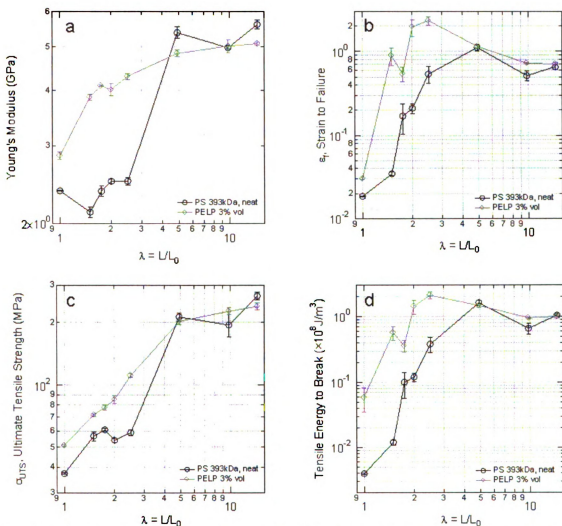


Figure V-4. The Young's Modulus (a), strain to failure (b), ultimate tensile strength (c), and tensile energy to break (d) of hot-drawn PS 393 kDa with 3v% PELP as a function of hot draw ratio. All four key tensile properties are increased at draw ratios less than five. At higher draw ratios, the behavior of the matrix dominates and the composite follows the tensile properties of unfilled polystyrene.

In addition to changes in Young's Modulus, changes in the strain-to-failure (ϵ_f) and mode of failure in simple tension are observed. The alignment induced by the hot drawing process is known to increase ϵ_f for unfilled PS. At low hot draw ratios, PS fails by an abrupt, brittle fracture mechanism at a very low strain value, which increases slightly across the low draw ratio regime. Beyond a critical processing threshold, the failure occurs by a ductile mechanism, characterized by neck formation and failure at much higher strain values. For the test and processing conditions of the present study, that transition occurs for unfilled PS at $\lambda \geq 2$. The PS-PELP blend undergoes a similar shift in tensile failure mechanism, but at a hot draw ratio of 1.5. The stress-strain curves of unfilled PS and PS-PELP 3.2v%, each processed to a hot draw ratio of 1.5 are shown in Figure V-5. The two samples show the classic stress-strain curves for their respective failure modes. The unfilled polymer fails abruptly and completely at a low strain value after a monotonic increase in stress. The ductile PS-PELP blend shows a maximum stress at a strain similar to ϵ_f of the unfilled polymer. This stress maximum occurs at the yield point and is indicative of the onset of necking. After the constant stress necking process has propagated across the length of the specimen, a strain hardening process occurs before final rupture.

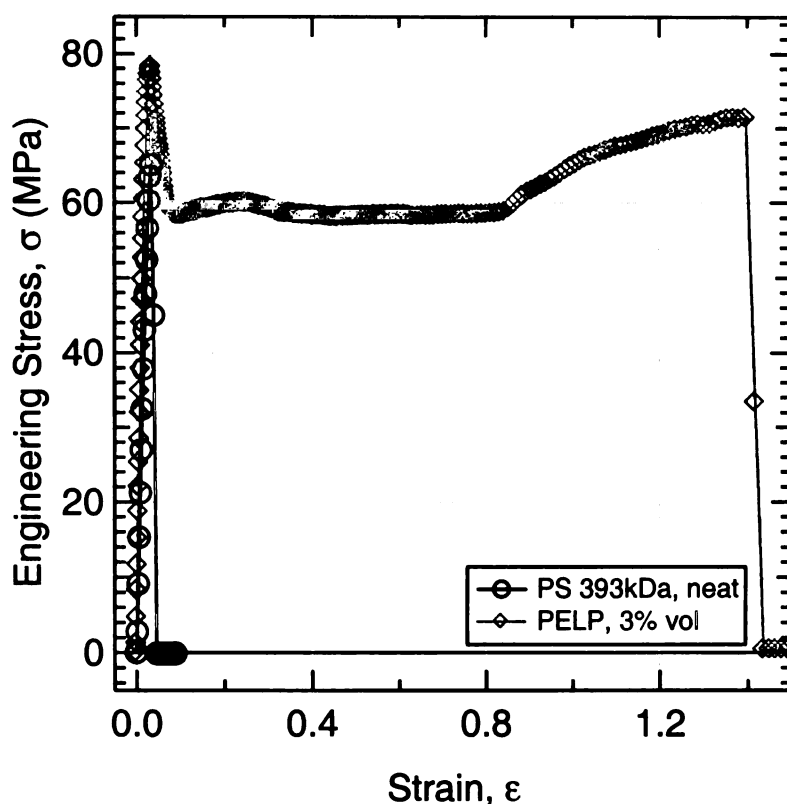


Figure V-5. Stress-strain curves for polystyrene with (green diamonds) and without (black circles) PELP, each processed to a hot-draw ratio of 1.5. The PELP induces ductile failure under conditions for which the unfilled polymer fails by a brittle mechanism at low strains.

In addition to shifting the critical hot draw ratio needed to induce ductility, the addition of PELP increases ϵ_f at all draw ratios up to 2.5 by as much as 825% relative to the unfilled polymer (Figure V-4b). Both of these effects reflect the low modulus of PELP and weak interaction at the interface between PS and PELP. This weak interface, which has been previously evaluated by trends in K_0 , permits an avenue for stress relief in the PS matrix. The even special distribution of these sites for stress relief throughout the sample allows the material to distribute stress evenly throughout the sample, permitting larger deformations. In the absence of these stress relief sites, internal stresses become concentrated at a single sample flaw or cross-sectional area minimum. Eventually, the

accumulation of stress at this location gives rise to failure at lower deformations than would be expected if stress were more evenly distributed.

At the higher draw ratios PELP is less effective at improving sample ductility. With the continuous matrix more oriented by the hot drawing process, tensile stress is propagated more directly along the polymer chain backbone. In this case, the matrix is less capable of distributing stress to the matrix-filler interface and the ϵ_f of the blend is dominated by the continuous phase.

V.D. Conclusion

Hyperbranched polyethylene macromolecules (PELP) can be well-dispersed in linear PS. Like other nanoparticle fillers, the addition of PELP at low volume fractions has been shown by DSC and PVT to increase the free volume and mobility of the material due to the poor interaction between PS and PELP. The increase in free volume is reflected by a decrease of the bulk modulus of nearly 20%. Estimates of the free volume fraction from the bulk modulus indicate that the free volume fraction is as much as five times the particle volume fraction. This free volume appears to be well-dispersed and leads to an increase in polymer mobility, and therefore, ductility rather than nucleating stress concentrations.

The unfavorable polymer-particle interaction is also found to cause chain strain in the polymer, which leads to an increase in the tensile modulus, an unexpected observation based on the addition of a low modulus material to one of higher modulus and the observed free volume increase. The increase in tensile modulus (E) and the decrease in bulk modulus (K) suggest a change in the shear modulus (G) as well. Based



on the well known relation between the moduli for the three modes of strain, an estimate can be attained for the shear modulus with and without PELP addition.

$$\text{Eq. 22} \quad E^{-1} = (3G)^{-1} + (9K)^{-1}$$

For a 3% loading of PELP in PS, the shear modulus at 50 °C is expected to increase by *ca.*20%.

Chapter VI: Rigid nanoparticle inclusion with polystyrene

VI.A. Introduction

A class of nanoparticles that has garnered a great deal of attention for behavior peculiar to their nanometer size is semiconductor nanocrystals, also known as quantum dots. A particularly interesting and well-studied semi-conductor crystal type is II-VI semiconductors, such as CdS and CdSe. These materials have shown variation in a number of material properties based on the size of the crystal which includes a shift in band gap,¹⁰⁷ melting temperature,¹⁰⁸ and pressure required to induce a transformation in the crystalline structure.¹⁰⁹ This peculiar behavior arises from the quantum-confined nature of the semiconductor crystal. The potential functionality of these materials has garnered interest for potential use as light-emitting diodes,¹¹⁰⁻¹¹³ photovoltaic cells,¹¹⁴⁻¹¹⁶ and bio-sensors.¹¹⁷ In addition to these potential applications, these particles are attractive for composite formulation due to their small, well-defined size, rigid composition, and the ability to coat them with a variety of stabilizing layers.^{118, 119}

VI.B. Experimental

Polystyrene standards were purchased from Scientific Polymer Products (Ontario, NY) with $M_w = 393,400$ Da and $M_w/M_n = 1.16$. CdSe-pyr nanoparticles were generously provided by Michael Wong at Rice University. Linear polymer/nanoparticle blends were made by dissolving both the linear polymer and nanoparticle, which was originally in solution with pyridine, in a mutual solvent, THF. This quaternary solution was then dripped into a mutual non-solvent, water, where the polymer and nanoparticles rapidly precipitated, forming an intimately mixed, homogeneous dispersion of nanoparticles in the linear polymer.⁴³ After removing the majority of the liquid from the sample by

decanting and vacuum filtration with copious water rinsing, the blend was dried for a week in an oven at 50 °C and under rough vacuum. Sample processing and characterization techniques were identical to those described in section II.B. Samples for TEM were embedded in Polybed 812, which was prepared and cured according to the manufacturer's instructions. Thin section of the bulk samples were cut with an ultramicrotome and samples were observed and photographed with a JEOL 100 CXII.

VI.C. Results & Discussion

The glass transition temperature observed by DSC is an indicator of polymer chain mobility and may reveal signs of phase separation in a particle-polymer blend. In the case of PS blended with CdSe-pyr, the glass transition temperature is decrease by 1.0 to 1.5 °C with 0.9v% to 1.0v% loading of particles. This indicates that the mobility of the polymer is increased by the particle addition. This is likely due to weak adhesion between the particle and polymer which leads to a region of low polymer density near the particle surface.

The tensile behavior of a PS-CdSe-pyr blend is interesting due to the rigid structure of the particle and its intermediate size. Previous studies of the tensile behavior of nanoparticle filled polymers have been limited to particles that were of similar (PSNP, Chapter II:) or lower (PELP, Chapter V:) modulus than the matrix polymer, or had a size that was much smaller than the Kuhn segment length (C₆₀, Chapter IV:) of the matrix. The comparison to the previously described particles is complicated, however, by the presence of a chemical stabilizing layer attached to the particle. This layer permits the particle to be dissolved in solution, allowing blending with the matrix, but provides an obstacle at the polymer-particle interface. This interface has been shown to be weak in

other nanoparticle systems, often associated with a layer of free volume around the particle. This has been attributed to both poor polymer-particle interaction and geometric restrictions to efficient packing near the particle surface.

The Young's modulus of PS and PS blended with 0.9v% CdSe-pyr is shown in (Figure VI-1a). The tensile modulus of the polymer particle blend is nearly 50% greater than for the unfilled polymer. While a modulus increase is expected with the addition of a rigid filler, the observed increase is not necessarily due to the rigidity of the filler. A larger, softer particle filler (PELP) was shown to increase the modulus similarly, an effect attributed to polymer chain strain at the polymer-particle interface due to a negative interaction. Another filler of similar size to the present system but lower modulus was observed to bring about a similar increase in E , attributed to the close proximity of the particles to one another, complicating chain extension under stress by the additional friction of the filler. In that case, the interparticle center-to-center distance was 22.4 nm, less than twice the R_g of the matrix polymer. The interparticle center-to-center distance of the present case is 23.0 nm, still less than twice the R_g of the matrix.

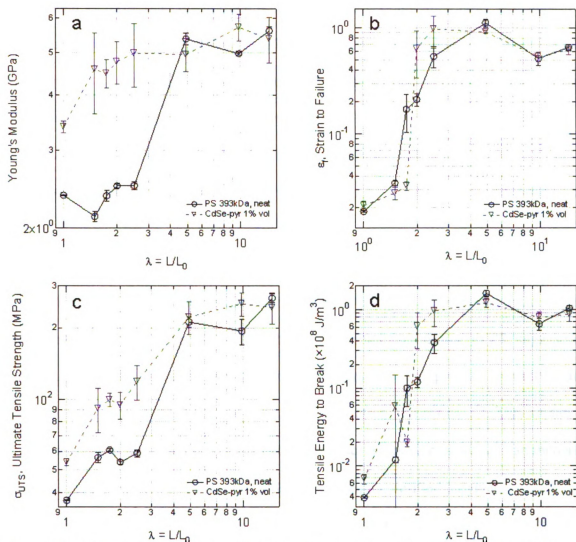


Figure VI-1. The Young's Modulus (a), strain to failure (b), ultimate tensile strength (c), and tensile energy to break (d) of hot-drawn PS 393 kDa with 1% CdSe-pyr as a function of hot draw ratio. The modulus and tensile strength are both increased at all draw ratios less than five. The strain to failure and tensile energy are increased at moderate (2 to 2.5) draw ratios but unchanged from the unfilled polymer under other processing conditions.

Like the unfilled polymer, the polymer-particle blend shown an increase in E with increasing λ . This is a natural consequence of the alignment process and reaches a plateau at high λ for the filled and unfilled polymer, which both show a similar high draw ratio plateau in modulus. The modulus of the particle filled system, however, increases much more quickly than the neat polymer. The CdSe-pyr particles improve the modulus

by as much as 100% over the unfilled polymer at an equivalent draw ratio. However, the maximum achievable value of Young's Modulus is not change significantly by CdSe-pyr inclusion. This supports the idea that the observed enhancement is caused by a change in the matrix polymer rather than the inherent rigidity of the additive. This is likely due to poor adhesion between the matrix and filler, hindering stress transfer across the interface. It is possible that this adhesion could be improved by the used of a different stabilizing ligand.^{118, 120, 121}

Experience with a different nanoparticle system suggests that the use of a compatible ligand may improve adhesion enough to bring about increases in modulus. Cross-linked polystyrene nanoparticles (PSNP) are chemically similar to PS, suggesting that adhesion between the two species would be favorable. The particle themselves are intramolecularly cross-linked, having an aver coordination number of 2.2. This creates a higher modulus filler with a favorable particle-polymer interaction, leading to an increase in the maximum Young's Modulus of 20% greater than the unfilled polymer.

The poor adhesion between the particle and matrix has consequences for the strain-to-failure in tension (Figure VI-1b). This weak interaction causes a layer of low density to form around the particle. While this region is ill-suited to transferring stress from the matrix to the filler for reinforcement, it does act as a soft region for stress relief. The effective range of ductility enhancement is limited, however, by the rigidity of the particle, with ϵ_f enhancement occurring primarily for hot draw ratios between 2 and 2.5 before conforming to the behavior of unfilled PS.

TEM micrographs indirectly support the conclusion of a weak particle-polymer interaction. Samples of drawn and undrawn PS-CdSe-pyr films were prepared for

observation by TEM to observe the influence of hot drawing on particle dispersion. However, the particles were so poorly adhered to the matrix that the ultramicrotomy process generated aggregates of CdSe-pyr particles and aligned them normal to the direction of cutting, or parallel to the knife edge. This orientation was observed regardless of sample processing, and specifically for the undrawn film (Figure VI-2). This suggests that the loose adhesion of the particle to the polymer permitted the ultramicrotome knife to dislodge the particles, depositing them periodically as the knife moved across the sample surface. While not informative about the dispersion or orientation of the particles, this does confirm the poor state of adhesion of the particle to the polymer matrix.

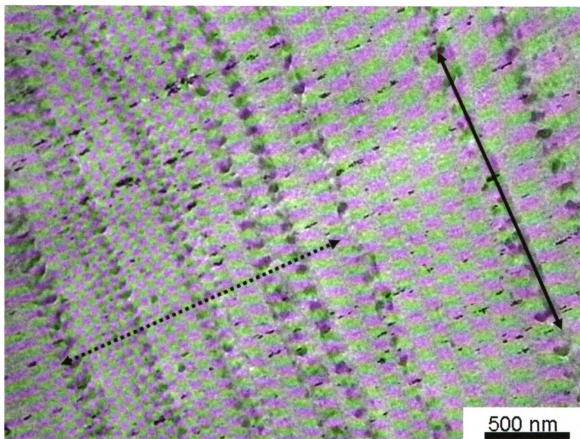


Figure VI-2. TEM micrograph of CdSe-pyr in PS. The wrinkles in the film are a familiar artifact of ultramicrotomy, reflecting imperfections in the knife edge. The particles are oriented perpendicular to these striations, suggesting that the particles are disturbed during the microtomy process and deposited intermittently as the knife moves across the sample.

VI.D. Conclusion

Blends of CdSe nanocrystals stabilized with a pyridine ligand were blended with linear polystyrene and characterized according to their thermal and mechanical behaviors. Similar to other nanoparticle-polymer blends, the interface between the particle and polymer is found to be quite weak, leading to a decrease in the glass transition temperature and modest improvement of the strain-to-failure for solid samples tested in tension. The Young's Modulus of the blend is greater than the unfilled polymer processed



to the same conditions, but does not exceed the maximum value for the unfilled polymer. The failure of the rigid particle to increase the modulus of the composite beyond the maximum for the polymer is attributed to poor stress transfer across the particle-polymer interface.

Chapter VII: Conclusions

Blends of polystyrene with four different classes of nanoparticles have been investigated to better understand the particle-polymer interaction and its significance for mechanical property enhancement. Cross-linked polystyrene nanoparticles (PSNP) are used as an enthalpically simple system with moderate particle stiffness. Buckminsterfullerenes (C_{60}) are rigid, high modulus particles with a size scale much smaller than PSNP. Hyperbranched polyethylene macromolecules (PELP) are a low modulus filler with an unfavorable interaction with PS and a size on the order of the PS chains' R_g . Finally, pyridine stabilized cadmium selenide nanocrystals are rigid particles with a size scale comparable to PSNP.

Generally, the particle inclusion increased polymer mobility and free volume. This is observed through decreases in the glass transition temperature, bulk modulus, and internal pressure, as well as increases in the free energy anharmonicity, and strain-to-failure for a sample in tension. In fact, the particles behave in a manner similar to a good solvent, increasing polymer chain mobility and ductility. Neutron scattering results confirm this, showing the chains to swell the polymer matrix, increasing the R_g and changing the chain conformation from that of a random coil with a Gaussian distribution to a swollen coil. The free volume layer size is dependent on particle size, increasing with increasing particle size (Figure VII-1a). The ratio of free volume to particle volume is less dependent on particle size (Figure VII-1b), having values of 1.5 to 3 for the studied systems in the melt state. The exception to this trend is C_{60} in PS, which leads to a free volume fraction approximately 13 times greater than the included particle fraction.

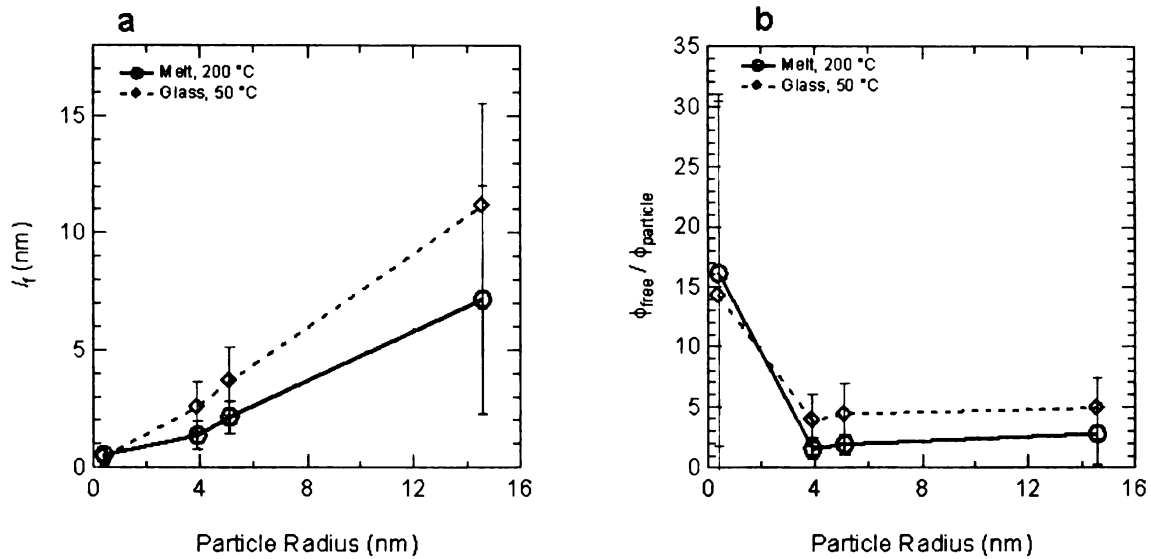


Figure VII-1. The calculated free volume layer size (a) and free volume fraction relative to particle volume fraction (b) for nanoparticles for four different sizes. The free volume thickness associated with the particle addition increases with particle size. With the exception of the extreme case of C60 ($a = 0.38$ nm), the ratio of free volume to particle volume is independent of particle size.

The details of the size, loading, and type of particle introduce other nuances to the polymer-particle behavior. Bulk modulus increases have been observed for many systems, although this increase is rarely beyond the maximum value for the matrix. This suggests a different mode for nanocomposite property enhancement than that of traditional macroscale composites. The nanoscale additive improves the behavior of the composite by changing the conformation of the matrix polymer, rather than simply by transferring stress to the particle. The increased ductility and, sometimes, stiffness leads to a general observation of increase in the materials' ability to dissipate energy, its toughness. This supports the application of nanoparticles as additives for improving engineering materials.

Appendix A. Notes on PVT Analysis

Specific Volume Measurements: A simple probe of free volume in a sample is to measure its specific volume under ambient conditions. Deviations in the observed specific volume (V_{obs}) from predictions based on relative composition (V_{pred}) and specific volume of each pure species may indicate a more or less tightly packed system. This can be quantified by the Excess Volume Fraction, measure of the free volume fraction.

$$\text{Eq. 23} \quad \phi_{\text{excess}} = (V_{\text{obs}} - V_{\text{pred}})/V_{\text{obs}}$$

The measured specific volume and the corresponding Excess Volume Fraction are shown in Figure A-1. While trends can be readily observed in the specific volume, the changes in Excess Volume Fraction are not beyond the error of measurement.

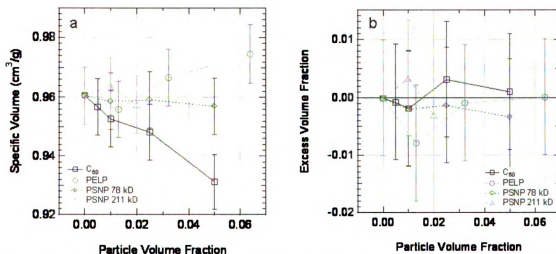


Figure A-1. The measured specific volume (a) of polystyrene-nanoparticle blends. Blends of polystyrene with nanoparticles follow close to a rule-of-mixtures type trend for specific volume. The deviation from that trend is apparent in the Excess Free Volume (b) for which a positive value represents the presence of free volume in the blend. It must be noted that the measurement technique is very subject to environmental variations and small changes in free volume may not be apparent in specific volume measurements.

Free Volume Calculation From Bulk Modulus: The bulk modulus of a nanoparticle linear polymer blend provides information about the presence of free volume in the composite. If a value of the bulk modulus for the nanoparticles is assumed, a relative amount of free volume present in the sample can be computed based on a volumetric average of the moduli of the three components: the continuous PS (c), particulate filler (p), and free volume (f).

$$\text{Eq. 24} \quad 1 = \varphi_c + \varphi_p + \varphi_f$$

$$\text{Eq. 25} \quad K_0 = \varphi_p K_{0,p} + \varphi_c K_{0,c}$$

The known bulk modulus of the composite, K_0 , and the nominal volume fraction of filler, $\varphi_{n,p}$, can be used to calculate the free volume fraction.

$$\text{Eq. 26} \quad \varphi_{n,p} = V_p / (V_p + V_c)$$

$$\text{Eq. 27} \quad \varphi_f = 1 - K_0 [(1 - \varphi_{n,p}) K_{0,c} + \varphi_{n,p} K_{0,p}]^{-1}$$

If one assumes that the free volume is concentrated in an even layer around the particle, with a radius a , the free volume layer thickness, l_f , can also be calculated.

$$\text{Eq. 28} \quad l_f = a [(((\varphi_p + \varphi_f) \varphi_p^2)^{1/3} / \varphi_p) - 1]$$

The free volume sizes of certain blends have been discussed previously. Values for each particle type and concentration are presented below.

Table A-1: Values of free volume layer sizes based on the bulk moduli of composites at 200 °C

Nanoparticle Blends with PS 393 kDa		
Particle	ϕ	l_f (nm)
PSNP 78kD	1.0%	1.98 ± 0.31
PSNP 78kD	2.5%	0.95 ± 0.45
PSNP 78kD	5.0%	1.16 ± 0.42
PSNP 211kD	1.0%	2.63 ± 0.40
PSNP 211kD	2.0%	1.65 ± 0.52
C ₆₀	0.5%	0.90 ± 0.11
C ₆₀	1.0%	0.42 ± 0.23
C ₆₀	2.5%	0.39 ± 0.24
C ₆₀	5.0%	0.43 ± 0.22
PELP	1.3%	4.69 ± 1.43
PELP	3.2%	13.45 ± 0.80
PELP	6.4%	3.37 ± 1.76

The Tait Equation: The empirical Tait equation has been used to model the PVT behavior of polymer in both the melt and glass states.^{52, 122-125}

$$\text{Eq. 29} \quad 1 - V/V_0 = C \ln(1 + P/B)$$

The parameter C is a constant with a value of 0.0894, V_0 is the initial volume at ambient pressure, and B is a function of temperature given by Eq. 30.

$$\text{Eq. 30} \quad B(T) = B_0 \exp(-B_1 T)$$

While some effort has been made to associate theoretical importance to the empirical parameters,¹²⁶ the values are reported primarily for completeness of comparison to other such characterized polymer systems.

Table A-2: Tait EOS parameters in the melt state of polymer/nanoparticle blends

Nanoparticle Blends with PS 393 kD			
Particle	ϕ	B_0 (MPa)	$B_1 \times 10^3$ ($^{\circ}\text{C}^{-1}$)
Unfilled PS	0.0%	214.9	3.235
PSNP 78kD	1.0%	219.5	3.451
PSNP 78kD	2.5%	216.4	3.369
PSNP 78kD	5.0%	211.2	3.172
PSNP 211kD	1.0%	225.3	3.529
PSNP 211kD	2.0%	220.1	3.410
C_{60}	0.5%	211.3	3.704
C_{60}	1.0%	210.2	3.035
C_{60}	2.5%	212.4	2.971
C_{60}	5.0%	353.0	5.799
PELP	1.3%	206.7	3.194
PELP	3.2%	200.6	3.756
PELP	6.4%	202.7	3.308

The Coefficient of Thermal Expansivity: The coefficient of thermal expansion has been used as an indicator of the system's free volume. Simha and Boyer⁴⁹ suggested that thermal expansivity in the glassy state was due entirely to occupied volume ($\alpha_g \approx \alpha_{occ,m}$). The increase in the coefficient of thermal expansion in the melt state was attributed to thermal expansivity due to free volume:

$$\text{Eq. 31} \quad \alpha_{f,m} \approx \alpha_m - \alpha_g$$

This allowed the difference between coefficients of thermal expansion in the melt or glass states to provide a relative measure of system free volume. In later work Dlubek,⁵¹ and later Kilburn,¹²⁷ used the Simha-Somcynski equation of state (S-S eos) hole fraction to separately determine the specific free ($V_f = hV$) and occupied ($V_{occ} = (1-h)V$) volumes where h is the statistical hole fraction in the melt state. From these quantities, the

coefficients of thermal expansion of the free volume in the glass and melt states were determined by

$$\text{Eq. 32} \quad \alpha_{f.g} = V_g^{-1}(\partial V_f / \partial T) (T < T_g)$$

$$\text{Eq. 33} \quad \alpha_{f.m} = V_g^{-1}(\partial V_f / \partial T) (T > T_g)$$

It is shown in these studies that α_g is significantly greater than $\alpha_{occ,m}$ and $\alpha_m - \alpha_g < \alpha_{f,m}$, contrary to the earlier work of Simha and Boyer. Each of these studies are confounded by the difficulty in measuring α in the glassy state. The restricted mobility of materials in their glassy state means that external conditions, especially pressure, are not necessarily transferred uniformly throughout the sample. This stress transfer is a time dependent process and often exceeds the time-scale of measurement. While some empirical relations, specifically the Tait equation, have been successful in modeling the PVT surface in the glassy state, true thermodynamic conclusions should generally not be drawn from PVT behavior of the glassy state.

The Simha-Somcynsky (S-S) equation of state: Several equations of state have been proposed to model the behavior of polymer melts,^{125, 128-130} but one of the most successful and widely used¹³¹ has been the Simha-Somcynsky (S-S) equation of state.³⁸ The melt is described in this model as an amorphous assembly of chain segments that occupy a lattice with a certain fraction (h) of unoccupied sites, representative of free volume within the melt. The thermodynamic properties of the melt are characterized by three key parameters: the maximum interaction energy between two chain segments (ϵ^*), the segmental repulsion volume (v^*), and the number of volume-dependent external degrees of freedom ($3c$). In turn, the characteristic pressure, volume, and temperature are defined as

$$\text{Eq. 34} \quad P^* = zq\varepsilon^*/(sv^*); \quad T^* = zq\varepsilon^*/(Rc); \quad V^* = v^*/M_s$$

where R is the universal gas constant, s is the number of chain segments, M_s is the molar segmental mass, z is the lattice coordination number ($z = 12$), and $zq = s(z-2)+2$. These characteristic parameters, P^* , V^* , and T^* scale their respective physical parameters, P , V , and T to produce a universal, reduced \tilde{P} - \tilde{V} - \tilde{T} surface.

Table A-3: Simha-Somcynsky EOS parameters in the melt state of polymer/nanoparticle blends

Nanoparticle Blends with PS 393 kD				
	ϕ	P^* (MPa)	V^* (cm ³ /g)	T^* (K)
Unfilled PS	0.0%	826.6	0.9486	11946.7
PSNP 78kD	1.0%	830.5	0.9505	11805.9
PSNP 78kD	2.5%	847.1	0.9489	11644.8
PSNP 78kD	5.0%	837.3	0.9459	11817.6
PSNP 211kD	1.0%	861.7	0.9506	11638.1
PSNP 211kD	2.0%	840.9	0.9501	11797.6
C ₆₀	0.5%	831.8	0.9448	11255.9
C ₆₀	1.0%	825.2	0.9456	12051.8
C ₆₀	2.5%	830.2	0.9404	12168.7
C ₆₀	5.0%	824.3	0.9261	12149.8
PELP	1.3%	819.4	0.9471	11795.1
PELP	3.2%	819.8	0.9472	10993.8
PELP	6.4%	799.1	0.9656	11700.1

The S-S eos is based on the free energy function, \tilde{F} , defined as

$$\text{Eq. 35} \quad \tilde{F} = \tilde{F}[\tilde{V}, \tilde{T}, h(\tilde{V}, \tilde{T})]$$

The free volume fraction, h , is a function of the reduced temperature and volume, which arises from the minimization of the free energy at a given temperature and pressure:

$$\text{Eq. 36} \quad (\partial\tilde{F}/\partial h)_{\tilde{V}, \tilde{T}} = 0$$

and the reduced pressure is described as:

$$\text{Eq. 37} \quad \tilde{P} = -(\partial \tilde{F} / \partial \tilde{V})_{T}$$

The solution to the reduced pressure term yields the first of two equations that constitute the equation of state:

$$\text{Eq. 38} \quad \tilde{P}\tilde{V}/\tilde{T} = (1-\eta)^{-1} + 2yQ^2(1.011Q^2 - 1.2045)/\tilde{T}$$

where y is the occupied site fraction ($1-y = h$), $Q = (y\tilde{V})^{-1}$, and $\eta = 2^{-1/6}yQ^{1/3}$. The free energy minimization yields the second equation:

$$\text{Eq. 39} \quad 3c[(\eta - 1/3)/(1 - \eta) - yQ^2(3.033Q^2 - 2.409)/6\tilde{T}] + (1 - s) - (s/y)\ln(1 - y) = 0$$

The statistical hole fraction, h , is computed from the S-S eos and presented as a function of particle volume fraction (Figure A-2) for samples at 200 °C and 0 MPa. It is interesting to note that all the samples show an increase in the hole fraction with nanoparticle addition, regardless of the change in bulk modulus or coefficient of thermal expansivity. It is counterintuitive that the statistical hole fraction, h , increases, regardless of the relative change in bulk modulus or thermal expansivity. This may indicate that free volume is introduced around the exterior of all nanoparticles. However, changes in physical properties may be due to the way in which the occupied volume is filled. Different nanoparticles may differently affect the packing of the polymer chains outside the excluded volume region.

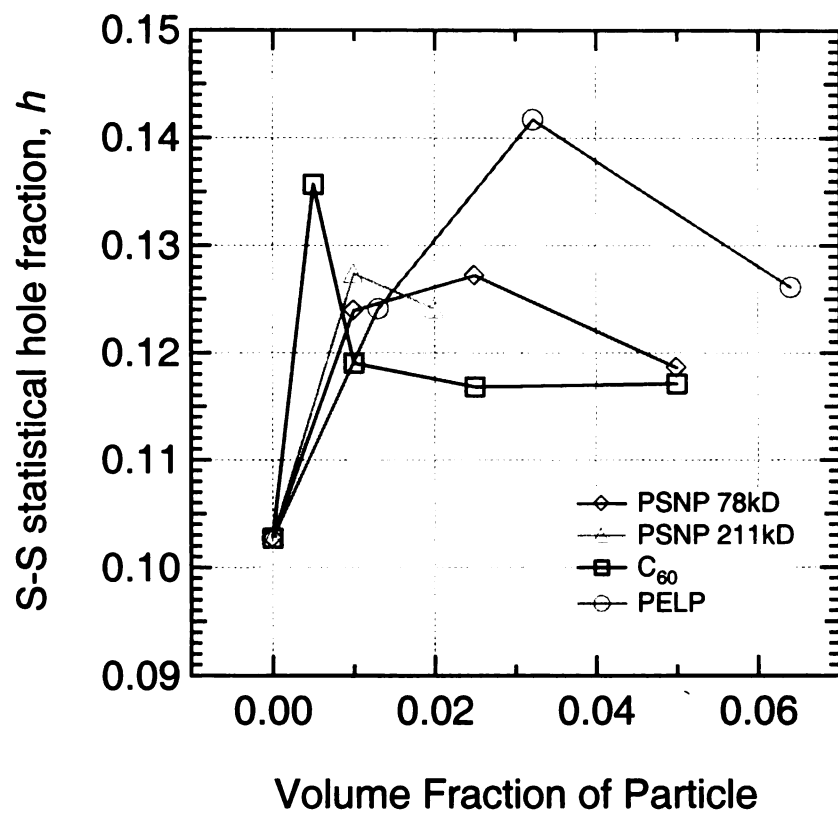


Figure A-2. The Simha-Somcynsky statistical hole fraction for blends of PS 393 kD with four different nanoparticle types.

Appendix B. Additional Tensile Data

In addition to the low loadings (1v%) presented in Chapter II, the tensile behavior of 5v% blends of PSNP has also been measured (Figure B-1). The behavior tends to be similar to the 1v% loading described previously.

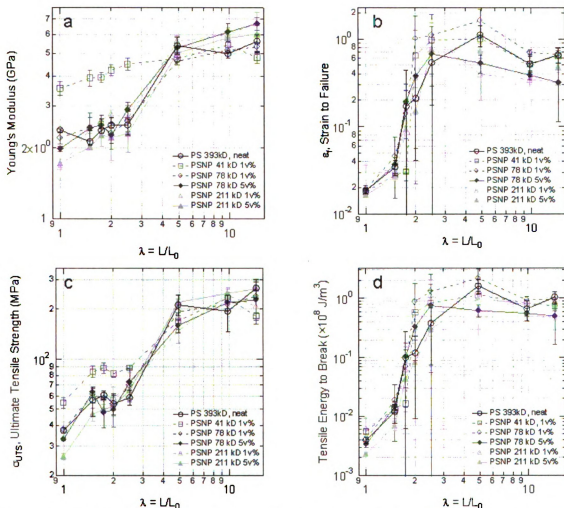


Figure B-1. The Young's Modulus (a), strain to failure (b), ultimate tensile strength (c), and tensile energy to break (d) of hot-drawn PS 393 kD with PSNP as a function of hot draw ratio. Blends of 1% PSNP are represented by open symbols while blends of 5% PSNP are represented by closed symbols. Larger PSNP species have very little effect on Young's Modulus or ultimate tensile strength, while smaller (41 kD) particles increase these properties for the unprocessed and slightly processed case. The ductility (b) is increased for all cases at low draw ratios and at all draw ratios for PSNP 78 kD, which gives rise to an increase in the material toughness (d).

REFERENCES

1. Seydel, T.; Kolln, K.; Krasnov, I.; Diddens, I.; Hauptmann, N.; Helms, G.; Ogurreck, M.; Kang, S. G.; Koza, M. M.; Muller, M., Silkworm Silk under Tensile Strain Investigated by Synchrotron X-ray Diffraction and Neutron Spectroscopy. *Macromolecules* **2007**, 40, (4), 1035-1042.
2. Vollrath, F.; Knight, D. P., Liquid crystalline spinning of spider silk. *Nature* **2001**, 410, (6828), 541-548.
3. Liu, Y.; Shao, Z. Z.; Vollrath, F., Relationships between supercontraction and mechanical properties of spider silk. *Nature Materials* **2005**, 4, (12), 901-905.
4. Liu, Y.; Shao, Z. Z.; Vollrath, F., Extended wet-spinning can modify spider silk properties. *Chemical Communications* **2005**, (19), 2489-2491.
5. Gersappe, D., Molecular mechanisms of failure in polymer nanocomposites. *Physical Review Letters* **2002**, 89, (5), -.
6. Tang, Z. Y.; Kotov, N. A.; Magonov, S.; Ozturk, B., Nanostructured artificial nacre. *Nature Materials* **2003**, 2, (6), 413-U8.
7. Tanner, D.; Fitzgerald, J. A.; Phillips, B. R., The Kevlar Story - an Advanced Materials Case Study. *Angewandte Chemie International Edition in English* **1989**, 28, (5), 649-654.
8. Mackay, M. E.; Dao, T. T.; Tuteja, A.; Ho, D. L.; Van Horn, B.; Kim, H. C.; Hawker, C. J., Nanoscale effects leading to non-Einstein-like decrease in viscosity. *Nature Materials* **2003**, 2, (11), 762-766.
9. Tuteja, A.; Mackay, M. E.; Hawker, C. J.; Van Horn, B., Effect of ideal, organic nanoparticles on the flow properties of linear polymers: Non-Einstein-like behavior. *Macromolecules* **2005**, 38, (19), 8000-8011.
10. Mackay, M. E.; Tuteja, A.; Duxbury, P. M.; Hawker, C. J.; Van Horn, B.; Guan, Z.; Chen, G.; Krishnan, R. S., General Strategies for Nanoparticle Dispersion. *Science* **2006**, 311, (5768), 1740-1743.

11. Simha, R.; Utracki, L. A.; Garcia-Rejon, A., Pressure-volume-temperature relations of a poly-epsilon-caprolactam and its nanocomposite. *Composite Interfaces* **2001**, 8, (5), 345-353.
12. Utracki, L. A.; Simha, R.; Garcia-Rejon, A., Pressure-volume-temperature dependence of poly-epsilon-caprolactam/clay nanocomposites. *Macromolecules* **2003**, 36, (6), 2114-2121.
13. Utracki, L. A.; Simha, R., Pressure-volume-temperature dependence of polypropylene/organoclay nanocomposites. *Macromolecules* **2004**, 37, (26), 10123-10133.
14. Winberg, P.; Eldrup, M.; Pedersen, N. J.; van Es, M. A.; Maurer, F. H. J., Free volume sizes in intercalated polyamide 6/clay nanocomposites. *Polymer* **2005**, 46, (19), 8239-8249.
15. Dionne, P. J.; Ozisik, R.; Picu, C. R., Structure and dynamics of polyethylene nanocomposites. *Macromolecules* **2005**, 38, (22), 9351-9358.
16. Cerda, J. J.; Sintes, T.; Chakrabarti, A., Excluded volume effects on polymer chains confined to spherical surfaces. *Macromolecules* **2005**, 38, (4), 1469-1477.
17. Vacatello, M., Phantom chain simulations of realistically sized polymer-based nanocomposites. *Macromolecular Theory and Simulations* **2006**, 15, (4), 303-310.
18. Papakonstantopoulos, G. J.; Yoshimoto, K.; Doxastakis, M.; Nealey, P. F.; de Pablo, J. J., Local mechanical properties of polymeric nanocomposites. *Physical Review E* **2005**, 72, (3).
19. Desai, T.; Koblinski, P.; Kumar, S. K., Molecular dynamics simulations of polymer transport in nanocomposites. *Journal of Chemical Physics* **2005**, 122, (13).
20. Brown, D.; Mele, P.; Marceau, S.; Alberola, N. D., A molecular dynamics study of a model nanoparticle embedded in a polymer matrix. *Macromolecules* **2003**, 36, (4), 1395-1406.
21. Brown, D.; Clarke, J. H. R.; Okuda, M.; Yamazaki, T., The Preparation of Polymer Melt Samples for Computer-Simulation Studies. *Journal of Chemical Physics* **1994**, 100, (8), 6011-6018.

22. Neyertz, S.; Brown, D., Preparation of bulk melt chain configurations of polycyclic polymers. *Journal of Chemical Physics* **2001**, 115, (2), 708-717.
23. Merkel, T. C.; Freeman, B. D.; Spontak, R. J.; He, Z.; Pinnau, I.; Meakin, P.; Hill, A. J., Ultraparpermeable, reverse-selective nanocomposite membranes. *Science* **2002**, 296, (5567), 519-522.
24. Boyer, R. F., Dynamics and Thermodynamics of the Liquid-State (T Greater-Than T_g) of Amorphous Polymers. *Journal of Macromolecular Science-Physics* **1980**, B18, (3), 461-553.
25. Priestley, R. D.; Ellison, C. J.; Broadbelt, L. J.; Torkelson, J. M., Structural relaxation of polymer glasses at surfaces, interfaces and in between. *Science* **2005**, 309, (5733), 456-459.
26. McCoy, J. D.; Curro, J. G., Conjectures on the glass transition of polymers in confined geometries. *Journal of Chemical Physics* **2002**, 116, (21), 9154-9157.
27. Alcoutlabi, M.; McKenna, G. B., Effects of confinement on material behaviour at the nanometre size scale. *Journal of Physics-Condensed Matter* **2005**, 17, (15), R461-R524.
28. Xiao, P.; Xiao, M.; Gong, K. C., Preparation of exfoliated graphite/polystyrene composite by polymerization-filling technique. *Polymer* **2001**, 42, (11), 4813-4816.
29. Fragiadakis, D.; Pissis, P.; Bokobza, L., Glass transition and molecular dynamics in poly (dimethylsiloxane)/silica nanocomposites. *Polymer* **2005**, 46, (16), 6001-6008.
30. Bansal, A.; Yang, H.; Li, C.; Benicewicz, B. C.; Kumar, S. K.; Schadler, L. S., Controlling the thermomechanical properties of polymer nanocomposites by tailoring the polymer-particle interface. *Journal of Polymer Science Part B: Polymer Physics* **2006**, 44, (20), 2944-2950.
31. Bansal, A.; Yang, H. C.; Li, C. Z.; Cho, K. W.; Benicewicz, B. C.; Kumar, S. K.; Schadler, L. S., Quantitative equivalence between polymer nanocomposites and thin polymer films. *Nature Materials* **2005**, 4, (9), 693-698.
32. Rittigstein, P.; Torkelson, J. M., Polymer-nanoparticle interfacial interactions in polymer nanocomposites: Confinement effects on glass transition temperature and

suppression of physical aging. *Journal of Polymer Science Part B: Polymer Physics* **2006**, 44, (20), 2935-2943.

33. Xu, H. Y.; Yang, B. H.; Wang, J. F.; Guang, S. Y.; Li, C., Preparation, thermal properties, and T-g increase mechanism of poly(acetoxystyrene-co-octavinyl-polyhedral oligomeric silsesquioxane) hybrid nanocomposites. *Macromolecules* **2005**, 38, (25), 10455-10460.

34. Cheatham, R. G.; Dietz, A. G. H., Effect of Orientation on the Mechanical Properties of Polystyrene. *Modern Plastics* **1951**, September, 113-192.

35. Cleereman, K. J.; Karam, H. J.; Williams, J. L., Polystyrene Monofilaments and Bristles. *Modern Plastics* **1953**, May, 119.

36. Stendahl, J. C.; Li, L. M.; Zubarev, R.; Chen, Y. R.; Stupp, S. I., Toughening of polymers by self-assembling molecules. *Advanced Materials* **2002**, 14, (21), 1540-+.

37. Stendahl, J. C.; Zubarev, E. R.; Arnold, M. S.; Hersam, M. C.; Sue, H. J.; Stupp, S. I., Structural modifications to polystyrene via self-assembling molecules. *Advanced Functional Materials* **2005**, 15, (3), 487-493.

38. Harth, E.; Van Horn, B.; Lee, V. Y.; Germack, D. S.; Gonzales, C. P.; Miller, R. D.; Hawker, C. J., A facile approach to architecturally defined nanoparticles via intramolecular chain collapse. *Journal of the American Chemical Society* **2002**, 124, (29), 8653-8660.

39. Potschke, P.; Brunig, H.; Janke, A.; Fischer, D.; Jehnichen, D., Orientation of multiwalled carbon nanotubes in composites with polycarbonate by melt spinning. *Polymer* **2005**, 46, (23), 10355-10363.

40. Miaudet, P.; Badaire, S.; Maugey, M.; Derre, A.; Pichot, V.; Launois, P.; Poulin, P.; Zakri, C., Hot-drawing of single and multiwall carbon nanotube fibers for high toughness and alignment. *Nano Letters* **2005**, 5, (11), 2212-2215.

41. Dror, Y.; Salalha, W.; Khalfin, R. L.; Cohen, Y.; Yarin, A. L.; Zussman, E., Carbon nanotubes embedded in oriented polymer nanofibers by electrospinning. *Langmuir* **2003**, 19, (17), 7012-7020.

42. Ruan, S.; Yu, T. X.; Gao, P., Ultra-strong gel-spun UHMWPE fibers reinforced using multiwalled carbon nanotubes. *Polymer* **2006**, *47*, (5), 1604-1611.
43. Zoller, P.; Bolli, P.; Pahud, V.; Ackermann, H., Apparatus for Measuring Pressure-Volume-Temperature Relationships of Polymers to 350Degreesc and 2200 Kg/Cm2. *Review of Scientific Instruments* **1976**, *47*, (8), 948-952.
44. Jain, R. K.; Simha, R., On the Equation of State of Argon and Organic Liquids. *Journal of Chemical Physics* **1980**, *72*, (9), 4909-4912.
45. Tuteja, A.; Mackay, M. E.; Narayanan, S.; Asokan, S.; Wong, M. S., Breakdown of the Continuum Stokes-Einstein Relation for Nanoparticle Diffusion. *Nano Lett.* **2007**, *7*, (5), 1276-1281.
46. Lodge, T. P.; Wood, E. R.; Haley, J. C., Two calorimetric glass transitions do not necessarily indicate immiscibility: The case of PEO/PMMA. *Journal of Polymer Science Part B: Polymer Physics* **2006**, *44*, (4), 756-763.
47. Yu, S. Z.; Hing, P.; Hu, X., Thermal expansion behaviour of polystyrene-aluminium nitride composites. *Journal of Physics D-Applied Physics* **2000**, *33*, (13), 1606-1610.
48. Tuteja, A.; Mackay, M. E.; Hawker, C. J.; Van Horn, B.; Ho, D. L., Molecular architecture and rheological characterization of novel intramolecularly crosslinked polystyrene nanoparticles. *Journal of Polymer Science Part B-Polymer Physics* **2006**, *44*, (14), 1930-1947.
49. Simha, R.; Boyer, R. F., On a General Relation Involving the Glass Temperature and Coefficients of Expansion of Polymers. *The Journal of Chemical Physics* **1962**, *37*, (5), 1003-1007.
50. Dlubek, G.; Sen Gupta, A.; Pionteck, J.; Krause-Rehberg, R.; Kaspar, H.; Lochhaas, K. H., Temperature dependence of the free volume in fluoroelastomers from positron lifetime and PVT experiments. *Macromolecules* **2004**, *37*, (17), 6606-6618.
51. Dlubek, G.; Bondarenko, V.; Pionteck, J.; Supej, M.; Wutzler, A.; Krause-Rehberg, R., Free volume in two differently plasticized poly(vinyl chloride)s: a positron lifetime and PVT study. *Polymer* **2003**, *44*, (6), 1921-1926.

52. Schmidt, M.; Maurer, F. H. J., Pressure-volume-temperature properties and free volume parameters of PEO/PMMA blends. *Journal of Polymer Science Part B-Polymer Physics* **1998**, 36, (6), 1061-1080.
53. Sanchez, I. C.; Cho, J.; Chen, W. J., Universal Response of Polymers, Solvents, and Solutions to Pressure. *Macromolecules* **1993**, 26, (16), 4234-4241.
54. Cho, J.; Sanchez, I. C., An analytical free energy and the temperature-pressure superposition principle for pure polymeric liquids. *Macromolecules* **1998**, 31, (19), 6650-6661.
55. Sauer, B. B.; Dee, G. T., Surface tension and melt cohesive energy density of polymer melts including high melting and high glass transition polymers. *Macromolecules* **2002**, 35, (18), 7024-7030.
56. Hildebrand, J.; Prausnitz, J. M.; Scott, R. L., *Regular and Related Solutions: The Solubility of Gases, Liquids, and Solids*. Van Nostrand Reinhold: New York, 1970.
57. Anderson, S. L.; Grulke, E. A.; Delassus, P. T.; Smith, P. B.; Kocher, C. W.; Landes, B. G., A Model for Antiplasticization in Polystyrene. *Macromolecules* **1995**, 28, (8), 2944-2954.
58. Forsyth, M.; Meakin, P.; MacFarlane, D. R., C-13 NMR spin-lattice relaxation times as a probe of local polymer dynamics in plasticized polyethers. *Journal of Materials Chemistry* **1997**, 7, (2), 193-201.
59. Rehner, J., Theory of filler reinforcement in natural and synthetic rubber. The stresses in and about the particles. *Journal of Applied Physics* **1943**, 14, (12), 638-645.
60. Nielsen, L. E.; Landel, R. F., *Mechanical Properties of Polymers and Composites*. Marcel Dekker, Inc.: New York, 1994.
61. Choi, K. J.; Spruiell, J. E.; White, J. L., Structure Development in Biaxially Stretched Polystyrene Film .1. Property-Orientation Correlation. *Polymer Engineering and Science* **1989**, 29, (21), 1516-1523.
62. White, J. L.; Spruiell, J. E., The Specification of Orientation and Its Development in Polymer Processing. *Polymer Engineering and Science* **1983**, 23, (5), 247-256.

63. Choi, K. J.; Spruiell, J. E.; White, J. L., Structure Development in Biaxially Stretched Polystyrene Film .2. Theoretical-Analysis of Orientation Development. *Polymer Engineering and Science* **1989**, 29, (21), 1524-1527.
64. Picot, C.; Duplessix, R.; Decker, D.; Benoit, H.; Boue, F.; Cotton, J. P.; Daoud, M.; Farnoux, B.; Jannink, G.; Nierlich, M.; de Vries, A. J.; Pincus, P., Neutron-Scattering by Uniaxially Hot Stretched Polystyrene Samples. *Macromolecules* **1977**, 10, (2), 436-442.
65. Ramzi, A.; Hakiki, A.; Bastide, J.; Boue, F., Uniaxial extension of end-linked polystyrene networks containing deuterated free chains studied by small-angle neutron scattering: Effect of the network chains and the size of the free chains. *Macromolecules* **1997**, 30, (10), 2963-2977.
66. Embery, J.; Graham, R. S.; Duckett, R. A.; Groves, D.; Collis, M.; Mackley, M. R.; McLeish, T. C. B., Tearing energy study of "oriented and relaxed" polystyrene in the glassy state. *Journal of Polymer Science Part B: Polymer Physics* **2007**, 45, (4), 377-394.
67. Ender, D. H.; Andrews, R. D., Cold Drawing of Glassy Polystyrene under Dead Load. *Journal of Applied Physics* **1965**, 36, (10), 3057-&.
68. Tanabe, Y.; Kanetsuna, H., Structure of Oriented Polystyrene Monofilaments and Its Relationship to Brittle-to-Ductile Transition. *Journal of Applied Polymer Science* **1978**, 22, (6), 1619-1630.
69. Boue, F.; Nierlich, M.; Jannink, G.; Ball, R., Polymer Coil Relaxation in Uniaxially Strained Polystyrene Observed by Small-Angle Neutron-Scattering. *Journal De Physique* **1982**, 43, (1), 137-148.
70. Pellerin, C.; Prud'homme, R. E.; Pezolet, M.; Weinstock, B. A.; Griffiths, P. R., Deformation and Relaxation of Polymers Studied by Ultrarapid Scanning FT-IR Spectrometry. *Macromolecules* **2003**, 36, (13), 4838-4843.
71. Bent, J.; Hutchings, L. R.; Richards, R. W.; Gough, T.; Spares, R.; Coates, P. D.; Grillo, I.; Harlen, O. G.; Read, D. J.; Graham, R. S.; Likhtman, A. E.; Groves, D. J.; Nicholson, T. M.; McLeish, T. C. B., Neutron-mapping polymer flow: Scattering, flow visualization, and molecular theory. *Science* **2003**, 301, (5640), 1691-1695.
72. De Francesco, A.; Duckett, R. A., Effects of orientation on mechanical properties of uniaxially oriented polystyrene films. *Polymer* **2004**, 45, (23), 8005-8011.

73. Theodorou, M.; Jasse, B.; Monnerie, L., Fourier-Transform Infrared Investigation of Conformational-Changes Occurring at the Yield-Point in Uniaxially Drawn Atactic Polystyrene. *Journal of Polymer Science Part B-Polymer Physics* **1985**, 23, (3), 445-450.
74. Yokouchi, M.; Yokota, A.; Kobayashi, Y., Tensile and Impact Behavior of Drawn Polystyrene and High-Impact Polystyrene. *Journal of Applied Polymer Science* **1982**, 27, (8), 3007-3018.
75. Dvoranek, L.; Machova, L.; Sorm, M.; Pelzbauer, Z.; Svantner, J.; Kubanek, V., Effects of Drawing Conditions on the Properties of Optical Fibers Made from Polystyrene and Poly(Methyl Methacrylate). *Angewandte Makromolekulare Chemie* **1990**, 174, 25-39.
76. Han, H. Z. Y.; Duckett, R. A.; McLeish, T. C. B.; Ward, N. J.; Johnson, A. F., Drawing and orientation-relaxation behaviour of monodisperse linear and 3-arm star polystyrenes. *Polymer* **1997**, 38, (7), 1545-1555.
77. King, S. M., Small-angle Neutron Scattering. In *Modern Techniques for Polymer Characterisation*, Pethrick, R. A.; Dawkins, J. V., Eds. John Wiley & Sons Ltd: 1999; pp 171-228.
78. Higgins, J. S.; Benoit, H. C., *Polymers and Neutron Scattering*. Clarendon Press: Oxford, 1994.
79. Forster, S.; Burger, C., Scattering Functions of Polymeric Core-Shell Structures and Excluded Volume Chains. *Macromolecules* **1998**, 31, (3), 879-891.
80. Li, Y. Q.; Ishida, H., A study of morphology and intercalation kinetics of polystyrene-organoclay nanocomposites. *Macromolecules* **2005**, 38, (15), 6513-6519.
81. Tung, J.; Gupta, R. K.; Simon, G. P.; Edward, G. H.; Bhattacharya, S. N., Rheological and mechanical comparative study of in situ polymerized and melt-blended nylon 6 nanocomposites. *Polymer* **2005**, 46, (23), 10405-10418.
82. Plummer, C. J. G.; Rodlert, M.; Bucaille, J. L.; Grunbauer, H. J. M.; Manson, J. A. E., Correlating the rheological and mechanical response of polyurethane nanocomposites containing hyperbranched polymers. *Polymer* **2005**, 46, (17), 6543-6553.

83. Weon, J. I.; Sue, H. J., Effects of clay orientation and aspect ratio on mechanical behavior of nylon-6 nanocomposite. *Polymer* **2005**, 46, (17), 6325-6334.
84. Tanoue, S.; Utracki, L. A.; Garcia-Rejon, A.; Tatibouet, J.; Cole, K. C.; Kamal, M. R., Melt compounding of different grades of polystyrene with organoclay. Part 1: Compounding and characterization. *Polymer Engineering and Science* **2004**, 44, (6), 1046-1060.
85. Chae, H. G.; Sreekumar, T. V.; Uchida, T.; Kumar, S., A comparison of reinforcement efficiency of various types of carbon nanotubes in poly acrylonitrile fiber. *Polymer* **2005**, 46, (24), 10925-10935.
86. Minus, M. L.; Chae, H. G.; Kumar, S., Single wall carbon nanotube templated oriented crystallization of poly(vinyl alcohol). *Polymer* **2006**, 47, (11), 3705-3710.
87. Kroto, H. W.; Heath, J. R.; O'Brien, S. C.; Curl, R. F.; Smalley, R. E., C-60 - Buckminsterfullerene. *Nature* **1985**, 318, (6042), 162-163.
88. Iijima, S., Helical Microtubules of Graphitic Carbon. *Nature* **1991**, 354, (6348), 56-58.
89. Affholter, K. A.; Henderson, S. J.; Wignall, G. D.; Bunick, G. J.; Haufler, R. E.; Compton, R. N., Structural Characterization of C-60 and C-70 Fullerenes by Small-Angle Neutron-Scattering. *Journal of Chemical Physics* **1993**, 99, (11), 9224-9229.
90. Ruoff, R. S.; Ruoff, A. L., The Bulk Modulus of C60 Molecules and Crystals - a Molecular Mechanics Approach. *Applied Physics Letters* **1991**, 59, (13), 1553-1555.
91. Ruoff, R. S.; Ruoff, A. L., Is C60 Stiffer Than Diamond. *Nature* **1991**, 350, (6320), 663-664.
92. Wang, Y.; Tomanek, D.; Bertsch, G. F., Stiffness of a Solid Composed of C60 Clusters. *Physical Review B* **1991**, 44, (12), 6562-6565.
93. Soifer, Y. M.; Kobelev, N. P.; Nikolaev, R. K.; Levin, V. M., Integral and Local Elastic Properties of C₆₀ Single Crystals. *physica status solidi (b)* **1999**, 214, (2), 303-308.

94. Lundin, A.; Sundqvist, B.; Skoglund, P.; Fransson, A.; Pettersson, S., Compressibility, specific heat capacity, and Grüneisen parameter for C60/C70. *Solid State Communications* **1992**, 84, (9), 879-883.
95. Schirber, J. E.; Kwei, G. H.; Jorgensen, J. D.; Hitterman, R. L.; Morosin, B., Room-temperature compressibility of C₆₀: Intercalation effects with He, Ne, and Ar. *Physical Review B* **1995**, 51, (17), 12014.
96. Sundqvist, B.; Andersson, O.; Lundin, A.; Soldatov, A., Phase diagram, structure, and disorder in C60 below 300 K and 1 GPa. *Solid State Communications* **1995**, 93, (2), 109-112.
97. Lundin, A.; Sundqvist, B., Compressibility of C-60 in the temperature range 150-335 K up to a pressure of 1 GPa. *Physical Review B* **1996**, 53, (13), 8329-8336.
98. Brazhkin, V. V.; Lyapin, A. G.; Hemley, R. J., Harder than diamond: dreams and reality. *Philosophical Magazine a-Physics of Condensed Matter Structure Defects and Mechanical Properties* **2002**, 82, (2), 231-253.
99. Ding, Y. F.; Kisliuk, A.; Sokolov, A. P., When does a molecule become a polymer? *Macromolecules* **2004**, 37, (1), 161-166.
100. Choi, K. J.; Spruiell, J. E.; White, J. L., Orientation and Morphology of High-Density Polyethylene Film Produced by the Tubular Blowing Method and Its Relationship to Process Conditions. *Journal of Polymer Science Part B-Polymer Physics* **1982**, 20, (1), 27-47.
101. White, J. L., Structure Development in Polymer Processing. *Pure and Applied Chemistry* **1983**, 55, (5), 765-776.
102. Guan, Z. B.; Cotts, P. M.; McCord, E. F.; McLain, S. J., Chain walking: A new strategy to control polymer topology. *Science* **1999**, 283, (5410), 2059-2062.
103. Guan, Z. B., Control of polymer topology through late-transition-metal catalysis. *Journal of Polymer Science Part a-Polymer Chemistry* **2003**, 41, (22), 3680-3692.
104. Suhr, J.; Koratkar, N.; Keblinski, P.; Ajayan, P., Viscoelasticity in carbon nanotube composites. *Nature Materials* **2005**, 4, (2), 134-137.

105. Chae, D. W.; Lee, K. H.; Kim, Y. C., Rheological properties of ferrite nanocomposites based on nylon-66. *Journal of Polymer Science Part B-Polymer Physics* **2006**, *44*, (2), 371-377.
106. Lee, J. Y.; Zhang, Q.; Wang, J. Y.; Emrick, T.; Crosby, A. J., Failure Mechanism of Glassy Polymer-Nanoparticle Composites. *Macromolecules* **2007**.
107. Vossmeier, T.; Katsikas, L.; Giersig, M.; Popovic, I. G.; Diesner, K.; Chemseddine, A.; Eychmuller, A.; Weller, H., Cds Nanoclusters - Synthesis, Characterization, Size-Dependent Oscillator Strength, Temperature Shift of the Excitonic-Transition Energy, and Reversible Absorbency Shift. *Journal of Physical Chemistry* **1994**, *98*, (31), 7665-7673.
108. Goldstein, A. N.; Echer, C. M.; Alivisatos, A. P., Melting in Semiconductor Nanocrystals. *Science* **1992**, *256*, (5062), 1425-1427.
109. Tolbert, S. H.; Alivisatos, A. P., High-Pressure Structural Transformations in Semiconductor Nanocrystals. *Annual Review of Physical Chemistry* **1995**, *46*, 595-625.
110. Alivisatos, A. P., Semiconductor Clusters, Nanocrystals, and Quantum Dots. *Science* **1996**, *271*, (5251), 933-937.
111. Lee, J.; Sundar, V. C.; Heine, J. R.; Bawendi, M. G.; Jensen, K. F., Full Color Emission from II-VI Semiconductor Quantum Dot-Polymer Composites. *Advanced Materials* **2000**, *12*, (15), 1102-1105.
112. Schlamp, M. C.; Peng, X. G.; Alivisatos, A. P., Improved efficiencies in light emitting diodes made with CdSe(CdS) core/shell type nanocrystals and a semiconducting polymer. *Journal of Applied Physics* **1997**, *82*, (11), 5837-5842.
113. Gao, M. Y.; Richter, B.; Kirstein, S., White-light electroluminescence from a self-assembled Q-CdSe/PPV multilayer structures. *Advanced Materials* **1997**, *9*, (10), 802-&.
114. Huynh, W. U.; Dittmer, J. J.; Alivisatos, A. P., Hybrid nanorod-polymer solar cells. *Science* **2002**, *295*, (5564), 2425-2427.
115. Leatherdale, C. A.; Kagan, C. R.; Morgan, N. Y.; Empedocles, S. A.; Kastner, M. A.; Bawendi, M. G., Photoconductivity in CdSe quantum dot solids. *Physical Review B* **2000**, *62*, (4), 2669-2680.

116. Wang, P.; Abrusci, A.; Wong, H. M. P.; Svensson, M.; Andersson, M. R.; Greenham, N. C., Photoinduced charge transfer and efficient solar energy conversion in a blend of a red polyfluorene copolymer with CdSe nanoparticles. *Nano Letters* **2006**, 6, (8), 1789-1793.
117. Kloepfer, J. A.; Mielke, R. E.; Wong, M. S.; Neelson, K. H.; Stucky, G.; Nadeau, J. L., Quantum dots as strain- and metabolism-specific microbiological labels. *Applied and Environmental Microbiology* **2003**, 69, (7), 4205-4213.
118. Skaff, H.; Sill, K.; Emrick, T., Quantum dots tailored with poly(para-phenylene vinylene). *Journal of the American Chemical Society* **2004**, 126, (36), 11322-11325.
119. Asokan, S.; Krueger, K. M.; Alkhaldeh, A.; Carreon, A. R.; Mu, Z. Z.; Colvin, V. L.; Mantzaris, N. V.; Wong, M. S., The use of heat transfer fluids in the synthesis of high-quality CdSe quantum dots, core/shell quantum dots, and quantum rods. *Nanotechnology* **2005**, 16, (10), 2000-2011.
120. Lee, J. Y.; Zhang, Q.; Emrick, T.; Crosby, A. J., Nanoparticle Alignment and Repulsion during Failure of Glassy Polymer Nanocomposites. *Macromolecules* **2006**, 39, (21), 7392-7396.
121. Zhang, Q.; Russell, T. P.; Emrick, T., Synthesis and Characterization of CdSe Nanorods Functionalized with Regioregular Poly(3-hexylthiophene). *Chem. Mater.* **2007**, 19, (15), 3712-3716.
122. Hay, G.; Mackay, M. E.; Hawker, C. J., Thermodynamic properties of dendrimers compared with linear polymers: General observations. *Journal of Polymer Science Part B-Polymer Physics* **2001**, 39, (15), 1766-1777.
123. Schmidt, M.; Maurer, F. H. J., Isotropic pressure-densified atactic poly(methyl methacrylate) glasses: Free-volume properties from equation-of-state data and positron annihilation lifetime spectroscopy. *Macromolecules* **2000**, 33, (10), 3879-3891.
124. Schmidt, M.; Olsson, M.; Maurer, F. H. J., Macroscopic pressure-volume-temperature properties versus free-volume characteristics of isotropic pressure-densified amorphous polymer glasses. *Journal of Chemical Physics* **2000**, 112, (24), 11095-11106.
125. Rodgers, P. A., Pressure Volume Temperature Relationships for Polymeric Liquids - a Review of Equations of State and Their Characteristic Parameters for 56 Polymers. *Journal of Applied Polymer Science* **1993**, 48, (6), 1061-1080.

126. Nanda, V. S.; Simha, R., Theoretical Interpretation of Tait Equation Parameters. *Journal of Chemical Physics* **1964**, 41, (6), 1884-&.
127. Kilburn, D.; Dlubek, G.; Pionteck, J.; Bamford, D.; Alam, M. A., Microstructure of free volume in SMA copolymers I. Free volume from Simha-Somcynsky analysis of PVT experiments. *Polymer* **2005**, 46, (3), 859-868.
128. Sanchez, I. C.; Cho, J., A Universal Equation of State for Polymer Liquids. *Polymer* **1995**, 36, (15), 2929-2939.
129. Dee, G. T.; Walsh, D. J., Equations of State for Polymer Liquids. *Macromolecules* **1988**, 21, (3), 811-815.
130. Flory, P. J.; Orwoll, R. A.; Vrij, A., Statistical Thermodynamics of Chain Molecule Liquids .I. Equation of State for Normal Paraffin Hydrocarbons. *Journal of the American Chemical Society* **1964**, 86, (17), 3507-&.
131. Simha, R.; Somcynsky, T., On the Statistical Thermodynamics of Spherical and Chain Molecule Fluids. *Macromolecules* **1969**, 2, (4), 342-350.

MICHIGAN STATE UNIV



3 1293 02